Study of Planetary Nebulae in the Galactic Plane: IPHAS and SCUBA

A thesis submitted to The University of Manchester for the degree of
Doctor of Philosophy
in the Faculty of Engineering and Physical Sciences

2008

Laurence SABIN

School of Physics and Astronomy

Contents

List of Figures **9**

List of Tables **15**

Abstract 19

Declaration 21

Copyright Statement 22

Dedication 24

Acknowledgements 25

The Author 26

Supporting Publications 27

1 Introduction: The Planetary Nebulae **31**

1.1 The extent of our knowledge about galactic PNe and its limitations . . 34

1.1.1 General distribution and size 34

1.1.2 Morphology 35

1.1.3 Chemical abundances 40

1.2 The unsolved problems in PN study 42

1.2.1 The detection problem 43

1.2.2 The derivation of the physical properties 44

1.2.3 The Morphology: determination and origin 44

I Discoveries of planetary nebulae in the framework of the IPHAS

survey of the Galactic Plane **47**

2 The contribution of the IPHAS survey: observation and classification of stellar populations **49**

2.1 The Hα emission line 49

2.2 Introduction to the survey 50

2.3 Mosaicing of the Galactic Plane 59

2.4 The populations in the IPHAS survey 65

2.4.1 The classification and number of extended nebulae 67

2.4.2 The IPHAS nebulae database 73

2.5 Summary 73

3 Classification of the candidate planetary nebulae **77**

3.1 Spectroscopic identification 78

3.1.1 Characteristic spectral lines 78

3.1.2 The IPHAS spectroscopy follow-up 82

3.2 The IRAS and MSX based classifications 98

3.2.1 The infrared emission of PNe and the use of colour-colour diagrams 98

3.2.2 The IRAS results 104

3.2.3 The MSX results 110

3.3 The radio based classification 115

3.4 Morphology based classification 132

3.5 Summary 145

II Analysis of the first IPHAS results **155**

4 General properties of the IPHAS PNe (and candidates) **157**

4.1 Galactic distributions 157

4.2 Discussion 167

5 Infrared properties of the IPHAS sources 173

5.1 Introduction 173

5.2 CLOUDY models 174

5.3 Fitting models for the IPHAS nebulae 182

5.4 Conclusion 187

6 Estimation of the Distances 191

6.1 Introduction 191

6.2 Surface brightness-radius relationship 193

6.3 The Shklovskii method 201

6.4 The IPHAS extinction method 201

6.4.1 Application to the IPHAS PNe 203

6.4.2 Accuracy of the method 208

6.5 Discussion 211

6.5.1 Comparison of the methods 211

6.5.2 IPHAS PNe in the Galactic Plane: height and galactocentric distances 222

6.6 Ionised Mass 226

7 Recombination process and age determination 231

7.1 Application to the sample of IPHAS PNe 231

7.2 Discussion 237

7.2.1 The age populations 237

7.2.2 Ionization or density bounded ? 242

8 Interaction with the interstellar medium 249

8.1 Classification of the IPHAS nebulae 249

8.2 Comparison with hydrodynamical models 268

8.3 Identification of the CS Candidates: Direction and Proper motions . . 274

8.4 Discussion 280

III Magnetic fields in planetary nebulae 287

9 Magnetic field detection via dust polarisation 289

9.1 Abstract 289

9.2 Introduction 290

9.3 Observations 291

9.4 The results 293

9.4.1 NGC 6537 293

9.4.2 NGC 7027 294

9.4.3 CRL 2688 297

9.4.4 NGC 6302 300

9.5 Discussion and Conclusion 303

9.5.1 Targets 304

9.5.2 Field location and orientation 305

9.5.3 Chemistry 306

9.5.4 Comparison of less evolved/ more evolved nebulae 308

9.5.5 Field strength and origin 308

9.5.6 Evolution 309

9.5.7 Summary 310

10 Other detection processes and magnetic field exhibition 313

10.1 Spectropolarimetry and radio measurements 313

10.2 Interstellar magnetic field 316

11 Conclusions and Perspectives 317

11.1 Summary of the investigation 317

11.2 Solved problems and future work 323

A The IPHAS extended PNe candidates 325

B Qualitative description of the IPHAS candidate PNe 335

C Spectroscopic observations of candidate PNe located after RA=20h 345

D Spectra for each models obtained with CLOUDY 351

E The case of the Supernovae Remnants 365

List of Figures

1 The Necklace nebula: a new IPHAS PN 29

1.1 HR diagram showing the evolution of an intermediate mass star . . . 35
1.2 Distribution of galactic planetary nebulae following Kohoutek (1) . . 36
1.3 Distribution of galactic planetary nebulae following Kohoutek (2) . . 37

2.1 The Barnard's loop 51
2.2 IPHAS Hα images of four known and new nebulae 52
2.3 The Isaac Newton Telescope in La Palma 53
2.4 Transmission profiles of the filters used in the IPHAS survey 54
2.5 Sky area covered by IPHAS 56
2.6 5 pixels x 5 pixels binning mosaic of the region 20h12m+38deg . . . 63
2.7 Distribution of compact PNe in the IPHAS color-color diagram 66
2.8 Example of the most common artefacts found in the mosaics 67
2.9 Other examples of common artefacts 68
2.10 EGAPS main page 74
2.11 Entries of the Nebulae database 74
2.12 Part of database body for the extended catalogue 75
2.13 An example of entry for IPHASX J183416.2+021215 75

3.1 Hα+NII inverted images of IPHAS candidate PNe (1) 90
3.2 Hα+NII inverted images of IPHAS candidate PNe (2) 91
3.3 Hα+NII inverted images of IPHAS candidate PNe (3) 92

3.4 IPHAS image of IPHASX J185525.7-004823 93
3.5 Line-ratio diagrams presented by Sabbadin et al. (1977) for the classification of the nebulae S176 94
3.6 New diagnostic diagrams presented by Riesgo and López (2006) . . . 95
3.7 IPHAS data in the Sabbadin et al. (1977) and Riesgo and López (2006) diagnostic diagrams 96
3.8 IRAS two-colours diagram for various objects from Pottasch et al. (1988) 101
3.9 IRAS two-colours diagram from Zijlstra et al. (2001) 102
3.10 MSX colour-colour diagram from (Ortiz et al. 2005) 104
3.11 IPHAS/IRAS two-colour diagram from Zijlstra 2001 108
3.12 IPHAS/IRAS two-colour diagram from Pottasch 1988 109
3.13 IPHAS planetary nebulae identified within IRAS 111
3.14 MSX colour diagram following Ortiz 2005 113
3.15 IPHAS planetary nebulae identified within MSX 114
3.16 6cm flux density distribution of known PNe from Ratag et al. (1990) . 116
3.17 Results of the NVSS/VLA survey applied to 60 IPHAS targets 118
3.18 Brightness temperature distribution of the IPHAS targets, known PNe and HII regions 120
3.19 IPHAS images of the new HII region IPHASX J192349.9+143330 . . 121
3.20 Comparison of the radio surface brightness of the IPHAS targets and known PNe 122
3.21 Limits on the location of PNe and HII regions on the T_b vs size diagram 123
3.22 Percentage of PNe for limiting fluxes of 100, 200 and 500 mJy 124
3.23 Fraction of PNe/HII regions according to the radio flux 125
3.24 IPHAS planetary nebulae identified thanks to their radio flux 131
3.25 Hα+NII images of the IPHAS candidate PNe 133
3.26 Young IPHAS SNR candidates also classified as PN candidates 148

4.1 Galactic Distribution of the IPHAS nebulae and known PNe 158

4.2 Galactic distribution of newly discovered objects and known PNe . . . 160
4.3 Distribution on the Plane of the IPHAS nebulae according their size . 161
4.4 Morphological distribution of the IPHAS and known PNe 164
4.5 Number and morphology of the IPHAS and known PNe 165
4.6 Morphological distribution of populations detected in IPHAS in terms of the latitudes 166
4.7 IPHAS nebulae according their morphology and relative size 169
4.8 Expected versus observed nebulae in the Galactic plane between 18h and 20h 171

5.1 Closed geometry assumed in the CLOUDY models 175
5.2 CLOUDY models for a density of 100 cm^{-3} with the Pottasch limits . 177
5.3 CLOUDY models for a density of 1000 cm^{-3} with the Pottasch limits 178
5.4 CLOUDY models for a density of 10 000 cm^{-3} with the Pottasch limits 179
5.5 CLOUDY model A with different physical conditions 180
5.6 Known and IPHAS nebulae in the IR diagram from Pottasch et al. (1988) 182
5.7 Fitting models for the IPHAS nebulae with CLOUDY 184
5.8 Spectra of the different CLOUDY models 186
5.9 New version of the Pottasch et al. (1988) diagram 189

6.1 The early-A reddening line 204
6.2 Extinction curves for the IPHAS PNe 206
6.3 Slit position on the PN IPHASX J192847.1+093439 209
6.4 Extinction variation in the PN IPHASX J192847.1+093439 210
6.5 Comparison of the SB methods with the extinction method (1) 213
6.6 Comparison of the SB methods with the extinction method (2) 214
6.7 Distribution of the distances and height above the plane of the IPHAS PNe 223
6.8 z distribution for bipolar and round PNe 224
6.9 Galactic location of IPHAS and known PNe 225

6.10 Nebular mass against radius for IPHAS and known PNe 228

7.1 Electron Density versus radius diagram for the IPHAS and known PNe 235
7.2 IPHASX J195657.6+265714: an evolved recombining PN 236
7.3 Age determination of the IPHAS PNe 237
7.4 Density versus radius diagram for the IPHAS and known PNe 238
7.5 Determination of ionisation and density bounded IPHAS PNe (1) . . . 244
7.6 Determination of ionisation and density bounded IPHAS PNe (2) . . . 245
7.7 Ionisation bounded IPHAS PNe 246
7.8 Density bounded IPHAS PNe 247

8.1 Successive stages of ISM interaction in PNe 251
8.2 Nebular shapes for the four stages of interaction defined by Wareing et al. (2007) 252
8.3 WZO2: IPHASX J185322.1+083018 254
8.4 WZO2: IPHASX J190338.5+104227 254
8.5 WZO2: IPHASX J190419.4+152126 255
8.6 WZO2: IPHASX J190454.0+101801 256
8.7 WZO2: IPHASX J190512.4+161347 256
8.8 WZO2: IPHASX J190654.9+052216 257
8.9 WZO2: IPHASX J191421.1+140936 258
8.10 WZO2: IPHASX J192436.3+154402 258
8.11 WZO2: IPHASX J192543.2+143546 259
8.12 WZO2: IPHASX J193630.3+312810 259
8.13 WZO2: IPHASX J193637.3+123808 260
8.14 WZO2: IPHASX J194204.9+231932 261
8.15 WZO2: IPHASX J194240.6+275109 261
8.16 WZO2: IPHASX J194645.3+262211 262
8.17 WZO2: IPHASX J194727.6+230816 263
8.18 WZO2: IPHASX J194852.7+222516 264

8.19 WZO2: IPHASX J195357.9+312130 264
8.20 WZO3: IPHASX J185744.5+105053 265
8.21 WZO3: IPHASX J190700.7+043041 266
8.22 WZO3: IPHASX J192221.5+151550 267
8.23 WZO4: IPHASX J190227.3+020815 267
8.24 Comparison observation/model for the general WZO2 interaction process 270
8.25 Comparison observation/model for IPHASX J190454.0+101801 . . . 271
8.26 Comparison observation/model for IPHASX J190512.4+161347 . . . 272
8.27 Comparison observation/model for WZO3 type (1) 272
8.28 Comparison observation/model for WZO3 type (2) 273
8.29 Comparison observation/model for WZO4 type 274
8.30 Distribution of the candidate ISM/PNe in the plane according their size and stage of interaction 283
8.31 A case of WZO1 stage: IPHASX J205013.7+465518 284
8.32 Supernovae or large PN with ISM interaction 285
8.33 Presentation of two difficult cases to analyse 286

9.1 SCUBA 850μm results on NGC 6537 295
9.2 SCUBA 450μm results on NGC 7027 296
9.3 SCUBA 850 and 450μm results on CRL2688 298
9.4 Continuum-subtracted H_2 (HST) of CRL 2688 301
9.5 SCUBA 450μm results on NGC 6302 302
9.6 Location of the SCUBA dust emission compared to HST images . . . 306

10.1 Polarization of spectral lines 314

C.1 Hα IPHAS images of the nebulae with spectra in the 20h-7h region . . 347
C.2 Extinction curves of nebulae outside the 18h-20h boundary 349

D.1 CLOUDY model A for a density of 100 cm^{-3} 352
D.2 CLOUDY model B for a density of 100 cm^{-3} 353

D.3 CLOUDY model C for a density of 100 cm^{-3} 354
D.4 CLOUDY model D for a density of 100 cm^{-3} 355
D.5 CLOUDY model A for a density of 1000 cm^{-3} 356
D.6 CLOUDY model B for a density of 1000 cm^{-3} 357
D.7 CLOUDY model C for a density of 1000 cm^{-3} 358
D.8 CLOUDY model D for a density of 1000 cm^{-3} 359
D.9 CLOUDY model A for a density of 10000 cm^{-3} 360
D.10 CLOUDY model B for a density of 10000 cm^{-3} 361
D.11 CLOUDY model C for a density of 10000 cm^{-3} 362
D.12 CLOUDY model D for a density of 10000 cm^{-3} 363

List of Tables

1.1 Summary of the number of PNe known in the Galaxy 38
1.2 Number, mean scale height and morphological class of PNe 39
1.3 Chemical abundances in Planetary Nebulae 41
1.4 Planetary Nebulae Types reviewed by Quireza et al. (2007) 42

2.1 Main characteristics of the predecessors of the IPHAS survey 59
2.2 Criteria for the mosaics construction 61
2.3 Morphological classification of nebulae 72
2.4 Listing of the 8 types of nebulae localised with the visual search on mosaics with 18h <Ra< 20h 72

3.1 Sample of optical emission lines found in planetary nebulae 79
3.2 Spectroscopic configurations used for the different telescopes 84
3.3 Listing of the 18 IPHAS candidates PNe with available spectroscopic data 86
3.4 Classification of the IPHAS candidates following Sabbadin et al. (1977) and Riesgo and López (2006) 97
3.5 Results of the IPHAS/IRAS diagnostic diagrams 107
3.6 MSX identification of IPHAS sources 112
3.7 VLA characteristics for data taken at 6 cm and 21 cm 117
3.8 Probability on the nature of IPHAS nebulae based on radio data . . . 123
3.9 Radio classification of the candidate PNe identified in the NVSS survey 127

3.10 Summary of the classification of IPHAS candidate PNe 149

4.1 Number of IPHAS nebulae and known planetary nebulae in the galactic plane according their size 159
4.2 Number of IPHAS nebulae and known planetary nebulae according their morphology 163
4.3 Mean latitude and dispersion of each morphological population 164

5.1 Main parameters for the CLOUDY models 176
5.2 Radius for each CLOUDY models 176
5.3 Best CLOUDY fits for 3 formely misclassified PNe 183
5.4 Emission line contribution for the CLOUDY models 187

6.1 Logarithm of the surface brightness 197
6.2 Logarithm of the radius in pc 198
6.3 Distances in kpc obtained via the four methods 199
6.4 radius and distances obtained using the SB law for the bipolar nebulae 200
6.5 Distances obtained with the Shklovskii method 202
6.6 Extinction and distances of a set of IPHAS nebulae 205
6.7 Summary of the distances obtained 212
6.8 Summary of the radius obtained 216
6.9 Distances comparison for known PNe between the SB-R method, the Cahn et al. (1992) and Zhang (1995) results 218
6.10 Galactocentric distances of the IPHAS PNe 226
6.11 Derived ionised masses for the IPHAS targets 229

7.1 List of IPHAS PNe showing a nitrogen enhancement 232
7.2 Recombination time scale in a set of IPHAS planetary nebulae 233
7.3 Nebular parameters and dynamical age for known and IPHAS PNe . . 240
7.4 Evolutionary status of the IPHAS PNe and occurence of recombination 241

8.1 Definition of the four ISM interaction stages by Wareing et al. (2007) 252
8.2 Summary of the IPHAS nebulae with signs of ISM interaction 269
8.3 Proper motions of the candidates CS and direction of motion 277

9.1 Mean values of the polarimetric parameters for the Post-AGB objects 303

A.1 Full listing of the planetary nebulae candidate in the 18h to 20h region 325

C.1 List of 14 IPHAS nebulae with spectral data and localised between 20h and 00h in RA 346
C.2 Distances and extinction for some of the nebulae outside the 18h-20h boundary 348

E.1 The 17 known SNRs in the 18h-20h region 366
E.2 SNR candidates with X-ray emission nearby and/or adequate morphology 367
E.3 Young Pulsars close to nebulae found within IPHAS 368

The University of Manchester

ABSTRACT OF THESIS submitted by Laurence Sabin for the Degree of Doctor of Philosophy and entitled: "Study of planetary nebulae in the Galactic Plane: IPHAS and SCUBA."

This thesis sheds new light on two main subjects. First, the discovery of new extended planetary nebulae (PNe) in the Galactic Plane, thanks to the recent Isaac Newton Telescope Photometric Hα Survey (IPHAS). The new objects, located in a right ascension range between 18h and 20h, were identified using different diagnostic diagrams in the optical, infrared and radio regimes. We investigated their nature and distribution on the Plane compared to known planetary nebulae and found some "hidden populations" of PNe. These new findings also confirm the efficiency of the survey to detect faint planetary nebulae at low latitudes. The analysis of the radio and infrared properties of the newly found nebulae, allowed us to constrain and correct the diagnostic diagrams used so far and which are mostly dedicated to bright PNe. Combined with an investigation of the recombination status and the age of the nebulae, our analysis suggests that we are dealing with large, old and generally dusty objects. A totally new aspect of PNe has therefore been revealed. The issue of distance estimation has also been approached with the use of a new extinction-distance method developed within the framework of IPHAS. The last investigation carried out by IPHAS concerns the interaction with the interstellar medium (ISM). We observed several examples of interaction which were compared with hydrodynamical models. The interactions are classified into four stages according to the degree of disruption of the nebula, and we were able to identify objects at each stage i.e. from the undisturbed to the totally disrupted morphology.

The second part of the thesis is dedicated to the discovery and the study of magnetic fields in planetary nebulae and the role that they can play in their shaping. This point

was already mentioned while studying the ISM interaction for the IPHAS nebulae and how magnetic fields could disrupt the PNe. The observation of 4 bipolar PNe and Proto-PNe (NGC 7027, NGC 6537, NGC 6302 and CRL2688) in the sub-mm regime with SCUBA, has indicated the occurrence of toroidal magnetic fields in all the objects via dust grain alignment. The toroidal fields could account for the bipolar morphology observed but the lack of information concerning the strength of the field prevents us from jumping to such a conclusion. We also investigated the possible relation between magnetic fields and, first the chemistry of the selected targets: we showed two oxygen-rich and two carbon-rich nebulae (and we observed two different fields' organisation), and then their evolutionary stage: we showed nebulae from the Proto-PN to the PN stage (and we identified long-lived fields). Finally we discussed the methods that would allow us to derive the strength, as well as all those helping to define how magnetic fields act in planetary nebulae.

Declaration

I declare that no portion of the work referred to in the thesis has been submitted in support of an application for another degree or qualification of this or any other university or other institute of learning.

Copyright Statement

(i) Copyright in text of this thesis rests with the Author. Copies (by any process) either in full, or of extracts, may be made only in accordance with instructions given by the Author and lodged in the John Rylands University Library of Manchester. Details may be obtained from the Librarian. This page must form part of any such copies made. Further copies (by any process) of copies made in accordance with such instructions may not be made without the permission (in writing) of the Author.

(ii) The ownership of any intellectual property rights which may be described in this thesis is vested in The University of Manchester, subject to any prior agreement to the contrary, and may not be made available for use by third parties without the written permission of the University, which will prescribe the terms and conditions of any such agreement.

(iii) Further information on the conditions under which disclosures and exploitation may take place is available from the Head of School of Physics and Astronomy.

"All truths are easy to understand once they are discovered;

the point is to discover them."

Galileo Galilei

"Pli ou chiré, pli chien ralé'w alò sé fos épi courage ki rété !!!"

Creole saying

Dedication

To my parents

Acknowledgements

First I would like to thank my parents for their support during those 4 years. Then, my supervisor Albert Zijlstra with whom I've learnt a lot on the physics of late type stars and nebulae. I do not forget Romano Corradi and Antonio Mampaso who taught me about observational and instrumental procedures and analysis when I was in the Canary Islands. Above the PhD student-Supervisor link, I think that we all developed a quite good friendship !

I'd also like to mention the people who were there in good and bad times and/or with whom I've worked : Stecy (my "Caribbean friend" who will definitely agree with the Creole quote), Eric, Kerttu, Robert, Karen and Manuela (for the long hours of interesting discussions and long laughs too), Brent, Quentin , Nick, Mikako, Elisabeth, Yin, and the last but not the least, Claire.

Jonathan Irwin, David Frew, Chris Wareing, Stuart Sale, and Peter Van Hoof have been of great help at different stages of this work.

Finally, I'd like to thank Chris Rock and Dave Chapelle who make life better to live!

This thesis was typeset with LaTeX.

The Author

Has completed her degrees up to the Master in Physics, in the French Overseas Regions (Guyane, Martinique and Guadeloupe). After one year at the University of Nice (France) to complete the Master in Astronomy and Astrophysics, she started her thesis with Albert Zijlstra at The University of Manchester (UMIST). Due to the observational nature of the thesis, the latter was conducted abroad during 2 years: one in the islands of La Palma (Canary Islands, Spain), where she was a support astronomer on the Isaac Newton Telescope, and one in Tenerife (Canary Islands, Spain), where she obtained a Marie Curie Fellowship to work on the IPHAS project.

Supporting Publications

Publication in refereed journals

1. *Magnetic fields in planetary nebulae and post-AGB nebulae*"
   Sabin L.; Zijlstra, Albert A.; Greaves, J. S., MNRAS,Vol.376, 378-386, 2007

2. *Initial Data Release from the INT Photometric H-alpha Survey of the Northern Galactic Plane (IPHAS)*
   Gonzalez-Solares, E. A.; Walton, N. A.; Greimel, R.; Drew, J. E.; Irwin, M. J.; Sale, S. E.; Andrews, K.; Aungwerojwit, A.; Barlow, M. J.; van den Besselaar, E.; and 40 coauthors (among: Sabin L.), submitted to MNRAS, arXiv:0712.0384, 2007

3. *IPHAS and the symbiotic stars. I. Selection method and first discoveries*
   Corradi, R. L. M.; Rodrguez-Flores, E. R.; Mampaso, A.; Greimel, R.; Viironen, K.; Drew, J. E.; Lennon, D. J.; Mikolajewska, J.; Sabin L.; Sokoloski, J. L, Accepted for publication on Astronomy and Astrophysics, arXiv:0712.2391, 2007

Conference publication

1. *New Planetary Nebulae found by the IPHAS Survey*
   Viironen, K.; Sabin L.; Rodrguez-Flores, E. R.; Mampaso, A.; Corradi, R. L. M.; Greimel, R. , Planetary Nebulae in our Galaxy and Beyond, Proceedings of the International Astronomical Union, Symposium 234. Edited by Michael J. Barlow and Roberto H. Mndez. Cambridge: Cambridge University Press, 2006., pp.533-534

2. *IPHAS discovers hundreds of new planetary nebulae on the galactic plane.* Mampaso, A., Corradi, R.L.M.; Viironen, K., Sabin, L., Drew, J.E., Greimel, R. and the IPHAS Collaboration. , JENAM 2007, To be published in EAS.

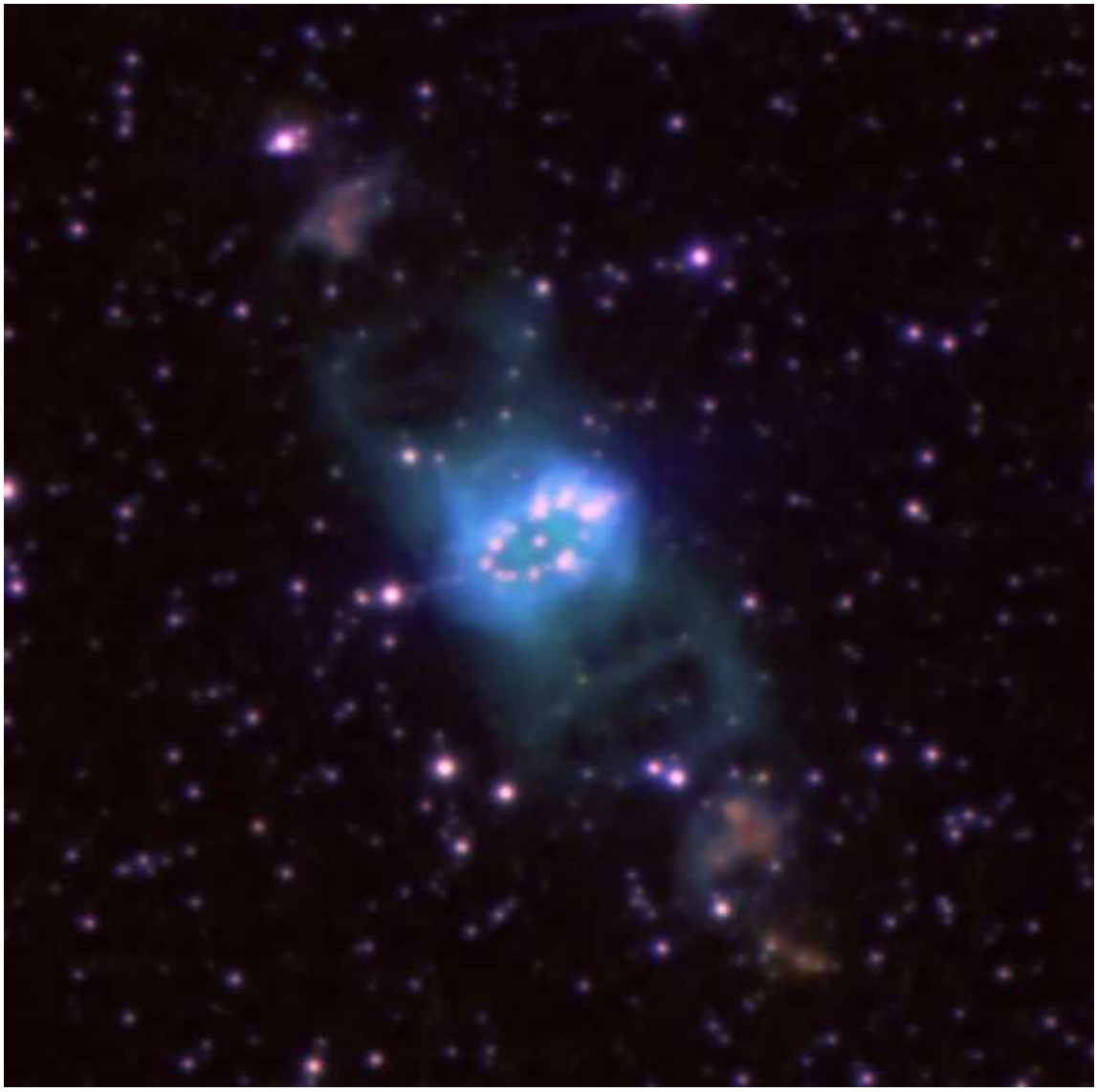

Figure 1: The Necklace nebula: a new Planetary Nebula discovered within IPHAS.

1

Introduction: The Planetary Nebulae

First discovered by Charles Messier in 1764, Planetary Nebulae (PNe) are the end products of the evolution of low and intermediate mass stars. To understand how these shells of ionised dust and gas have been expelled from their associated stars, I will briefly trace the evolution process from the main sequence.

Stars with masses high enough to ignite helium on the Red Giant Branch (RGB) i.e. between roughly 0.8 and 8 $M_\odot$, will conduct helium burning in their core until exhaustion. Subsequently, the stars will develop a core composed of carbon and oxygen. This is the Asymptotic Giant Branch (AGB) stage. The C/O core is surrounded by a nuclear burning shell where alternatively helium and hydrogen are burning. The stars with sufficient masses will undergo so-called thermal pulses, more commonly called He-shell flashes. The convective envelope surrounding the shell is also subject to periodic pulsations. The latter induce an outer envelope (the atmosphere) allowing, via radiation pressure, an important loss of matter led by slow winds (from 10^{-7} $M_\odot$ yr^{-1} to 10^{-4} $M_\odot$ yr^{-1}). This process occurs until the envelope reaches a mass limit of ~0.02 M⊙ and the core starts to be exposed (with an increase in temperature). There follows a short phase, the **Post-AGB** or Proto Planetary Nebulae (PPN) stage , where the temperature is not hot enough to totally ionise the gas (3000 K < T < 25000 K). With time the star contracts further and the temperature increases in such a way that the surrounding matter is fully ionised (from ~30 000 K) and forms a detached and expanding ionised

shell: the **Planetary Nebula**.
The central star of the PNe will finally start to decrease in luminosity and will be unable to ionise the surrounding gas (as the number of photons decrease). The end product is a C/O white dwarf (WD) with a recombination of the ejecta (Fig.1.1).

The PNe, which are short lived objects, from normally 10 000 to 20 000 yrs, are fundamental to our study: they strongly contribute to the enrichment of the interstellar medium in C,O ,N ,metals and other products of nucleosynthesis, but they also allow us to better understand the physical processes occurring in those stars during their final stage of stellar evolution.
The two components of planetary nebulae, namely the envelope and the central star (CS), have been extensively studied and each reveals more about the conditions reached in evolved stars.
The envelope or nebula expands relatively slowly, on average 25 km/s (Robinson et al. (1982), Weinberger (1989)). Any variation (increase) of this velocity as a function of the age of the PN has not been proved yet. The PN shell is composed of dust which will enrich the interstellar medium (ISM). The presence and amount of nebular material is linked to the physical processes taking place in the nebulae, like photoionisation (absorption of UV photons and release of electrons) which is a heating process and recombination (electronic capture) and collisional excitation which are cooling processes[1]. The two main physical parameters involved in the nebular shells are density and temperature, which are derived from the numerous emission lines observed in the PNe. The distribution range in densities varies from roughly 10^4 cm^{-3} (for young, bright and/or compact PNe) to less than 100 cm^{-3} (for large, faint and/or old PN, Osterbrock (1974), Zhang et al. (2004)). This lower limit even reaches 1 cm^{-3} according to Peimbert (1990). In the same way, the electronic temperatures vary from 25 000 K to 3000 K. The nebular studies also include the understanding of more parameters: the

[1]In the case of collisional excitation, the cooling is due to the weak collisions between particules in PNe. This leads to a small energy difference from the ground state.

size reached by the shell and the morphology, as well as the abundances, are among the items which will characterise a planetary nebula (see next section).

The central stars of PNe are not often discernible because of their faintness and the presence of the nebular shell. However, more and more CS-PNe are now studied thanks to the improvement of instruments, the use of models and the extension of the observations to other ranges than the visible (Gesicki and Zijlstra (2007), Rauch et al. (2007)). Temperature is one of the most important criteria and for the same reasons which prevent the observation of the CS, it is quite difficult to measure. The most popular method is the Zanstra method which relies on nebular parameters. This assumes that all the Lyman continuum photons absorbed correspond in number to the recombinations at all levels except the ground level [2]. But this method depends on the thickness of the shell and the magnitude of the stars and both are subject to large variations in their determination. The temperatures observed in CS-PNe range from ~30 000 K to ~100 000 K. These high values have led to the extension of observations to ranges other than the visible, i.e.at UV and X-ray wavelengths (Kastner (2007), Guerrero (2006)). CS-PNe are generally classified according their spectral properties, which depends on the quantity of hydrogen in the atmosphere (namely H-rich and H-poor). H-poor stars have spectra which are close to the Wolf-Rayet (WR) spectral type (in emission), and are either WC or WN depending on the concentration of C over N. H-rich CS-PNe show, as indicated by their name, a large number of H lines but also He lines. In terms of occurrence rate, we found more WC than WN CS-PNe. This is related to their respective progenitors and their masses, which allow to bring to the surface the different elements (C,N). Hence WC stars have more or less rare carbon stars as progenitors and WN stars have as progenitors even rarer massive AGB stars undergoing Hot Bottom Burning. The winds from the CS have also been investigated. These are due to the reinitiation of the mass loss process (because of radiation pressure on resonance lines) and are characterised by their high velocity. The encounter with the slow AGB wind,

[2] A detailed calculation for the obtention of the Zanstra temperatures is given by Pottasch (1984) pp 168-172

expelled beforehand, is part of a theory for the formation of planetary nebulae (Interacting Stellar Winds model by Kwok et al. (1978a)). Finally, efforts have been made to detect binary central stars using radial velocities, photometric fluctuation, spectroscopy or simple imaging (Iben and Tutukov (1989), De Marco (2006), Zijlstra (2007)). The goals of such research are mainly to increase our understanding of mass transfer processes (common envelope) (De Marco and Moe 2005) and the possible implications for nebulae morphology (Soker 1998).

Although short, the PN phase involves rather complex and intriguing physical processes which are far from being fully understood. Nevertheless, past surveys have helped us to have a better comprehension of this evolutionary phase.

1.1 The extent of our knowledge about galactic PNe and its limitations

So far, around 2000 true and candidate PNe are known in the Galaxy (Table 1.1). They are mainly listed in the Perek and Kohoutek catalogue (Perek and Kohoutek 1967), the Strasbourg-ESO Catalogue (Acker et al. 1992) and its 1st supplement (Acker et al. 1996) and the recent Macquarie-AAO-Strasbourg Hα Planetary Nebula Catalogue: MASH (data obtained from the AAO/UKST survey: Parker et al. (2006a).

1.1.1 General distribution and size

With the detected objects we can study the distribution of planetary nebulae in the Galaxy. Figures 1.2 and 1.3 show that the majority of the sources are concentrated towards the galactic centre, more precisely in a latitude range $-10° < b < +10°$. Pottasch (1984) found that in addition to the general trend observed (more nebulae towards the galactic centre), the majority of PNe located between l=± 10 deg have a diameter smaller than 20 arcsec. The ones with a diameter greater than 20 arcsec are quasi

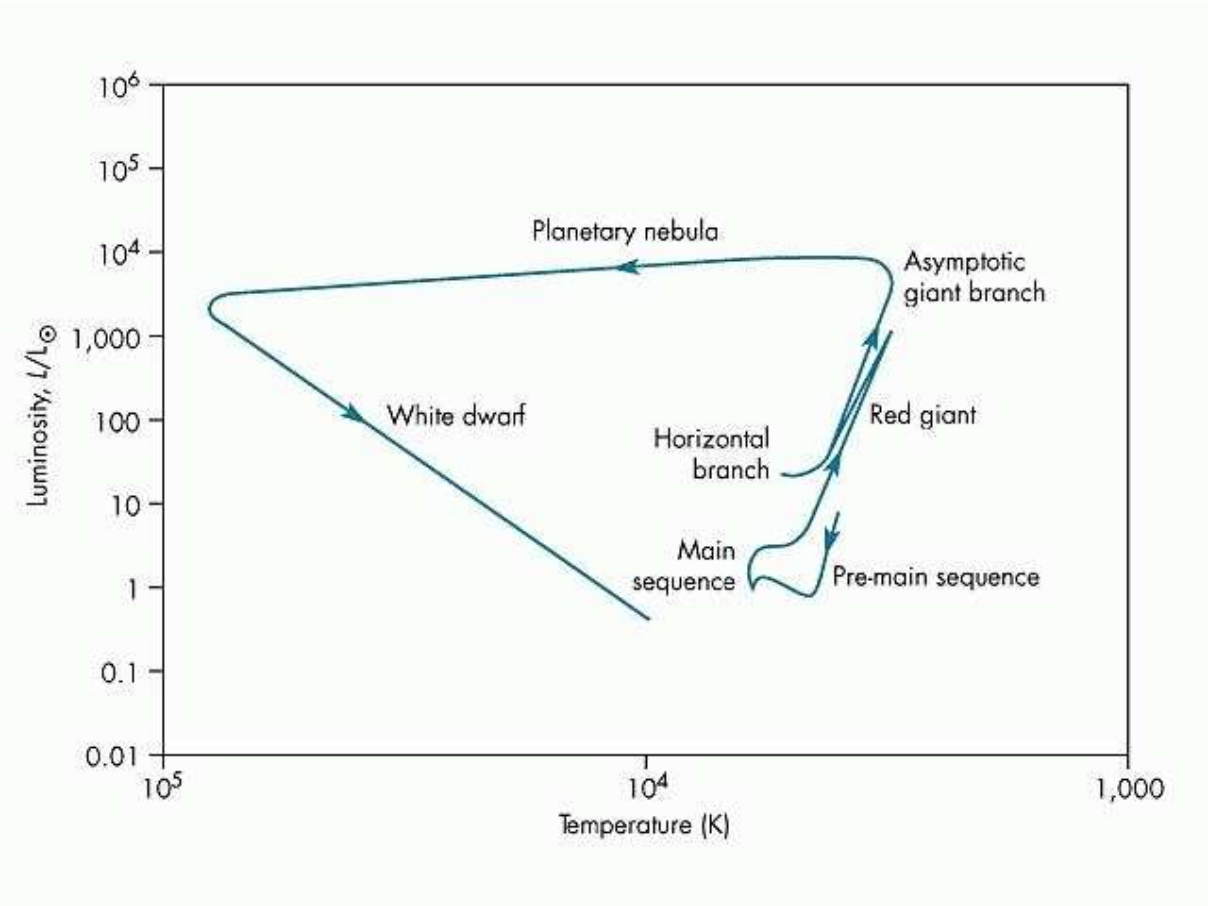

Figure 1.1: HR diagram showing the evolution of an intermediate mass star from the main sequence to the white dwarf stage. We point out that stars with masses greater than ~1.5-2 M⊙ do not go through the Horizontal Branch phase. Their cores are not fully electron-degenerate and do not experience a full ignition following a helium flash.

absent from the galactic centre. The anticentre (from 90° to 270°) in all cases is less populated.

1.1.2 Morphology

The most obvious point concerning PNe, and which made them famous, is their peculiar and extraordinary morphology. The Hubble Space Telescope obtained really interesting and good pictures, showing the different aspects of some PNe. While some

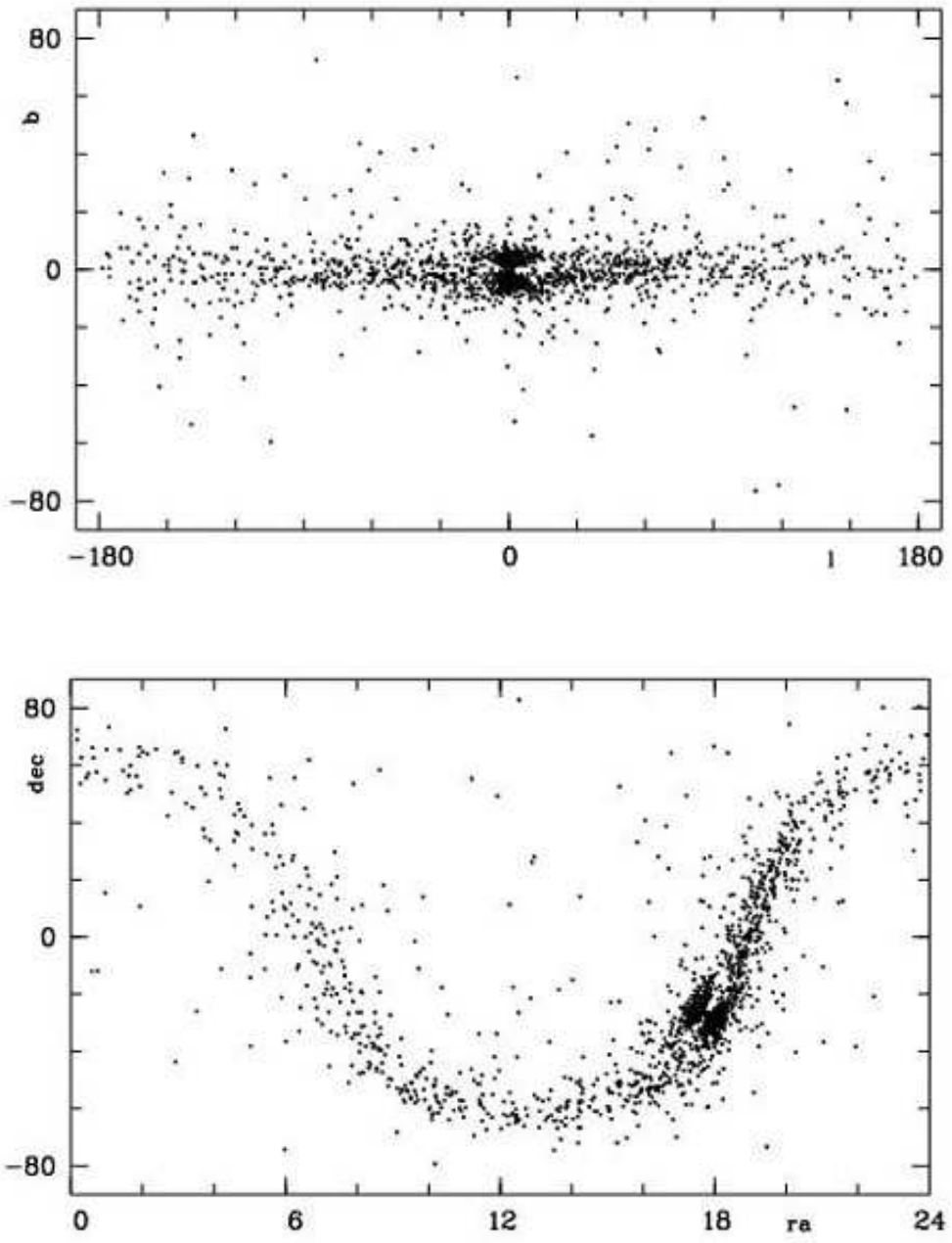

Figure 1.2: Distribution of galactic planetary nebulae according Kohoutek (2001) in galactic coordinates (top panel) and equatorial coordinates (bottom panel).

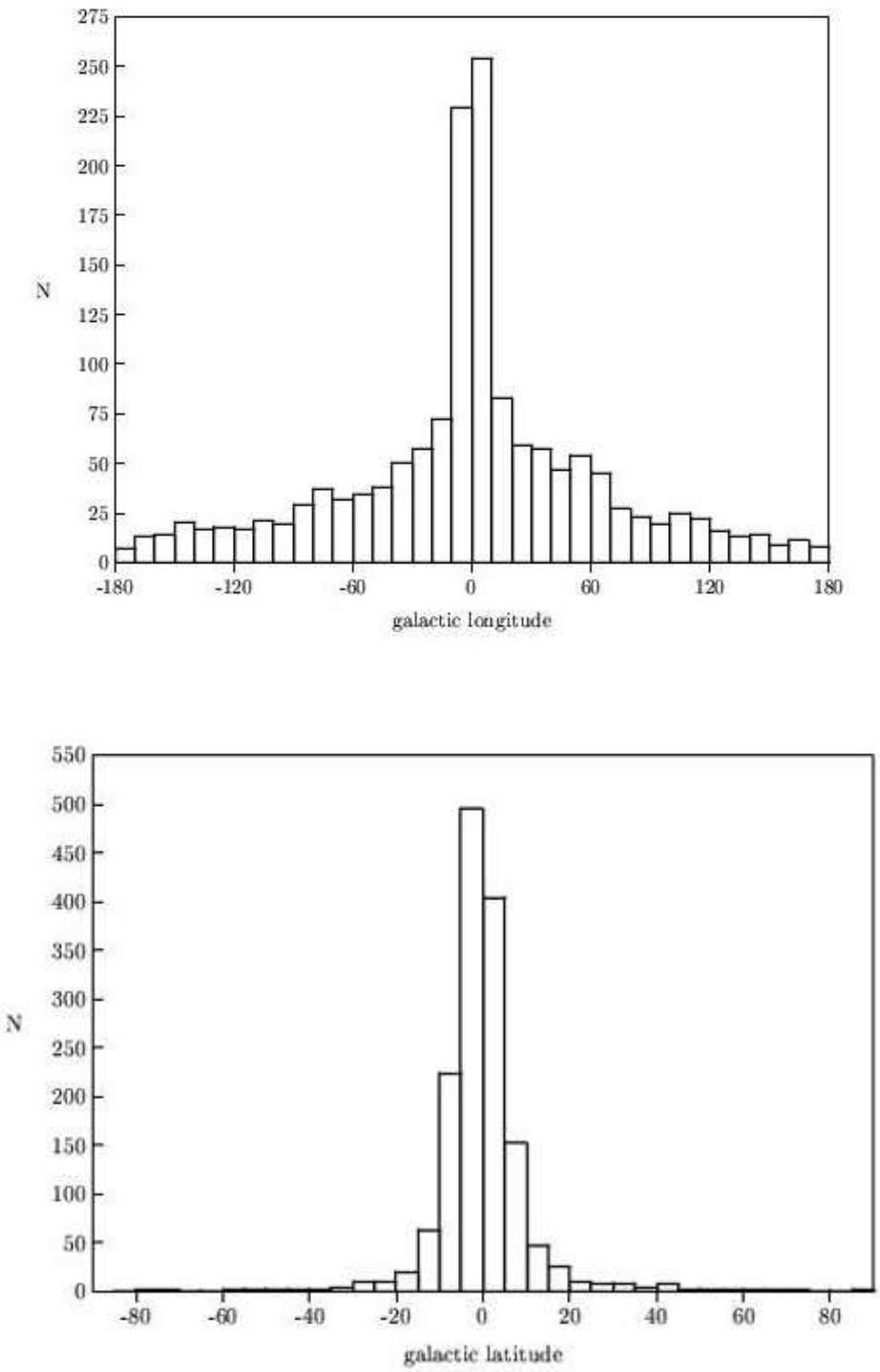

Figure 1.3: Distribution of Galactic Planetary nebulae from Kohoutek (2001) according the galactic longitude (top panel) and the galactic latitude (bottom panel).

Table 1.1: Summary of the number of PNe known in the Galaxy by Parker et al. (2006b). The asterisk refers to "possible" PNe.

Investigator	Epoch	Number of PNe
Messier, Darquier, Mechain	1764-1782	4
William Herschel	~ 1800	20
Curtis	1918	78
Vorontsov-Velyaminov, Parenago	1931	121
Vorontsov-Velyaminov	1948	288
Minkowski	1950	371
Perek, Kohoutek; CGPN	1967	1036
Kohoutek supplements	1978-2000	721
Acker et al.;SECGPN	1992	1143+347*
Acker et al.;SECGPN (supplements)	1996	243+142*
Kohoutek; CGPN updated	2001	1510
Parker et al.; MASH	2003,2006	756+146*

demonstrate a spherical symmetry (which is what one would expect from a spherical MS star, RGB star and AGB star), a good number of them appear aspherical or show an asymmetry: they are bipolar, elliptical, quadrupolar or point symmetric. The eclectic variety of shapes has been classified by different authors like Balick (1987), Balick and Frank (2002), Corradi and Schwarz (1995), Stanghellini et al. (1993) and Manchado et al. (1996), Manchado et al. (2000). Most of these studies came to similar conclusions about the number of PNe, their morphology and their location in the galaxy:

- The number of elliptical and round PNe is higher than the number of bipolar PNe (included bipolar with point symmetry and quadrupolar).
- The morphology of PNe is related to the mean galactic scale height <z>. Bipolar PNe have a lower mean scale height, so are closer to the galactic plane than the

Table 1.2: Results from the IAC catalogue of Manchado et al. (2000) and the survey from Corradi and Schwarz (1995). The progenitors mass estimations come from Phillips (2001) and are related to the morphological class in general.

Survey	Morphology	Number %	<z> in pc
Manchado (2000)	Bipolar	13	139
	Elliptical	60	308
	Round	26	753
Corradi & Schwarz (1995)	Bipolar	14	130
	Elliptical + Round	64	325
	Irregular	18	181
	Point symmetry	4	-
	Stellar	22*	-

* In Corradi & Schwarz (1995) the class other than stellar concerns the extended PNe.

elliptical PNe. The latter are located closer to the galactic plane than the round PNe (see Table 1.2).

- Miller and Scalo (1979) found a correlation between the mass of a stellar population and its scale height in the Galaxy (more precisely in the solar neighbourhood). They derived for <z>=110 pc: M > 1.9 $M_\odot$, for <z>=150 pc: M > 1.5 $M_\odot$, for <z>=230 pc: M > 1.2 $M_\odot$ and for <z>=300 pc: M < 1 $M_\odot$. The progenitor masses derived later by Phillips (2001a) differ from the ones of Miller & Scalo. In comparison to these scale heights, bipolar PNe have a progenitor mass (PM)> 2.3 $M_\odot$, elliptical PNe have 1.2 $M_\odot$ > PM > 2.3 $M_\odot$ and round PNe have 1 > PM > 1.2 $M_\odot$. In conclusion, bipolar PNe have higher mass progenitors (which evolve more rapidly) than elliptical PNe and round PNe (Table 1.2)

More recently Sahai et al. (2007) undertook a survey of candidate preplanetary nebulae (PPNs) using the HST and also derived a new morphological classification system.

1.1.3 Chemical abundances

The abundance of planetary nebulae are good tools to trace the enrichment of the interstellar medium, and to trace back the history of their progenitors. During the long phase from the main sequence to the PN stage, the different events of convection and dredge-ups will bring to the surface the products of the triple-α process (^{12}C and ^{16}O). Depending on the initial mass, ^{4}He and ^{14}N can become overabundant. He-flashes and dredge-ups will bring the He, C and s-process elements to the surface increasing the C/O ratio. During the first dredge-up in the RGB phase, we observed a mix of matter in the convective envelope going from the hydrogen burning shell in fusion to the stellar surface. Chemical studies can constrain stellar evolution models (Charbonnel 2005) and the nucleosynthesis processes (Palmerini and Busso 2007). The PNe have therefore been investigated from the "chemical" point of view by several authors: Aller and Czyzak (1983), Koeppen et al. (1991) and Perinotto (1991) amongst others for the galactic disk; and Ratag (1991) for example for the galactic bulge. The most popular study still remains the one of Peimbert (1978), Peimbert and Torres-Peimbert (1983). Peimbert (1978) computed the abundance of H, He, C, N, O and Ne in galactic planetary nebulae and found that they could be split into 4 types as summarised in Table 1.3. To measure abundances, the line strengths of the objects measured from spectroscopy are used to determine the temperature (with the [OIII] lines for example) and electron density (with the [SII] lines for example). The abundances of the different species are calculated relative to H and are obtained from models using recombination or collisional excitation and which solve statistical equilibrium equations. The total abundance of an element is only obtained if lines are available for all its ionisation stages, which may require UV and IR observations. This is not always available and to obtain a good value, one should apply an ionisation correction factor.

In addition to these chemical criteria, it has been observed by Peimbert (1978) that:

- Type I: The PNe are extremely filamentary. They are He and N rich due to the occurrence of a second and even third dredge up, implying progenitor masses

larger than ~3 M⊙.

- Type II: These PNe belong to the intermediate disk population and are older than the Type I PNe. The Type II PNe are C-rich because they have gone through the third dredge-up and carbon star phase on the AGB but they have not experienced hot bottom burning. This implies masses between ~1 M⊙ and ~3 M⊙ for the progenitors.

- Type III: The PNe have a high velocity, and typically concern objects with $|\Delta v|>$ 60 km s^{-1} but are not part of the Halo population.

- Type IV: The PNe belong to the Halo population and have indeed a slight He deficiency. This deficiency as well as that of O and N is due to the low mass of the progenitors, less than ~1 M⊙, and then the inability to processes these elements.

A recent statistical review by Quireza et al. (2007) has re-analysed the classification of 476 planetary nebulae with known abundances according to the Peimbert Types.

Table 1.3: Chemical abundances in Planetary Nebulae and the Sun by Peimbert (1978). The "N(X)/N(H)" notation shows the abundance of the element X at all stage of ionization, with respect to hydrogen. The "Log N(X)" notation corresponds to 12+log(N(X)/N(H)).

	Type I He-N Rich	Type II Intermediate pop.	Type III High Velocity	Type IV Halo pop.	Sun
N(He)/N(H)	0.16	0.11	0.11	0.10	...
log N(C)	...	9.5	...	...	8.5
log N(O)	8.8	8.9	8.8	7.7	8.7
log N(N)	9.0	8.3	8.2	7.4	7.9
log N(Ne)	8.2	8.3	8.2	7.0	7.9

Their new classification is given in Table 1.4.

Table 1.4: Planetary Nebulae Types reviewed by Quireza et al. (2007).

Interval	Type
He/H > 0.147	I
log N/O > -0.005	I
-0.513 < log N/O < -0.324	IIa
0.95 < |z| < 1.60 kpc	III
|z| > 1.99 kpc	IV
66 < |Δv| < 101 km s^{-1}	III
|Δv| > 121 km s^{-1}	IV

Finally, several studies have attempted to find a correlation between the PNe morphology and their abundances (nebula and central star) (Peimbert and Torres-Peimbert (1983), Gorny et al. (1997), Stanghellini et al. (2002), Phillips (2003)). This is of particular interest as we could then derive information on the PN progenitor and better understand their morphologies and maybe their origin. Peimbert and Torres-Peimbert (1983) found that most of the type I PNe are bipolar. Quireza et al. (2007) confirmed this behaviour and noticed that elliptical PNe mainly belong to the types II and III; and the round PNe mainly belong to the type IV. The latter group of PNe may show a different type as Soker and Subag (2005) suggested that only a small percentage of those have been discovered so far.

1.2 The unsolved problems in PN study

Although enormous progress has been made over the years in terms of observations (using high resolution spectroscopy (Lee et al. 2007b), integral field spectroscopy (Tsamis et al. 2008), interferometry (Lykou et al. 2007), CCD cameras ...etc) and modelling (with photoionization codes for example, Morisset et al. (2005)), our knowledge

of planetary nebulae is far from complete. Only a fraction of Galactic PNe are known, for various reasons.

1.2.1 The detection problem

- Some PNe are hidden by the interstellar medium. As most of the PNe have a low height on the galactic plane, their detection is complicated by the interstellar extinction. Moreover, as the scale height is linked to the morphology, as we saw earlier, then we also have a bias on this parameter.
- Old PNe have a very low surface brightness.
- Some PNe are located in less explored regions, such as the Galactic Anticenter region.
- Very distant PNe maybe be unresolved, and not distinguishable as nebulae.
- They are hidden in crowded areas, such as in the galactic plane.

As an illustration, fewer than 200 PNe are known as PNe with ISM interaction, which is the last step before the complete dilution of the nebulae in the interstellar medium. These objects have a low surface brightness and only the interacting rim is well seen (Wareing et al. 2007) (see later in this thesis). Phillips (2001b) and Soker and Subag (2005) both discuss the missing populations of respectively bipolar and round PNe.

Zijlstra and Pottasch (1991) gave an estimation of the total number of planetary nebulae in the galactic disk of $\sim$ 23 000 $\pm$ 6 000. Shklovsky (1956) found a number of $6x10^4$ PNe in the entire Galaxy. In any case, this is far from what we actually see.

1.2.2 The derivation of the physical properties

The bias mentioned above is also reflected in the derivation of the most elemental parameters e.g. the size, the distance distribution (which will be discussed in more in detail in chapter 6) and the radial velocity. Other physical parameters like the luminosity function and the abundances are generally based on nearby (young) and very bright PNe. This is understandable with regard to abundances as these PNe will give a higher number of emission lines, strong enough to derive the exact chemistry. Unfortunately this does not take into account the whole PN diversity.

1.2.3 The Morphology: determination and origin

The morphology of a planetary nebula is not always easy to determine (nor its exact size). It will depend not only on the exposure depth but also on the wavelength used. It will also depend on human subjectivity.

Short exposure times will only bring out the very bright structures in the PN which can be the central star, knots or jets. The halo, for example, which is generally fainter would require much deeper exposures. If a PN is nitrogen rich for example, most of its morphology will be seen at the [NII] wavelength. But using other wavelengths, like Hα or molecular lines, other contours like the halo or any recombined structure, can be revealed. Thus depending on the structures which are meant to be observed, the choice of the wavelength (or filter) is important.

A “hot topic” in the PN field is the question of the origin of the aspherical symmetry observed in many objects. So far four processes are considered as responsible for it:

- A “wind-wind” interaction between a slow asymptotic giant branch (AGB) wind and a faster post-AGB wind ((Kwok et al. 1978b), (Reimers et al. 2000)).
- A binary interaction ((Bond and Murdin 2000), (Ciardullo et al. 2005)).
- The action of magnetic fields ((Blackman et al. 2001), (Sabin et al. 2007)).

- An ISM interaction which would shape the outer part of the PN (Wareing et al. 2007).

Each of them has its strong and weak points. We will return in more detail to this problem in the last part of this thesis.

An unbiased and general study of planetary nebulae relies on an extended detection effort, going deeper in terms of sensitivity. The INT Photometric Hα Survey combines both coverage and depth, and is the tool that we are going to use to unveil and study the "missing PN population". This thesis is organised in three parts. The first one describes the IPHAS survey (Chapter 2) and the classification/identification of candidates PNe discovered (Chapter 3). The second part is dedicated to the analysis of the results obtained in the first part. Then follows an investigation of the distribution of the IPHAS nebulae (Chapter 4), their infrared properties (Chapter 5), their distance estimation (Chapter 6), their recombination and age (Chapter 7) and finally their interaction with the interstellar medium (Chapter 8). The third part of this thesis deals with the analysis of magnetic fields in planetary nebulae in order to answer the question regarding the origin of their morphology. The fields detection via dust polarisation for a set of PNe is discussed in Chapter 9 and other types of magnetic field detections are discussed in Chapter 10. The final chapter describes our conclusions and perspectives.

Part I

Discoveries of planetary nebulae in the framework of the IPHAS survey of the Galactic Plane

2

The contribution of the IPHAS survey: observation and classification of stellar populations

2.1 The Hα emission line

Hα emission is well known for being a good tracer of star formation activity through large HII regions. It allows us to trace the large scale outflows in HII regions, supernovae and stellar winds, as well as the identification of details (like filaments, rings and knots) in their morphology as they evolve in the interstellar medium (ISM). Hα emission is also used to measure star formation rates in external galaxies (Kennicutt 1992). Moreover the Universe is more transparent to Balmer lines than Lyman lines and even if Lyman lines are intrinsically brighter, Balmer lines are often more useful (Lyman lines are observable in the UV regime and are absorbed by dust, which is less the case for the Balmer lines).

The Hα emission outlines ionised nebulae and is commonly associated with stars and stellar systems in short lived phases of evolution that remain relatively poorly understood. This is particularly the case for the PNe, a phase which lasts around 10^4 years.

We can add to this group pre and post main sequence stars, massive stars and interacting binary stars. These stars and nebulae are quite numerous in the Galaxy and are generally linked to objects located at both ends of the stellar evolution (see an example of nebula in Fig 2.1):

- Young stars: T Tauri, Herbig-Haro objects, HII regions.
- Evolved stars: Post-AGB, Planetary Nebulae (PNe), Wolf-Rayet, LBV, Supergiants, massive Be, Supernovae, symbiotic nebulae.

The importance of the hydrogen line as a tracer has encouraged people to conduct Hα imaging "surveys" since the 50's. We can cite Sharpless (1953) and Sharpless (1959b), Gum (1955), Johnson (1955) and Johnson (1956), Rodgers et al. (1960), Georgelin and Georgelin (1970) and Sivan (1974). But their surveys were generally targeted and the fainter objects were not detected. Thus, the photographic survey from Georgelin and Georgelin (1970) was undertaken with 1 arcmin resolution for 44 areas located between $|b|=\pm 10$ deg and 250 deg $< l <$ 360 deg. Although the authors do not give information on the brightness of the objects and the depth of the survey, they state that the faintest objects were not detected. In order to have a wider view of the Galaxy in Hα, a more complete type of survey is therefore necessary.

2.2 Introduction to the survey

IPHAS is the acronym for Isaac Newton Telescope (INT) Photometric Hα Survey. This new fully photometric CCD survey of the Northern Galactic Plane started in 2003 under the supervision of Dr. Janet Drew (P.I., UCL) (Drew et al. (2005), Gonzalez-Solares et al. (2007)). IPHAS targets the Galactic plane in the Northern hemisphere, with a latitude range of $-5^\circ < b < 5^\circ$ and covers 1800 deg^2. The restriction on the latitude range comes from the total amount of telescope time necessary to complete the survey (22 weeks) and also from the amount of new detections that would be discovered: most of the stellar population is located in the chosen boundaries.

Figure 2.1: The Barnard's loop is an example of emission nebula which is part of the Orion nebula, a large HII region. It is therefore well mapped in Hα. The Barnard's loop is also thought to originate from a supernova explosion.

All the IPHAS data have been obtained from the Isaac Newton Telescope (INT) (La Palma, Canary Islands, SPAIN) (Fig 2.3) equipped with a 2.5 m primary mirror, using the Wide Field Camera (WFC) and offering a field of view of 34.2 arcmin thanks to its L-shaped 4 EEV 2kx4k CCDs[1]. This long-term international survey, which aims to identify new Hα emission sources, is made by comparing broad band R and I images with matched Hα-filter data to look for Hα excess (Fig 2.2). As just mentioned, in addition to the narrow-band Hα filter (95Å FWHM), IPHAS is also conducted with a continuum filter in the same part of the spectrum as Hα, and a second continuum filter to enable the determination of the continuum colours of stellar sources. The continuum filters are respectively the Sloan r' and i', chosen because of their box-like pass-bands (see Fig. 2.4). The broad r' filter, with a central wavelength of 6240Å, encompasses Hα, while the second continuum filter is chosen to be i' because it can be used in bright time too. After appropriate background subtraction to obtain the Hα magnitudes, can-

[1]For more details on the telescope and instrument see http://www.ing.iac.es/Astronomy/telescopes/int/

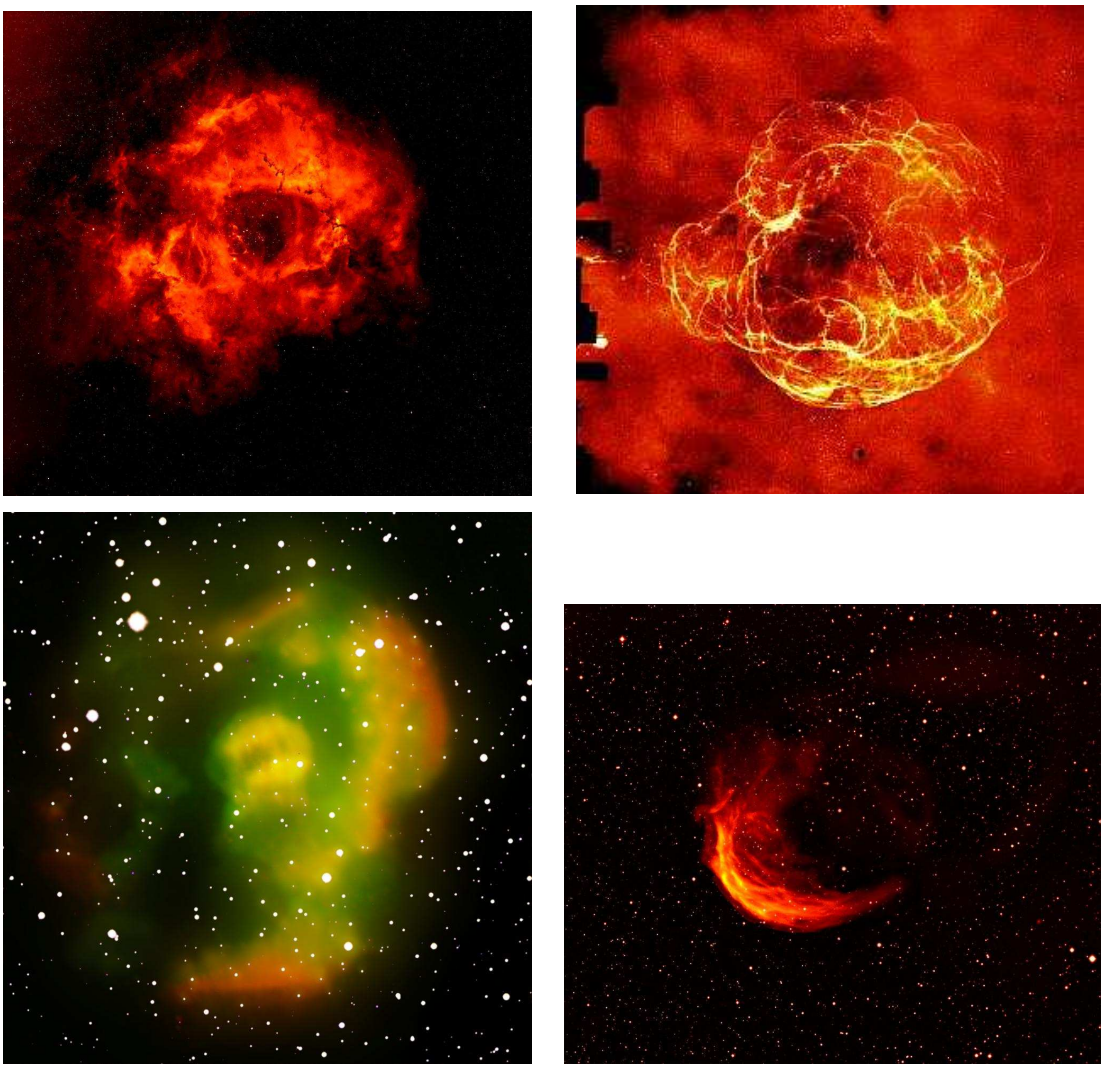

Figure 2.2: Top-Left: IPHAS Hα image of the Rosette Nebula. Top-right: A 5°×3.5° mosaic of the supernova remnant S147 in Hα. Bottom-Left: Two-colour image of a new ~6 arcminutes long Planetary Nebula, red for H-alpha and green for [OIII]. Bottom-Right: Sh 2-188, a wind blown planetary nebula in Cassiopeia. Images based on data obtained as part of the INT Photometric H-Alpha Survey of the Northern Galactic Plane, obtained and/or prepared by Nick Wright (University College London), Jonathan Irwin (Cambridge University), Albert Zijlstra (University of Manchester) and Laurence Sabin (University of Manchester), on behalf of the IPHAS Collaboration.

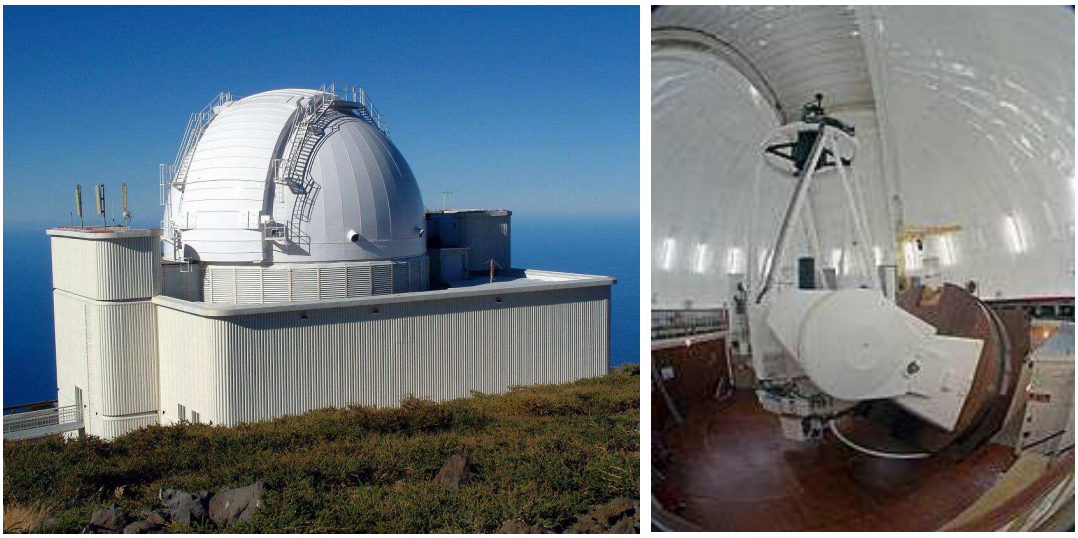

Figure 2.3: The Isaac Newton Telescope in La Palma.

didate point-sources Hα emitters are identified by means of their (r'-Hα) excess in plots of (r'-Hα) vs. (r'-i'). Spatially resolved Hα emission will be directly discernible in the Hα filter images.

IPHAS has been carried out as a complement and, in certain respects, as an enhancement, to the recent photographic Hα survey of the Southern Galactic Plane using the AAO UK Schmidt Telescope (SHS, see below). The photographic survey had some calibration problems, such as the non-linearity in regions of bright background nebulosity, which complicated a reliable extraction and identification of likely Hα point sources. The use of the INT/WFC for our survey sidestepped this difficulty. Another desirable feature of the WFC is its small pixel scale (0.33 arcsec pix^{-1}). The other advantage of IPHAS is the depth reached. All point sources with a r' magnitude between 13 and 19.5-20 could be detected, as well as extended emission with an Hα surface brightness down to 2×10^{-17} erg cm^{-2} s^{-1} arcsec^{-2}.

For the observations, the Galactic Plane was divided into 7635 fields each showing the roughly 0.3 deg^2 area allowed by the WFC. The observation process was fully au-

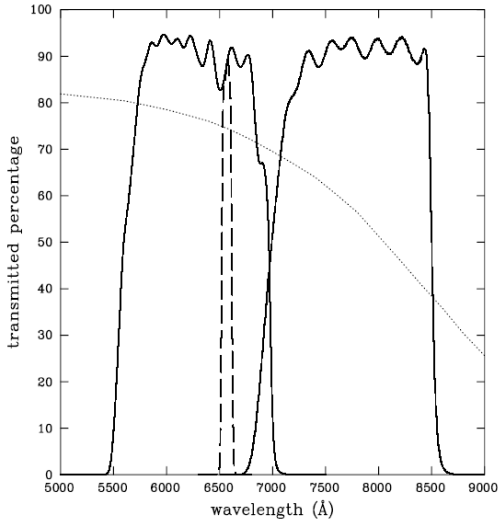

Figure 2.4: Transmission profiles of the Hα (dashed line), Sloan r' and i' (solid lines) used in IPHAS. The dotted line shows the mean WFC CCD response at the cooled working temperature.

tomatic and each field was observed with a 120s exposure in Hα (central wavelength at 6568 Å), 30s in r' (central wavelength at 6240 Å) and 10s in i' (central wavelength at 7743 Å). This operation was repeated with a telescope offset of 5 arcmin West and 5 arcmin South. This second pointing ensured the CCD borders, the CCD gaps and any other perturbing elements did not affect the data quality. Moreover a field was reobserved if it did not satisfy the quality requirements that had been fixed, for the seeing, the average stellar ellipticity, the sky brightness and sky noise. Concerning the seeing, the mean value during the observations was approximately 1.26 arcsec but to deal with bad weather conditions the limit was set at 2 arcsec in the three filters. The ellipticity should be lower than 0.2. The r' band sky count should be lower than 2000 ADU's, hence the observations had to be done without the presence of clouds and at a distance from the moon greater than 30 degrees (IPHAS has been designed as a flexible programme and the runs operate during bright and grey nights) and if possible at an airmass lower than 1.4. The most difficult area, to ensure good quality data, is the

right ascension range ~5h to ~7h corresponding to the galactic anticentre. It can only be observed during the winter time (November to April), and this period is the most delicate for obtaining good observations: we lost several nights due to heavy clouds, high humidity, rain, or snow.

An important "manual" step is the observation of standard stars. These are normally only of use if the night is photometric, in order to obtain photometric calibrations. But as the pipeline needs these observations to figure out if the observations were done in cloudy or dusty conditions, they are taken every night. The standards are observed every ~ 2 hours during the night and are chosen from 3 catalogues: Landolt (Landolt 1992), Sloan (Smith et al. 2002) and Stetson [2]. IPHAS also has its proper list of most used standards with indication about the necessary exposure times .

Once the raw data are obtained, they are processed in a pipeline specially designed by Irwin and Lewis (2001a) for the (mosaics) WFC on the INT. The pipeline includes non-linearity correction at the detector level; bias and overscan correction prior to trimming to the active detector areas; flat-fielding and fringing removal in the i' band. After the quality control, all the point sources in the fields are measured and catalogued by the pipeline.

The new detections will be named according the International Astronomical Union convention: IPHAS JHHMMSS.ss+DDMMSS.s if they are point sources and IPHASX JHHMMSS.s+DDMMSS if they are extended sources.

The large coverage (from the near Galactic Centre to the Galactic Anticentre) and depth of the INT Photometric Hα Survey are the keys for major discoveries in the Milky Way (Fig 2.5).

The imaging survey alone won't give us the necessary information for a complete study of the stellar objects we are discovering. To determine the chemistry, and veloc-

[2] At the Canadian Astronomy Data Centre, http://www3.cadc-ccda.hia-iha.nrc-cnrc.gc.ca/community/STETSON/index.html

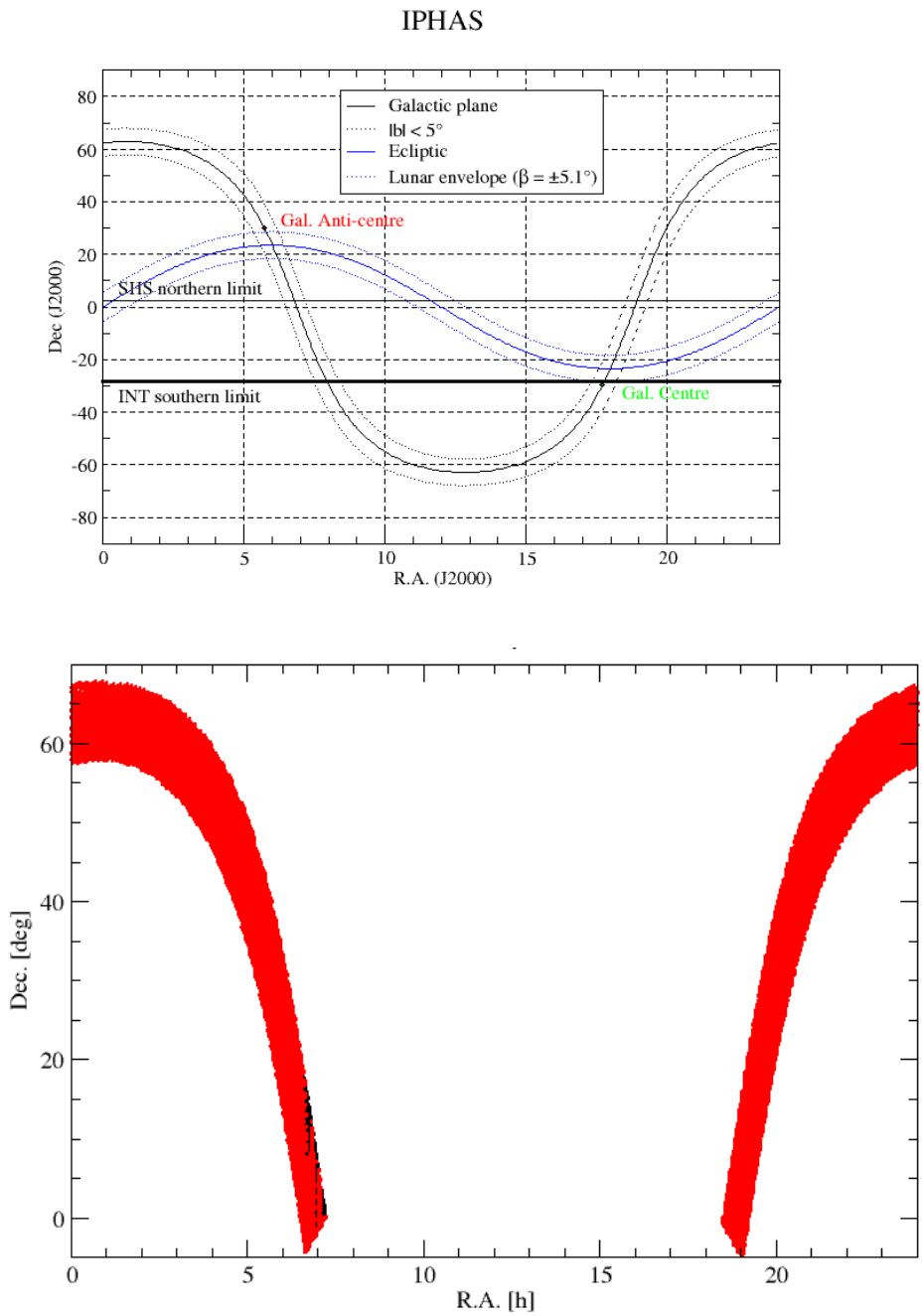

Figure 2.5: The upper map shows the total area covered by IPHAS: black path above the bold horizontal line and the INT southern limit. The lower map presents another view of the survey area with in red all the fields observed by December 06th 2007. Only the Anticenter region is not fully complete. Credit Robert Greimel.

ity among other things, we definitely need a spectroscopic analysis. The high amount of data to be checked requires a large amount of follow-up telescope time. We were awarded observing time via the International Telescope Time (ITP) programme to undertake a spectroscopic follow-up. Hence, the spectroscopic data come from the ING telescopes, using the Intermediate Dispersion Spectrograph (IDS) on the INT and ISIS on the 4.2 m William Herschel Telescope (WHT), ALFOSC on the 2.56m Nordic Optical Telescope (NOT) and the 3.58m Galileo Telescope (TNG). Independently, the 6.5m MMT is also giving data with Hectospec as well as the 2.1m Mexican San Pedro Martir (SPM) telescope. We have already obtained some spectra allowing us to start some deeper analysis. This phase of the survey is still going on.

Finally, IPHAS is part of the European Galactic Plane Surveys (EGAPS) which aims to map the full Milky Way at different wavelengths. Hence in the Southern hemisphere, VPHAS+ (VST/OMEGACAM Photometric H-alpha Survey) on the new VLT Survey Telescope is due to start by 2009 and will operate with the broadband filters u'g'r'i' and the narrowband Hα. UVEX is the ongoing "bluer" counterpart of IPHAS. It covers the same area and makes use of the u'g'r' and HeI5875 filters. All this new data will be used to study the different galactic stellar populations.

IPHAS is not the first Hα survey in the Galactic Plane. Indeed, among its predecessors we can cite the SuperCOSMOS H-alpha Survey (SHS) (Parker et al. 2005) linked to the AAO/UKST H-alpha survey (Parker et al. 1999). The Wisconsin H-Alpha Mapper, the Southern H-Alpha Sky Survey Atlas (SHASSA) and the Virginia Tech Spectral Line Survey (VTSS) complete the list. Here is a short review of their principal characteristics (Summary in Table 2.1).

• The SuperCOSMOS H-alpha Survey (SHS)[3] is the result of the digitisation of the data issued from the scans of survey films obtained during the AAO/UKST H-

[3]http://www-wfau.roe.ac.uk/sss/halpha/

alpha survey using the UK Schmidt Telescope. This **Southern Photographic** survey offers a coverage of -75 ° < Dec < +2 ° and -10° < b < 10 ° and a pixel resolution of 0.67 arcsec. The observations were carried out using a narrow-band H-alpha filter with a bandpass centred on 6590Å and a FWHM of 70Å combined with a broad-band Short-Red (SR) filter. Using this photographic imaging, 3 hour exposures were done in Hα and 15 minutes in SR.

• The Wisconsin H-Alpha Mapper (WHAM) [4] is a **Kinematic Survey** (Haffner et al. 2003) at high-resolution (R=25 000) using a Fabry-Perot spectrograph(dual-etalon 15-cm). The survey was carried out at Kitt Peak with a 0.6-metre telescope covering the Northern Galactic Plane above the declination dec=-30° and made use of a narrowband Hα filter with a FWHM of 20 Å. WHAM can reach 8-12 km/s velocity resolution from a one-degree, spatially integrated beam of the sky (i.e. 1 degree spatial resolution) and a level of detection of 0.05 Rayleighs [5] in a 30 second exposure.

• The Southern H-Alpha Sky Survey Atlas (SHASSA) [6] observations were taken at Cerro Tololo Inter-American Observatory (CTIO) in Chile with a robotic CCD camera providing a spatial resolution of 48 arcsec and 13deg^2 of field of view (Gaustad et al. 2001). The area covered is **the Southern Hemisphere** with a declination below +15 degrees. The 1014 x 998 images, with pixels of 0.8 arcminutes in width, are combined in the 542 fields, observed with a narrowband interference Hα filter of 32Å width and centred at 6563Å as well as a continuum filter of 61Å centred at 6440Å and 6770Å. The sensitivity in an H-alpha image is about 0.5 Rayleighs.

• The Virginia Tech Spectral Line Survey (VTSS)[7] (Dennison et al. 1998) is, **like SHASSA, an arcminute resolution imaging survey (CCD)**. It uses the Virginia Tech

[4] http://www.astro.wisc.edu/wham/survey/
[5] 1Rayleigh= $10^6/4\pi$ photons cm^{-2} s^{-1} sr^{-1} = 2.41 x 10^{-7} erg cm^{-2} s^{-1} sr^{-1} at Hα
[6] http://amundsen.swarthmore.edu/SHASSA/
[7] http://www.phys.vt.edu/ halpha/

Table 2.1: Main characteristics of the predecessors of the IPHAS survey.

Name	Location	Coverage	Technique	Spatial Resolution (pixel size)
SHS	South	-75 ° < Dec < +2 ° -10° < b < 10 °	Photographic plate digitisation	0.67 arcsec
WHAM	North	Dec > -30°	Kinematic survey	1° (beam)
SHASSA	South	Dec < 15°	CCD Camera	0.8 arcmin
VTSS	North	Dec > -15°	CCD Camera	1.6 arcmin

Spectral Line Imaging Camera (SLIC) to map the **Northern Hemisphere** with declinations greater than -15 degrees. The narrowband Hα filter used has a width of 17.5Å and is centred at 6563 Å (the [SII]6717 and 6731 lines are also observed in this survey). The wide-field images constituting the survey are circular with 10-degrees diameter. The pixels are 1.6 arcminutes in width and the sensitivity allows detection of sub-Rayleigh intensity structures.

From this range of surveys we can see that none of them combines large coverage and high spatial resolution (and a northern location)! **But IPHAS does**, which makes this survey the most complete of its type and generation.

2.3 Mosaicing of the Galactic Plane

In this thesis we are aiming to detect new extended Hα emitters and particularly new extended PNe (i.e. not point sources). The Northern Galactic Plane has therefore been divided into 2 deg^2 Hα-*r* (continuum removal) regions in order to create mosaics, made from the different IPHAS observations. The extended nebulae are searched for via a

visual inspection of those maps. The process to create the mosaics consists first in the selection of the $H\alpha$ and r images (given the mosaics centre coordinates), including the corresponding offset observations, to fill the inter-chip gaps on the Wide Field Camera. The next step is to set the quality parameters of the PostgreSQL database, generated automatically from the FITS headers of the pipeline object catalogues [8] (Irwin and Lewis (2001b), Drew et al. (2005) and Irwin et al., in preparation). We selected the used frames according to a number of constraints listed in Table 2.2. We used the images with the best calculated limiting magnitude. In most of the fields completed so far, less than 5% of the images are rejected. For our purpose the most interesting function is the one which sets the mosaic binning factor (in pixels). The advantage in using the binning technique in the mosaics is the multiple size and brightness detection levels which are possible. Hence we applied two different binning systems:

- 15 pixels x 15 pixels which correspond to 5 arcsec binning with the WFC (i.e 1 pixel represents 5 arcsec on the sky).
- 5 pixels x 5 pixels which correspond to 1.7 arcsec binning with the WFC (i.e 1 pixel represents 1.7 arcsec on the sky).

The first binning level helps to resolve low surface brightness objects (down to the IPHAS limit) and to accentuate the contours/shape of the nebulae (this is particularly useful to see, for example, the full extent of an outflow or a tail). The second set, is used to detect intermediate size nebulae i.e. smaller than ~15-20 arcsec in diameter. These objects are too small to be distinguishable at the first binning level (they are not resolved, and thus not distinguishable from emission line stars), and too faint or large to be detected via photometry (which is one of the methods also used). Hence, the first tests carried out have established that for objects with a size between 15 arcsec and 2-3 arcmin, a binning value of 3 to 5 pixels was enough to detect the details. We chose the 5 pixels binning due to the size of the mosaics, which reaches a mean of 135

[8] INT WFS (Wide Field Survey) archive. http://apm2.ast.cam.ac.uk/cgi-bin/wfs/dqc.cgi

Table 2.2: Criteria for the mosaics construction. The sky level is in count relative to the Hα filter and corresponds to the estimate of the ”median” sky brightness for the frame after removing background gradients. We set a magnitude limit greater than 18, knowing that in the initial quality control the values for the magnitude limit are 21.8 mag for r’, 20.2 mag for i’ and 20.6 in Hα. The magnitude limit corresponds to the 5-sigma flux limit for the standard aperture photometry measure.

Parameters	Boundary
Search box	120 arcmin
Filters	Ha,r
Sky level	< 600 ADU
Median image ellipticity	< 0.3
Seeing	< 2 arcsec
Maglim	> 18
Astrometric fit rms	< 0.75 arcsec
Binning	15 and 5 pixels

Megabytes, which increases the download time. For nebulae with a size greater than 3-4 arcmin, the 15 pixel binning is used to detect faint structures, and provides full morphological information.

At some point in the mosaics’ treatment, the allowed sky level value was raised to a limit of 2400 counts per pixel. This represents a degradation of the mosaics’ quality as we allow more “bad quality frames” to be used but it has the advantage of taking into account a higher number of frames. We operated this change while waiting for the re-observation of some areas, and to be able to continue the nebulae search. The level of 600 counts per pixel was reintroduced once the observations were redone.

The corresponding pairs of $H\alpha$ and r images (1 per CCD, amounting to 4 for each pointing, thus 8 counting the offset images) which composed the mosaics are subtracted via a "simple" pixel-by-pixel subtraction method, using the image world coordinate system to re-bin (using bilinear interpolation) the two images onto the same pixel coordinate system. According to Jonathan Irwin (private communication), who processed the mosaics, "the object catalogues are used to refine the frame-to-frame transformation by fitting for a standard 6-coefficient linear plate solution, since accurate astrometric registration is critical for difference imaging to avoid introducing artefacts into the images". Confidence maps, showing the less reliable image regions and bad pixels were also created. The subtracted images have their median sky background measured and the latter is subtracted from the pixel values. This allowed us to get rid of the possible sky background difference between the Hα and r images in the mosaic. In case of differences between the images in relation to the seeing for example, this subtraction method is more likely to produces artefacts. The process was therefore implemented with an adaptive kernel method based on that of Alard and Lupton (1998) and Alard (2000). Unfortunately, the amount and size of data to be processed and the number of mosaics to be made ($\sim$ 1500) prevented the use of this technique due to computational reasons. This functionality is nevertheless accessible on the Data Query Catalogue page for smaller data sets. The last step was the combination of subtracted images in all the chips in every concerned field, to obtain a complete mosaic. Those were subsequently binned using the factors defined above. The interpolation of the input images onto the output map was achieved by using the world coordinate system information stored in the FITS headers, and identifying bad pixels using the confidence maps.

The mosaics are named according their position as: HHMM±DD_ha-r_mosaics.fit. An example of a 5 pixels binning mosaic is shown in figure 2.6.

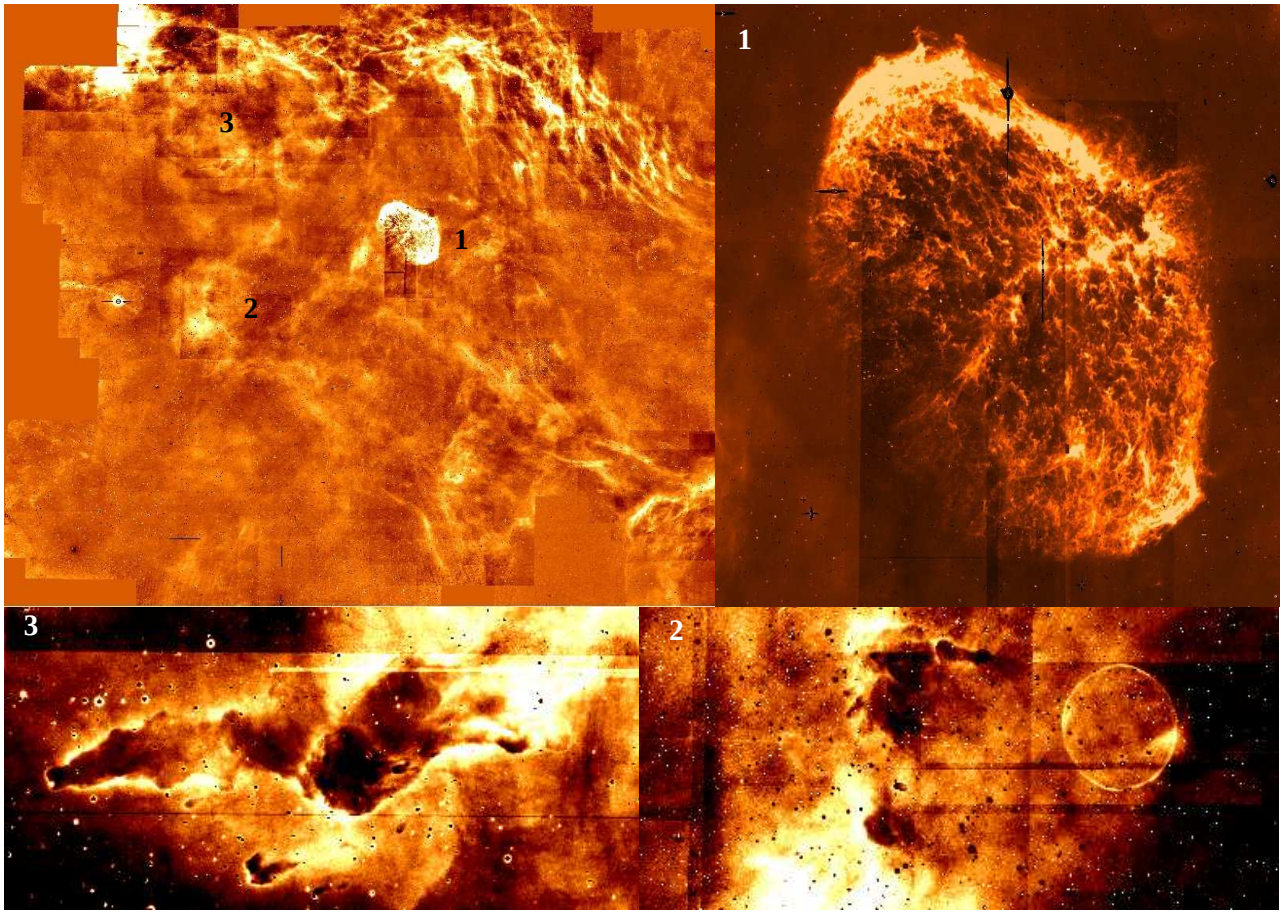

Figure 2.6: 5 pixels x 5 pixels binning mosaic created with the IPHAS observations centered on the region 20h12m+38deg.1- HII region G075.5+02.4, 2- New ionised sphere, 3-So called ”Elephant trunk”.

To be fully complete regarding the detection of Hα emitters within IPHAS, we must mention that two complementary search methods were adopted. The first one is dedicated to compact nebulae i.e. point sources (with a size up to 3-4 arcsec) where the prime targets are planetary nebulae (Viironen et al. 2006) (Viironen et al. 2008, in preparation). The compact nebulae are searched for automatically from the IPHAS data. The first criterion for PN candidate selection is that they should show strong excess in the IPHAS two-colour diagram (Fig 2.7). This cut (r' - H$\alpha \geq 0.25$(r' - i') + 0.55) is selected visually to exclude the main sequence stars, and to include the area where all the known planetaries are located in this diagram. The faint objects where the quality of IPHAS photometry decreases have to be removed (the objects should be brighter than 19.5 magnitudes in Hα). The final candidate selection is made visually. The semi-automated compact PN search overlaps with the mosaic visual search for extended nebulae. We also undertook an automatic detection of the PNe in order to be more complete, for the search of (faint) small size nebulae i.e. from 3-4 arcsec to 10-15 arcsec size, at 5 pixels binning. The method, also used in the southern MASH survey and applied with their collaboration, relies upon a quotient and difference imaging technique combining multi-wavelength data, Hα, r' and B (from imaging archives like DSS)[9]. Hence using colour-composite mosaics in Hα-r' and Hα/r' some intermediate size nebulae can be uncovered as we can discriminate them from "simple stars" and artefacts. The blue band can help to locate the central star. But this method can only work at its best for good to very good quality mosaics, as images must be clean. Moreover, the presence of artefacts can be a huge problem as they would pollute the field of search. Several valuable objects can be missed. We did the test on the 18h to 20h region, and half of the mosaics could not be automatically investigated due to the mosaic quality (presence of clouds, weather conditions at the limit of the selection criteria). This made the software unable to converge towards a proper result. Concerning

[9]A detailed explanation of the method applied to IPHAS can be found in the EGAPS website (http://www.ast.cam.ac.uk/meetings/egaps06/programme.html) in a talk by Brent Miszalski (MASH-IPHAS Team): "New techniques and tools for improving IPHAS detection of discrete nebulae".

the investigated mosaics the comparison with the visual search at the same binning led to very few discrepancies and sometimes interesting objects not detected by the software were identified visually. Although this tool is efficient and can be a plus for the detection of new nebulae and particularly new PNe, the visual inspection still remains predominant.

2.4 The populations in the IPHAS survey

The part of the northern galactic plane which is observable in IPHAS is the region between ~RA=18h to ~RA=7h15h. Although we performed an initial study of all the available mosaics (with the available data at the time), we decided to investigate and release data by sections of 2 hours in RA. The first field that has been fully observed and investigated at both binnings is the 18h to 20h region (as it was among the first areas to be fully processed). The census of the structures in the plane relies first on the validation of the objects as true structures, then if real, we must define their type or nature and their morphology.

The visual inspection of the mosaics to detect PNe or any other ionised nebulae faces two major problems: the bad quality of some mosaics and the presence of artefacts. The bad frames are generally due to the presence of clouds or images taken in not so good weather conditions. The case of the artefacts is more subtle in the sense that they can very easily be taken for real objects. We underline the issue of the artefacts as they represent a “population” that outnumber the population of “true nebulae” when the images are analysed.

All these “non-real” structures (Fig 2.8 and 2.9) generally result from instrumental effects (e.g. CCD edge reflection) or are generated during the Hα-r subtraction (mentioned earlier). Satellite traces are present but cannot be mistaken for nebulae. In order to differentiate a true nebula from an artefact, one simple way is to observe whether the concerned structure is repeated in several frames. As mentioned previously, in the

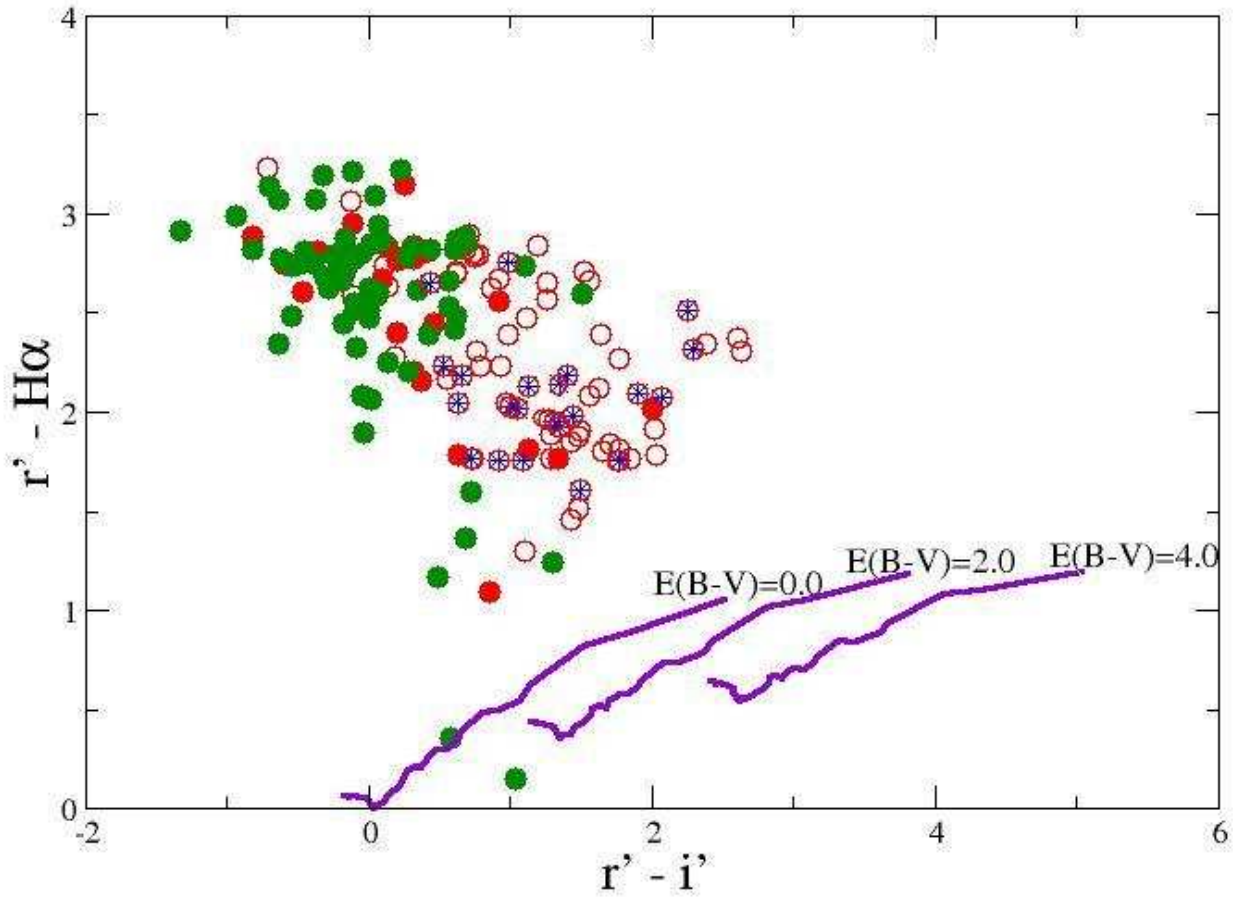

Figure 2.7: Distribution of compact planetary nebulae in the IPHAS color-color diagram. The known PNe are the green circles, the confirmed IPHAS PNe in filled red circles, the candidate PNe are the red open circles and the Hα IPHAS stars are in red circle with a blue filling. The violet solid lines show the location of MS stars at different reddening (Viironen et al. 2006) and (Drew et al. 2005).

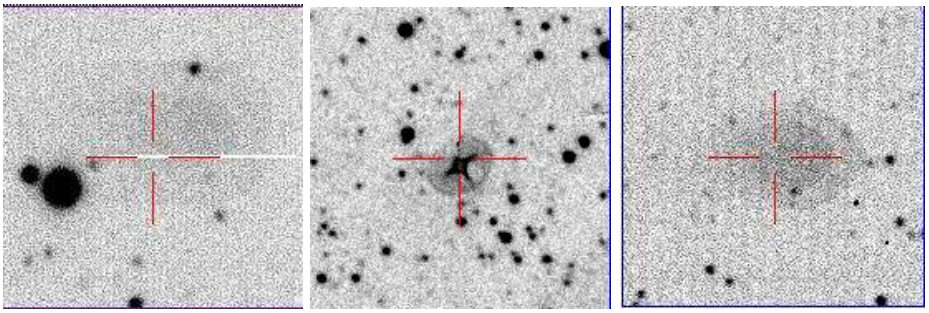

Figure 2.8: Example of the most common artefacts found in the mosaics.

IPHAS survey each field is observed at least twice, and even more depending on the observing conditions during the previous runs. But most importantly, successive observations of the same field are always offset, to avoid effects of bad pixels/area or to have any defect duplicated. All the data acquired can be seen in the IPHAS finding charts [10] and we can then probe the "reality" of an object: a real nebula must be seen in all the frames, an artefact is seen only once.

2.4.1 The classification and number of extended nebulae

The general catalogue for extended nebulae currently contains 722 known and new objects localised from **18h to 20h in RA** (see Table 2.4). All were found by visual search at 15 and 5 pixels binning. Each mosaic was viewed at least 3 times at both binnings. Once a new observing session was over (i.e. twice a year: summer and winter) the data was processed by the pipeline and the mosaics created. Each new session, since 2003, has brought more data which are new or of better quality, so the mosaics have been (re)created and examined several times.

In this section the terms "new" and "known" are quite relevant as the survey has not only found, unknown objects, but has also yielded better imaging of some already known sources and revealed new structures, as shown by Wareing et al. (2006) for Sh 2-188. Finally the survey aims to confirm the nature of the so-called "Nebula of un-

[10] http://apm3.ast.cam.ac.uk/iphas_finder.html

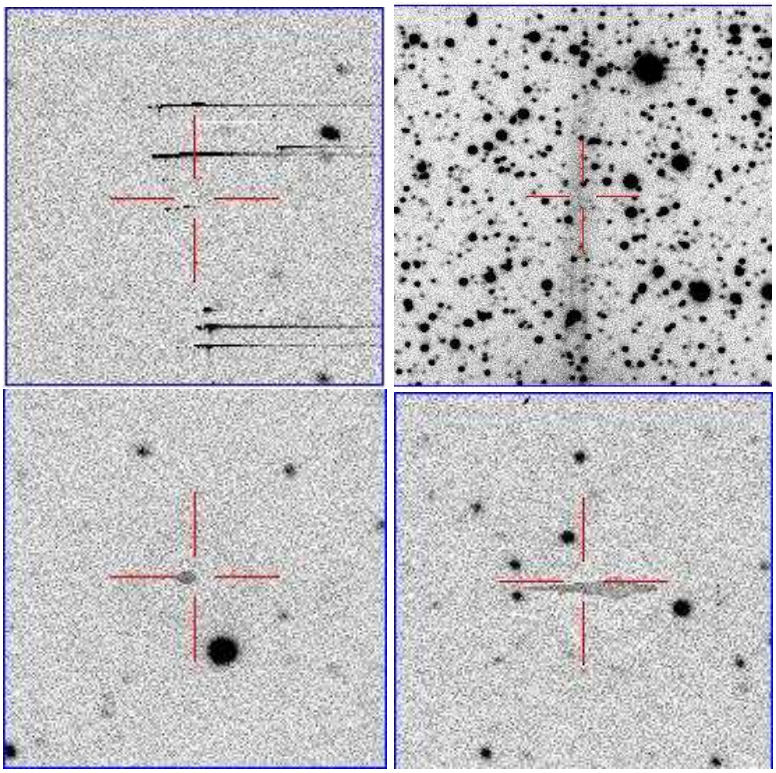

Figure 2.9: Other examples of common artefacts. Top Left: stripe-like features, Top Right: CCD edge reflection, Bottom Left: spot due to condensation or reflection effect and Bottom Right: larger condensation structure.

known nature" often listed in Simbad for which nothing is stated about the true nature of the nebula (HII, PN..etc).

Therefore we defined as **new** any object which has not been classified in any published catalogue (this is checked in Simbad[11] and VizieR[12]) or articles and which has an unknown nature. It can have infrared (IR) and radio counterparts for example, but the target is only listed as IR and as a radio source with no other information on the nature of the nebula. A **known** object is already listed in a catalogue i.e. it occurs in the literature, and it remains known even if its nature has not been unveiled yet. If its final classification is performed in the framework of IPHAS then it will be a known nebulae

[11] http://simbad.u-strasbg.fr/simbad/

[12] http://vizier.u-strasbg.fr/viz-bin/VizieR

confirmed by IPHAS. In this context a candidate PN can already be known (e.g. PN PM 1-302).

We used a wide variety of types in order to cover most of the stellar populations encountered during the search in the Hα continuum subtracted mosaics. Hence we ended up with 8 different types (Table 2.4).

- The diffuse nebulae (DNeb) gather all the mostly large Hα emissions with no precise forms or boundaries. They can be linked to diffuse HII regions, relics of supernovae remnant (SNR) or fading planetary nebulae or even Strömgren spheres around young stars. This category is quite difficult to characterise as any shapeless and faint structure is included and they can be embedded in other large scale objects like SNRs or HII regions. We counted 288 DNeb with an angular size between 20 arcsec up to 3 degrees, only 2 of which are known. The size was defined by fitting a circular aperture around the target so its accuracy is not absolute.

- The class of emission line stars (eStar) is quite generic and refers to all Hα emitting point sources. Witham et al. (2008) and Drew et al. (2005) have defined an upper limit for r-Hα of 3 to 3.1 for the classification of an eStar. They can be B[e] stars or T Tauri stars. We included those objects as some of the largest can be detected with the small, binning system. The eStar and the candidate emission line stars (eStar?) are visually identified as small compact and roundish structures showing a more or less extended surrounding halo. This definition allows us to make a distinction with the Herbig-Haro objects which have a much more pronounced bow shock shape. The other kinds of stars cannot be differentiated visually. The mean angular size of the 11 eStar candidates is about 5.8 arcsec and 7 arcsec for the 11 known ones. We found two known objects showing a larger angular size (HD 344313 with 20 arcsec and the diffuse NGC 6823 HOAG 13 with 80 arcsec).

- The galaxy type (Gal) has been set as we could observe known or new galaxies

(with Hα excess) through the Milky Way in the clear windows through the heavy extinction zone near the galactic centre. Their observation is easier through the galactic arms in the galactic anticentre (where the extinction is much reduced). We did not identify any new object for this kind nor listed known ones as they won't normally appear in the subtracted images.

- Herbig-Haro (HH) objects are nebulae associated with young stars or massive protostars. They are formed when the gas ejected by young stars collides with clouds of gas and dust in the nearby interstellar medium, at high speeds (several hundred kilometres per second). These fast evolving objects can be visually identified via their bow-shock structures and sometimes a point symmetric appearance. We counted 5 known HHs in our sample.

- The HII regions (e.g. Orion Nebula and Eta Carinae) are large clouds of gas and plasma surrounding massive O/B stars, (up to several degrees in size) in which recent star formation took place. The newly born stars which are hot emit ultraviolet light, ionising the nebula surrounding them. Although HII regions often appear as shapeless, some "small size" ones can show different kinds of morphologies. They can be classified from the simple spherically symmetrie to sophisticated bipolar shape. (e.g HII-S106 Perkins et al. (1981)). The ultra-compact HII regions (diameter $\leq 10^{17}$ cm) also show these particular shapes. It is quite difficult to determine the boundaries of HII regions are they are often close to SNRs or close to each other. So their total number may be underestimated. We identified 56 known HII regions.

- The SNR class (Supernova Remnant) play an important role in the enrichment of the interstellar medium with heavy elements and in triggering stellar formation. The 17 objects that we detected are very large, reflecting the high speed of the explosion (one tenth the speed of light) and their relatively old age. We could measure angular sizes from a "small" 80 arcsec up to $\sim$3 degrees. The definition of the SNR's contours is problematic when they are embedded in each other, but

their differentiation from HII regions is “easier” as the explosions give rise to a general directional map and the filamentary structures follow these orientations. SNR are well seen at higher binning.

- Symbiotic stars (Symb) consist of two stars (so a binary system): a late type giant and a hot compact companion, surrounded by a gaseous nebula. This nebula does not belong to the family of Planetary nebulae even if both types have some characteristics in common. Analysing the spectra of a symbiotic we see the features of:
  -A cool star: AGB or RGB (SiO, TiO bands)
  -High energy-level elements (Hot): ionised by the white dwarf which accretes the AGB or RGB wind and ionises it ([OIII], Halpha, Hbeta...etc . These features are also found in PNe).
  The interacting system causes a particular shaping (bipolarity in general). This mechanism could also occur in PNe: Bipolar PNe may also result from a binary interaction (but this is still an open question). Symbiotic stars cannot be certified only visually. A spectroscopic identification is necessary. 1 known symbiotic has been found.

- Finally, the planetary nebulae, confirmed (PN) and candidates (PN?), form the most interesting group for our purpose. The classification as candidate PN is based on two factors. The first one, which is the most obvious, is the morphology. As said previously, PNe are known for their original symmetrical shapes: bipolar, elliptical, round, point-symmetric. The 120s exposure in Hα can only give us a first estimation of the PN’s shape but this time is enough for our purpose. Therefore, under the “PN?” type we put **ALL the well detached nebulae showing a rather well defined shape with symmetry and/or particular structures (bow shocks, filaments, knots)**. We defined a comprehensive morphological main classification for these objects, using sub-classes in the cases where more structures could be seen (see Table 2.3).

Table 2.3: Morphological classification of nebulae.

Main class		Sub-Class	
B	Bipolar	a	ansae
E	Elliptical	d	disk
I	Irregular	Ms	Multiple shells
M	Multipolar	r	ring(s)
R	Round	t	torus

Table 2.4: Listing of the 8 types of nebulae localised with the visual search on mosaics with 18h <Ra< 20h .

Abbreviation	Type	Number	Candidate
DNeb	Diffuse nebula i.e. with no defined form	288	-
eStar	Emission line star	11	11
Gal	Galaxy	0	-
HH	Herbig-Haro Object	5	-
HII	HII region	56	-
PN	Planetary Nebula	100	233
SNR	Supernova Remnant	17	-
Symb	Symbiotic Star	1	-

But this visual criterion is not always reliable as other nebulae can also show a symmetrical structure. Hence potential symbiotics, PPNe, Herbig-Haros or HII regions can belong to the group.

We identified 100 known PNe and 233 candidates (15 of which are previously listed in the Simbad database).

2.4.2 The IPHAS nebulae database

In order to compile, not only the PNe but all the nebulae discovered with IPHAS, a database was built and is stored at the Institute of Astrophysics in Cambridge (IoA). The database can be found in the EGAPS[13] - Group B section. Public access is due soon (Fig. 2.10). It shows three main entries relative to the compact nebulae, the extended nebulae, and the last group of data deals with the spectroscopy and other elements of interest (Fig. 2.11). In the extended catalogue all the objects are listed and we give as basic information their name, type, morphology, size and some comments. We used a colour code to differentiate the known nebulae (white) from the new ones (green) (Fig. 2.12). So far, 3 main links have been added: one giving the corresponding finding chart (F), one linked to Simbad (S) and the last giving more detailed information on the object (O) (image, available spectrum). The latest entry has been designed to add any new information about a nebula (Fig. 2.13).

2.5 Summary

In conclusion, if we wanted an unbiased survey of planetary nebulae in the Northern Galactic Plane we needed a survey which went deeper in terms of sensitivity and further in terms of distance to the galactic bulge. The INT Photometric Hα Survey combined both criteria and was the tool that we used to reveal the "missing populations". The use of mosaics at different binning levels in the IPHAS survey was revealed to be very successful. Hence, we were able to visually detect from bright to very faint nebulae, from a wide variety of types and morphology. The first results obtained on the extended planetary nebulae were quite encouraging as in only two hours in right ascension we identified 233 new potential PNe. We have to add to this results the 59 compact candidate PNe found via the photometric search.

[13] http://www.egaps.org/

European GAlactic Plane Surveys

	IPHAS	UVEX	VPHAS+	VVV
Project Pages	iphas.org (Herts) Initial Data Release (CASU) Internal News/Follow Up (Warwick)		vphas.org (Herts)	
CASU / Data Access	• DQC interface • Finding Charts • Catalogue Data (Mike Irwin)	• Catalogue Data (Mike Irwin)		
Observing	• IPHAS Observing and past nights • Survey Status • Standard Stars • Follow up observations	• Survey Status		
Survey Science	Group A Group B Group C Group D Group E Group F			
Other	• General Project Related Information • Publicity • Database Queries • IPHAS field finder • Object Finder			

Figure 2.10: EGAPS main page.

Compact Objects	Extended Objects	Other links
• Method of extraction • Catalogue • CCD	• Method of extraction • Catalogue	• Spectroscopy • Nomenclature • Search • Publications

Figure 2.11: Entries of the Nebulae database.

The next logical step was the confirmation of the nebulae candidates as potential true PNe.

RA	Dec	Object name [Name/New]	Type	Morphology	Diameter [arcsec]	Comments	Links
18:34:16.223	+02:12:15.95	IPHASX J183416.2+021215	PN?	I	556		FSO
18:34:38.678	+00:08:03.00	PN PM 1-242	PN?	E	8		FSO
18:36:02.400	-00:02:26.16	PN PM 1-246	PN?	I	12		FSO
18:36:52.778	-01:15:36.81	IPHASX J183652.8-011536	PN?	I	26		FSO
18:38:11.748	-01:05:12.37	IPHASX J183811.7-010512	PN?	I	42		FSO
18:39:11.850	+01:06:24.60	IRAS 18366+0103	PN?	R	5	wht20050528 (red+blue),"PN3",(AMR) faint PN many lines,Te?,int20050620,"iphas1",Ha,[OIII]	FSO
18:40:30.275	-00:38:20.86	IPHASX J184030.3-003820	PN?	I	22		FSO
18:41:04.600	-01:40:50.08	IPHASX J184104.6-014050	PN?	I	6		FSO
18:41:37.235	+04:40:25.04	IPHASX J184137.2+044025	PN?	I	35		FSO
18:42:11.390	+00:50:31.70	IPHASX J184211.4+005031	PN?	R	5	IRAS 18396+0047 -- Infra-Red source near	FSO
18:42:53.191	-02:26:42.51	IPHASX J184253.2-022642	PN?	I	376		FSO
18:43:20.059	+04:27:22.10	IPHASX J184320.1+042722	PN?	I	60		FSO
18:45:05.250	+00:11:58.72	IPHASX J184505.2+001158	PN?	R	4		FSO
18:45:40.555	-03:12:38.17	IPHASX J184540.6-031238	PN?	I	34		FSO
18:47:16.354	+03:09:29.13	IPHASX J184716.4+030929	PN?	I	20		FSO

Figure 2.12: Part of database body for the extended catalogue.

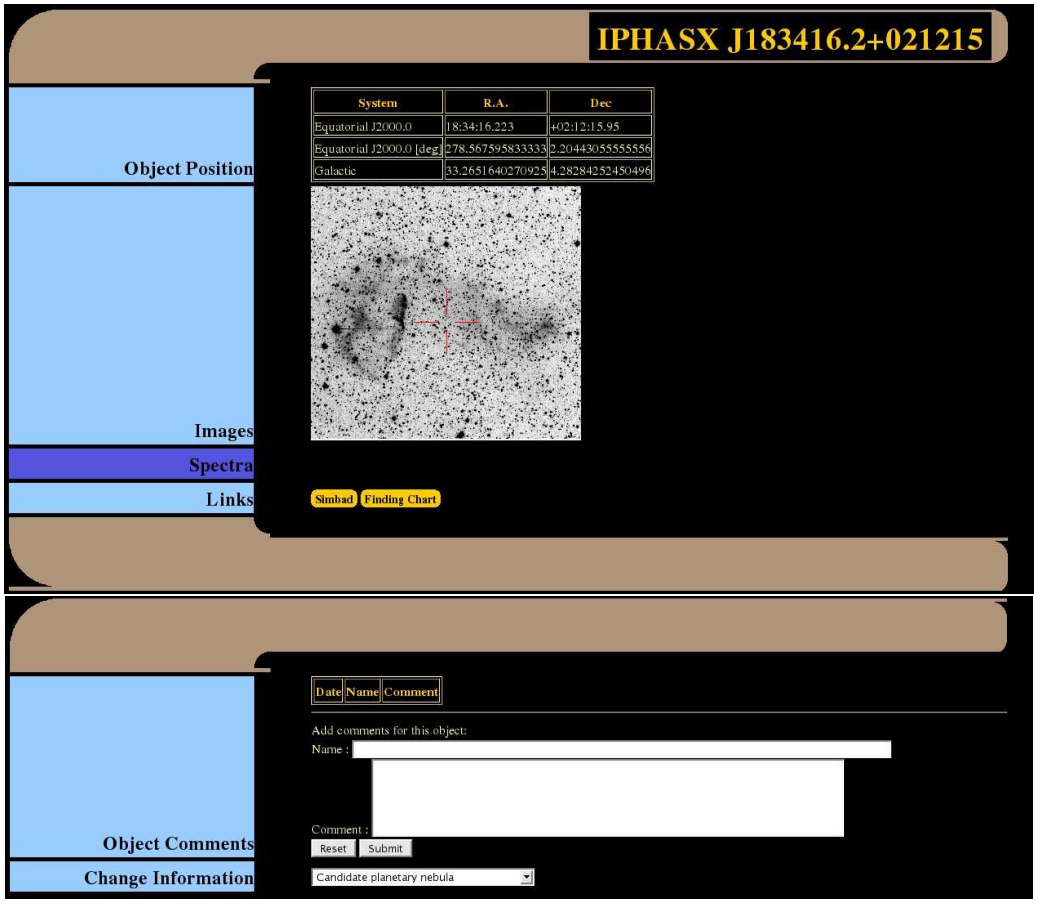

Figure 2.13: An example of entry for IPHASX J183416.2+021215.

3

Classification of the candidate planetary nebulae

From this point we will concentrate on planetary nebulae candidates and discard for the time being the other types of nebulae. The confirmation of the nature of the Hα emitters as PNe is the basis of our search. This operation can be achieved using different, complementary methods. The spectroscopic identification by detection of the characteristic emission lines of PNe is the most obvious tool. We also use colour-colour diagrams mainly with infra-red data and radio flux data to constrain the PNe range. Finally, by observing the objects' morphology we can still try to figure out if they are likely to be PNe, in case the methods listed above can not be applied.

We first introduced all the 233 nebulae classified as candidate PNe in the 18-20 hours area. The coordinates of each target were derived from the IPHAS finder chart with the images not binned, whenever possible. They are given for the nebula centre even in the case of arc-like nebulae. In this context, we defined as the centre the centroid of the geometric circular aperture which encloses the nebula. The angular diameters were derived visually by fitting a circular aperture around the nebulae in the case of large nebulae (where the object is much larger than the seeing), and we measured the seeing-deconvolved gaussian size for the very small (quasi point sources) nebulae. For

round objects we listed the circular diameter while for elliptical, bipolar and irregular nebulae the long axis was measured. The morphology is not definitive for some nebulae as we only have the short exposure images from the survey. The results are presented in Table A.1, in Appendix A, and in Appendix B.

3.1 Spectroscopic identification

3.1.1 Characteristic spectral lines

Spectroscopy is the best tool to identify a stellar object, as spectral classification allows us to derive its chemical signature, temperature and density. In the case of planetary nebulae, their optical spectrum is dominated by emission lines. This is due to the fact that the temperature of the exposed central star in a planetary nebula can be quite high (30,000 K to 100,000 K). These high temperatures and UV-dominated radiation field, cause a high degree of ionisation in the nebula. Planetary nebulae also provide the conditions for the occurrence of emission lines arising from transitions within the same electronic configuration (due to the low level of collisions in the nebulae environment). These transitions violate the LS coupling selection rules. The emitted lines issued from the decay of the upper states are called forbidden lines and are distinguished from the "normal " transition by brackets (e.g. [OIII]). These strong lines dominate the emission in planetary nebulae and their presence/absence marks the difference with other Hα emitters. Nevertheless, HII regions and symbiotics also show forbidden lines if the density is not too high. The forbidden lines are sensitive to densities ranging from 10^3 cm^{-3} to 10^8 cm^{-3}. Table 3.1 lists the names and wavelengths of some spectral lines characteristic of PNe.

Table 3.1: Sample of optical emission lines found in planetary nebulae.

Observed Wavelength (Å)	**Element**	**Laboratory Wavelength (Å) (Vacuum)**
3969	[Ne III]	3967.5
4026	He I	4026.2/4026.4
4072	[S II]	4068.6
4102	H I delta	4101.7
4340	H I gamma	4340.5
4363	[O III]	4363.2
4388	He I	4387.9
4472	He I	4471.5/4471.7
4542	He II	4541.6
4571	[Mg I]	4571.1
4686	He II	4685.7
4740	[Ar IV]	4740.3
4861	H I	4861.3
4922	He I	4921.9
4959	[O III]	4958.9
5007	[O III]	5006.8
5199	[N I]	5198.5
5412	He II	5411.5
5577	[O I]	5577.4
5754	[N II]	5754.8
5876	He I	5875.6/5876.0
6300	[O I]	6300.2
6312	[S III]	6310.2
6364	[O I]	6363.9

Table 3.1 – continued .

Observed Wavelength (Å)	Element	Laboratory Wavelength (Å)(Vacuum)
6435	[Ar V]	6434.9
6548	[N II]	6548.1
6563	H I alpha	6562.8
6583	[N II]	6583.6
6678	He I	6678.1
6716	[S II]	6717.0
6731	[S II]	6731.3
6891	He II	6890.7
7006	[Ar V]	7006.3
7065	He I	7065.2
7136	[Ar III]	7135.8
7176	He II	7177.5
7237	[Ar IV]	7236.0
7263	[Ar IV]	7263.3
7281	He I	7281.3
7325	[O II]	7318.6/7319.4/7329.9
7531	[Cl IV]	7530.54
7593	He II	7592.75
7751	[Ar III]	7751.06
8236	He II]	8236.79
9069	[SIII]	9069.6
9532	[SIII]	9532.55

As IPHAS targets quite faint extended nebulae, we do not expect to detect all these lines. We therefore have defined a list of “minimum necessary lines” which can probe

bona fide PNe. This is important as other type of nebulae (HII, SNR, Symb) can be confused with PNe when examining their spectra. Note that the following criteria to identify other nebulae are flexible.

• Planetary Nebulae may be discriminated from other emission nebulae by the fact that the oxygen line at 5007Å is normally about 3 to 5 times brighter than the red Hα line.

• The HII regions show strong HI recombination lines as well as [NII] and [OII] lines. The strength of the [OIII] and [Ne III] lines will vary depending on the temperature of the central star. The principal discriminant is the [NII]/Hα ratio (Kennicutt et al. 2000): lower than 0.7 it will probe the HII nature of the nebulosity, greater than 0.7 it will be linked to PNe, SNR or Population I Wolf Rayet ejecta nebulae, because it indicates N-enhancement. But we must also note that not all PNe show N-enrichment.

• The Supernovae remnants have very little continuum emission; strong lines of H, [OII], [OIII], [SII] and [NII]; and fainter lines of HeI, HeII, [OI], [NI], [NeIII], [FeII], [FeIII], [CaII] and [ArIII]. The difference with other species like HII regions and PNe lays principally on the very strong [SII], [OI] and [OII] lines.

• The Symbiotic stars can be separated from PNe by looking at the [OIII]5007 and 4363 lines (Gutierrez-Moreno 1988; Gutierrez-Moreno et al. 1995), and the [OIII]5007 and [OII]3727 lines (Schwarz 1988). In those papers, the ratio R1=I(4363)/Hγ plotted against the ratio R2=I(5007)/Hβ shows a net separation between both types of objects. This is based on the density difference between PNe and Symbiotics. In addition, the spectrum shows the existence of the strong emission of the forbidden lines and a late type giant spectrum (with the TiO bands for example). The particular emission lines (bands) at 6825Å and 7082Å are a signature of the symbiotics. They correspond to the Raman scattering of the OVI resonance lines at 1032Å and 1038Å (Schmid 1989).

Most of the parameters cited above can be used in the form of diagnostic diagrams. These tools differentiate the nebular populations using their different lines ratios for particular features. In the optical the most popular are the diagrams from Sabbadin and D'Odorico (1976b) and Sabbadin et al. (1977). The most recent diagnostic diagram

has been published by Riesgo and López (2006).

Hence, to confirm that an object is a PN we need at least to detect the following emission lines: Hβ (4863Å), [OIII] (4959Å), [OIII] (5007Å), [NII] (6548Å), Hα (6565Å), [NII] (6584Å), [SII] (6717Å) and [SII] (6731Å).

3.1.2 The IPHAS spectroscopy follow-up

Observing strategy and data reduction

In the framework of the IPHAS survey we undertook a spectroscopic follow-up of the newly detected objects. This follow-up, which concerns emission line stars and nebulae, was conducted through the International Time Programme (ITP). This programme from the European Northern Observatory (the International Scientific Committee (CCI)) allocates 5% of observing time on all the instruments located in the Canary Islands. As previously said, the ITP allows the use of a large number of telescopes and spectrometers based on La Palma i.e. (IDS on) the INT, (ISIS on) the WHT, (ALFOSC on) the Nordic Optical Telescope and the Telescopio Nazionale Galileo. The "nebulae group "of IPHAS also makes use of the San Pedro Martir Telescope in Mexico (Table 3.2).

The IPHAS survey is designed to detect the nebulae (in our case) that have not been detected before due mainly to their low surface brightness. Indeed we found a large number of faint objects, and the tools for their spectroscopic study as well as the observing strategy had to be chosen accordingly. They led to the following considerations:

- We performed a simple confirmation, hence we did not need to expose for a long time. In this case 30 min for each object on a 2m class telescope gave a reasonable S/N allowing the detection of the characteristic lines of the PNe. This had the advantage of allowing a maximum of candidates to be examined and we retrieved, in some cases, useful physical parameters like the extinction (using the

Balmer decrement method with the Hβ and Hα lines), the line fluxes (with the dereddened spectra), and the electron density (with the ratio [SII] (6717Å)/ [SII] (6731Å)).

- We performed deep observations only of good candidates, for further analysis. By good candidates we mean objects for which shape, colour in Ha, r and i, and possibly IR data left little doubt regarding the nature of the nebulae. In this context we intended to measure the [OIII] (4363Å) and/or [NII] (5755Å) lines which permit a derivation of the temperature of the nebulae. From previous observations we know that [OIII] (4363Å) is ~100 times fainter than Hα , so it requires much longer exposure times. The electron temperature is a fundamental parameter for PNe and needs to be derived if we want to determine abundances.

The spectroscopy of PNe was mainly done with IDS[1], ISIS[2] and the Boller & Chivens spectrograph (SPM)[3]. Due to the larger mirror (4m) of the WHT and higher efficiency spectrograph, ISIS was used for the PN candidates for which we expected to retrieve the [OIII] (4363Å)and/or [NII] (5755Å). IDS and SPM were used for object confirmation.

Due to the overlap with the Southern hemisphere observations, some candidate PNe were observed with the 2.3 m Telescope at the Siding Spring Observatory using the Dual Beam Spectrograph [4]. For future spectroscopic studies of IPHAS candidate PNe, the association of large mirrors and efficient spectrometers (with fibre for example, which will sum the signal received from each pixel on the whole object) will be required to detect more emission lines and to add fluxes.

The spectra were reduced using the IRAF packages and following the directives in the User's guide to slit spectra reduction [5]. Each spectrometer has its characteristics but the general reduction method still remains the same. We used both skyflats and

[1]For more details on IDS:http://www.ing.iac.es/Astronomy/instruments/ids/

[2]For more details on ISIS:http://www.ing.iac.es/Astronomy/instruments/isis/index.html

[3]For more details on Boller & Chivens spectrograph:http://www.astrossp.unam.mx/indexspm.html

[4]http://www.mso.anu.edu.au/observing/2.3m/DBS/

[5]Massey P., Valdes F. and Barnes J., 1992)

Table 3.2: Configurations used for the different telescopes. The numbers show the theoretical wavelength coverage for the spectrometer, as the effective cutoff may change from one spectrum to another.

Telescope	Instrument	Grating Dispersion Å/pixel	Central wavelength (Å)	Wavelength coverage (Å)	Slit length
WHT	ISIS	R300B and R158R 0.86 and 1.81	4249 & 7500	2330 and 2860	4’
INT	IDS	R300V 1.87	5500	5660	3.3’
SPM	B&C(1)	600 & 400 l/mm 3.2 & 4.8 (3)	4651& 6472	2113 & 2130	5’
SS1.9m(2)	DBS	300B 1.99	5600	4000	6’-7’

(1) Boller & Chivens,(2) Siding Spring’s Double Beam Spectrograph, (3) Resolution in Å.

lamp flats. As we also observed during bright nights e.g. when the moon was up, the skyflats were used to correct for the gradients in sky illumination. The arc calibration was achieved using mainly CuNe and CuAr lamps. In order to prevent any distortion in the wavelength calibration an arc frame was taken soon after the science frame it was supposed to calibrate i.e. at the same sky location. The final steps were the airmass correction, followed by the flux calibration where we used spectrophotometric standards available on the ING list [6].

We can see in Fig.3.4 a spectrum of one of the nebulae listed in Table 3.3 (and displayed in figures 3.1, 3.2 and 3.3). The table indicates the strength of the 6 characteristic emission lines (namely Hβ, Hα, [OIII]5007, [NII]6548, [NII]6584, [SII]6717 and [SII]6730) obtained from 18 candidate PNe. The hydrogen Balmer lines will provide the extinction so we can derive the line fluxes corrected from reddening. Following Acker et al. (1992), we assume the extinction law:

[6]http://catserver.ing.iac.es/landscape/tn065-100/workflux.php

$$\left(\frac{FH\alpha}{FH\beta}\right)^{theoretic} = \left(\frac{FH\alpha}{FH\beta}\right)^{observed} \times 10^{-c[0.325]} \tag{3.1}$$

where c is the extinction constant (also named c(Hβ)) and for a relative logarithmic extinction coefficient for Hα/Hβ equal to 0.325. We derive:

$$c(H\beta) = log\left(\frac{\left(\frac{FH\alpha}{FH\beta}\right)^{observed}}{\left(\frac{FH\alpha}{FH\beta}\right)^{theoretic}}\right) \times \frac{1}{0.325} \tag{3.2}$$

The theoretical F(Hα)/F(Hβ)=2.85, with all the fluxes normalised to F(Hβ)=100, the extinction constant c(Hβ) is finally defined as:

$$c(H\beta) = 3.08 logF(H\alpha)^{normalised} - 7.55 \tag{3.3}$$

Table 3.3: Listing of the 18 planetary nebula candidates with available spectroscopic data localised between 18h and 20h in RA. ”d” stands for dereddened.

Name	Telescope	c(Hβ)	Hβ	Hα	[OIII]5007d	[NII]6548d	[NII]6584d	[SII]6717d	[SII]6730d
IPHASX J183911.8+010624	WHT	2.71	100	2152	948	8	22	-(*)	1
IPHASX J184336.6+034640	SS	2.17	100	1438	78	130	386	15	22
IPHASX J184745.4+013248	INT	-(1)	-(*)	100	10	17	46	10	13
IPHASX J185224.2-004446	SS	2.56	100	1923	876	297	931	-(*)	-(*)
IPHASX J185525.7-004823	SS	1.93	100	1201	2032	509	1669	66	79
IPHASX J185925.8+001734	SS	3.73	100	4598	607	101	347	6	4
IPHASX J191124.8+002743	INT	1.32	100	759	1755	132	420	13	12
IPHASX J191345.6+174752	WHT	2.30	100	1581	1168	6	10	1	1
IPHASX J191445.1+133219	WHT	1.60	100	939	1210	823	2497	70	61
IPHASX J192847.1+093439	WHT	0.97	100	585	214	301	1003	64	54
IPHASX J192902.5+244646	WHT	0.88	100	546	271	-(*)	12	-(*)	-(*)
IPHASX J193827.9+265752	WHT	0.89	100	550	1837	-(*)	-(*)	-(*)	-(*)
IPHASX J193912.0+251105	WHT	2.21	100	1475	154	47	138	27	30
IPHASX J194359.5+170901	WHT	0.38	100	377	1618	111	366	62	69
IPHASX J194751.9+311818	WHT	2.79	100	2286	21	22	66	11	12
IPHASX J194940.9+261521	WHT	2.70	100	2130	872	165	503	46	45
IPHASX J195248.8+255359	WHT	3.93	100	5353	1021	262	780	15	25
IPHASX J195657.6+265714	WHT	3.05	100	2782	399	454	1296	70	45

(*) Emission lines with a signal to noise lower than 3, (1): The Hβ line was not detectable so the lines were not dereddened and are given scaled to F(Hα)=100.

From these observations, only IPHASXJ 194359.5+170901 and IPHASX J195248.8+255359 have their electron temperature determined with values of T_e[OIII]=11900 K and T_e[NII]=12820 K respectively.

In the small sample studied we noticed that half of the objects had their [NII]6584 line stronger than their Hα emission. Most of the PNe concerned are bipolar which is consistent with the studies performed by Peimbert and Torres-Peimbert (1983) and Quireza et al. (2007).

Classification using diagnostic diagrams

As seen in the previous section, the study of emission lines detected in spectra is a good tool (if not the best) to identify stellar species. This uses the fact that, in our case, the different nebulae will show different line ratios varying as a function of their internal physical processes (photoionisation, shock excitation ...etc) and evolutionary stage. Hence in a "lines ratio" diagram, the nebulae should be well separated. For example SNR have a generally low Hα/[NII] and Hα/[SII] as they are shock-excited compared to HII regions which are photoionised (Riesgo and López 2006). But the above criteria will also vary with the density and morphology of the nebula. In 1977, Sabbadin et al. (1977) introduced electron density based diagrams (Fig. 3.5) to unveil the true nature of Sharpless 176 i.e. PN, SNR or HII. They used as density indicator ratios, log [Hα/[NII]] versus [SII]6717/[SII]6731, described by Saraph and Seaton (1970) and adapted two new diagrams for further constraints: log [Hα/[NII]] versus log [Hα/[SII]] and log [Hα/[SII]] versus [SII]6717/[SII]6731. Later, Riesgo and López (2006) used and improved the same technique for 613 planetary nebulae using the diagnostic diagrams: log [Hα/[SII]] versus log[Hα/[NII]], log [Hα/[SII]] versus [SII]6717/[SII]6731 and log [Hα/[NII]] versus [SII]6717/[SII]6731 (Fig. 3.6). In both searches the data on HII regions are taken from Kaler (1976) and the data on SNR are from Daltabuit et al. (1976), Sabbadin and D'Odorico (1976a) and Dopita (1976). The line ratios should be de-reddened.

We therefore compared our results with the two sets of diagnostic diagrams. To constrain our identification we added the data of the known planetary nebulae located in our sky area, for which line fluxes are given by Acker et al. (1992). For these objects, the lines have been dereddened using as visual extinction at 5550 Å,

$$A(V) = R(V) * c(H\beta) * (0.61 + 0.024 * c(H\beta)) \tag{3.4}$$

and the ratio, R(V), of this extinction to the colour excess E(B-V) equal to 3.1 (Cardelli et al. 1989). Equation 3.4 is based on the relation between c(Hβ) and the broadband E(B-V). The Fitzpatrick parameterisation (Fitzpatrick 1999), based on the wavelength-dependence of Galactic interstellar extinction, was then used to correct the spectra. The results are shown in Fig 3.7 and Table 3.4.

From our 18 original candidates, 13 were able to have their ratios derived. As a result, all of them can be classified as "true" planetary nebulae. The 5 candidates without enough usable lines for the diagrams can be only be partially analysed according to their line strengths listed in Table 3.3 and additional data would be necessary to identify their type.

- IPHASX J183911.8+010624: Strong [OIII]5007 greater than Hα (PN?), low [SII] lines (not SNR), [NII]/Hα $< 0.7 \Rightarrow$ HII according Kennicutt et al. (2000), but is likely to be a PN.

- IPHASX J184745.4+013248: Low [SII] lines (not SNR), low [OIII]5007 and ratio [NII]/Hα just under the 0.7 limit $\Rightarrow$ HII/PN

- IPHASX J185224.2-004446: Strong [OIII]5007 greater than Hα (PN?), [NII]/Hα > 0.7 (PN?) $\Rightarrow$ Likely PN

- IPHASX J192902.5+244646: Low [OIII]5007, [NII]/Hα < 0.7 (assuming that [NII]6548~[NII]6584/3) $\Rightarrow$ HII?

- IPHASX J193827.9+265752: Strong [OIII]5007 greater than Hα $\Rightarrow$ Unclear due to the non-detection of [NII] and [SII] lines.

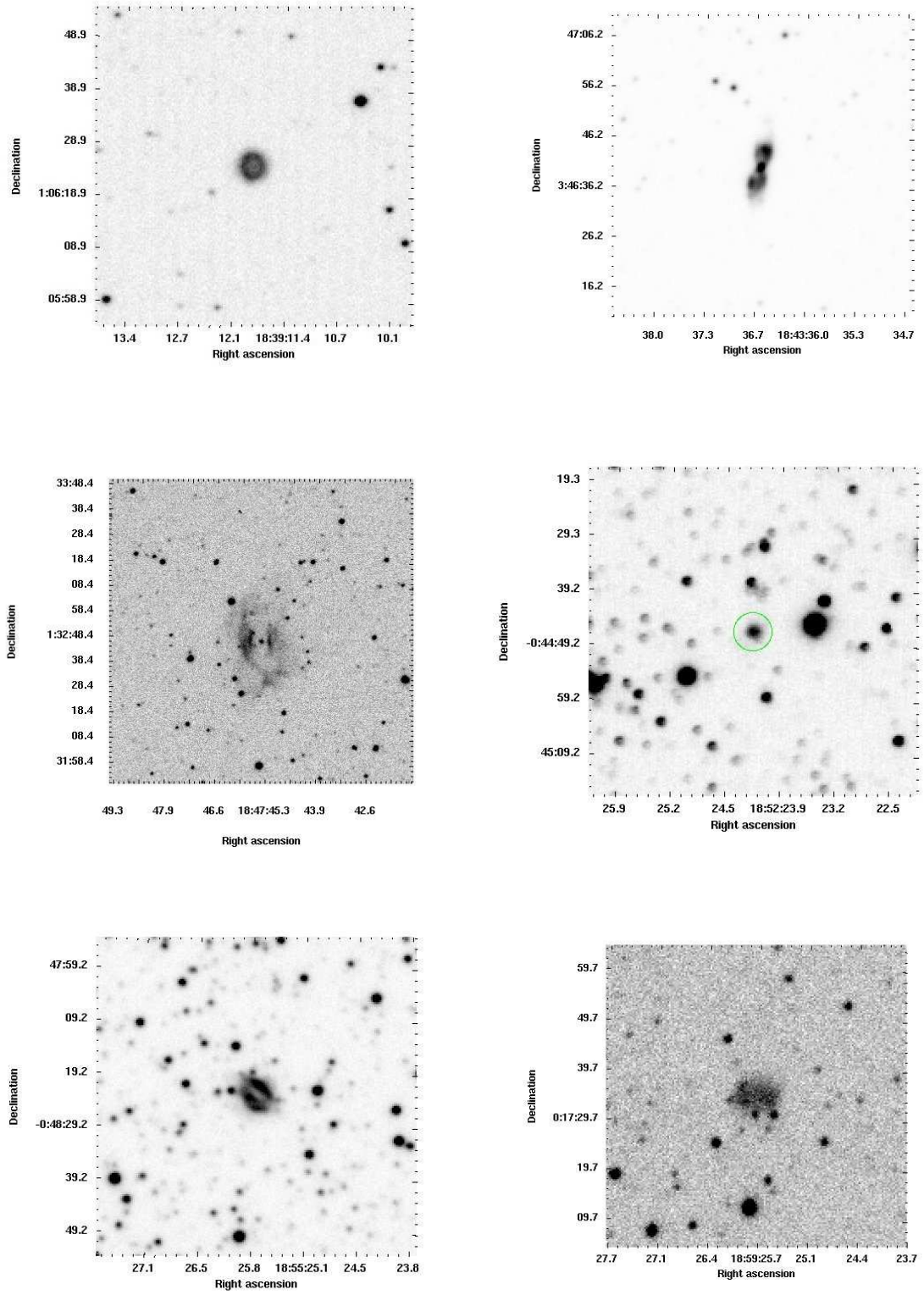

Figure 3.1: From Top to Bottom and Left to Right: Hα+[NII] inverted images of IPHASX J183911.8+010624, IPHASX J184336.6+034640, IPHASX J184745.4+013248, IPHASX J185224.2-004446, IPHASX J185525.7-004823 and IPHASX J185925.8+001734.

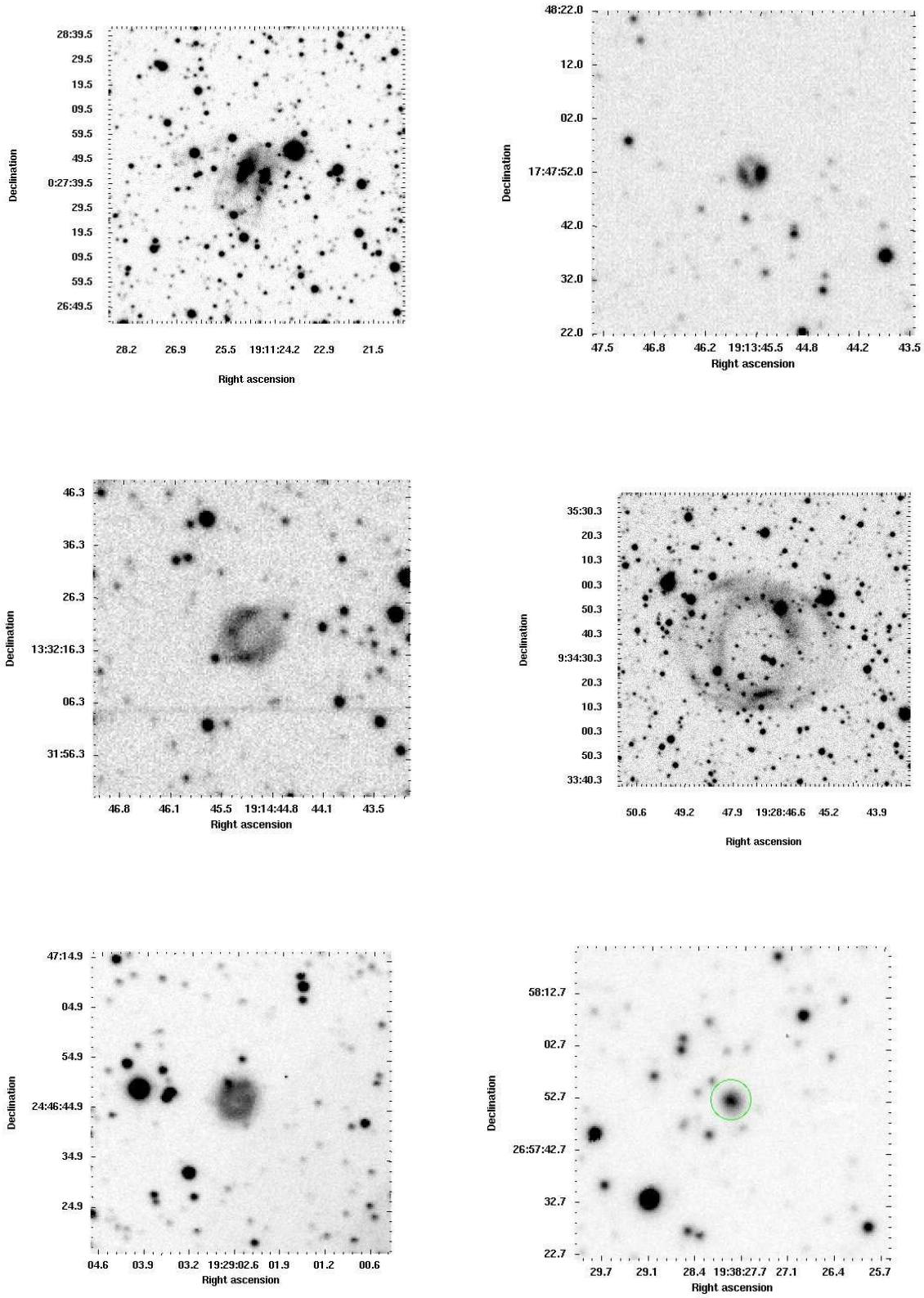

Figure 3.2: From Top to Bottom and Left to Right: Hα+[NII] inverted images of IPHASX J191124.8+002743, IPHASX J191345.6+174752 and IPHASX J191445.1+133219, IPHASX J192847.1+093439, IPHASX J192902.5+244646 and IPHASX J193827.9+265752.

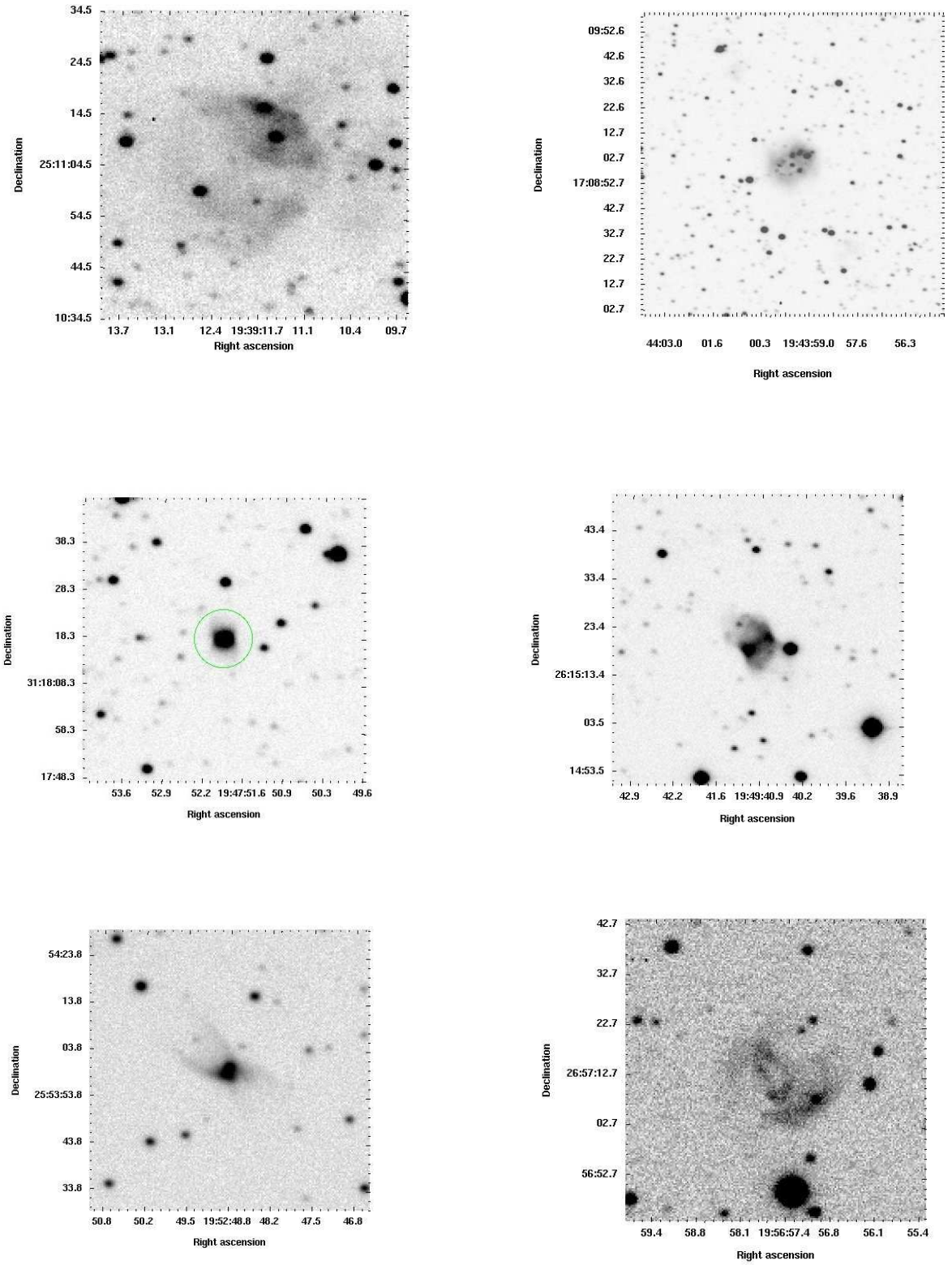

Figure 3.3: From Top to Bottom and Left to Right: Hα+[NII] inverted images of IPHASX J193912.0+251105, IPHASX J194359.5+170901, IPHASX J194751.9+311818, IPHASX J194940.9+261521, IPHASX J195248.8+255359 and IPHASX J195657.6+265714.

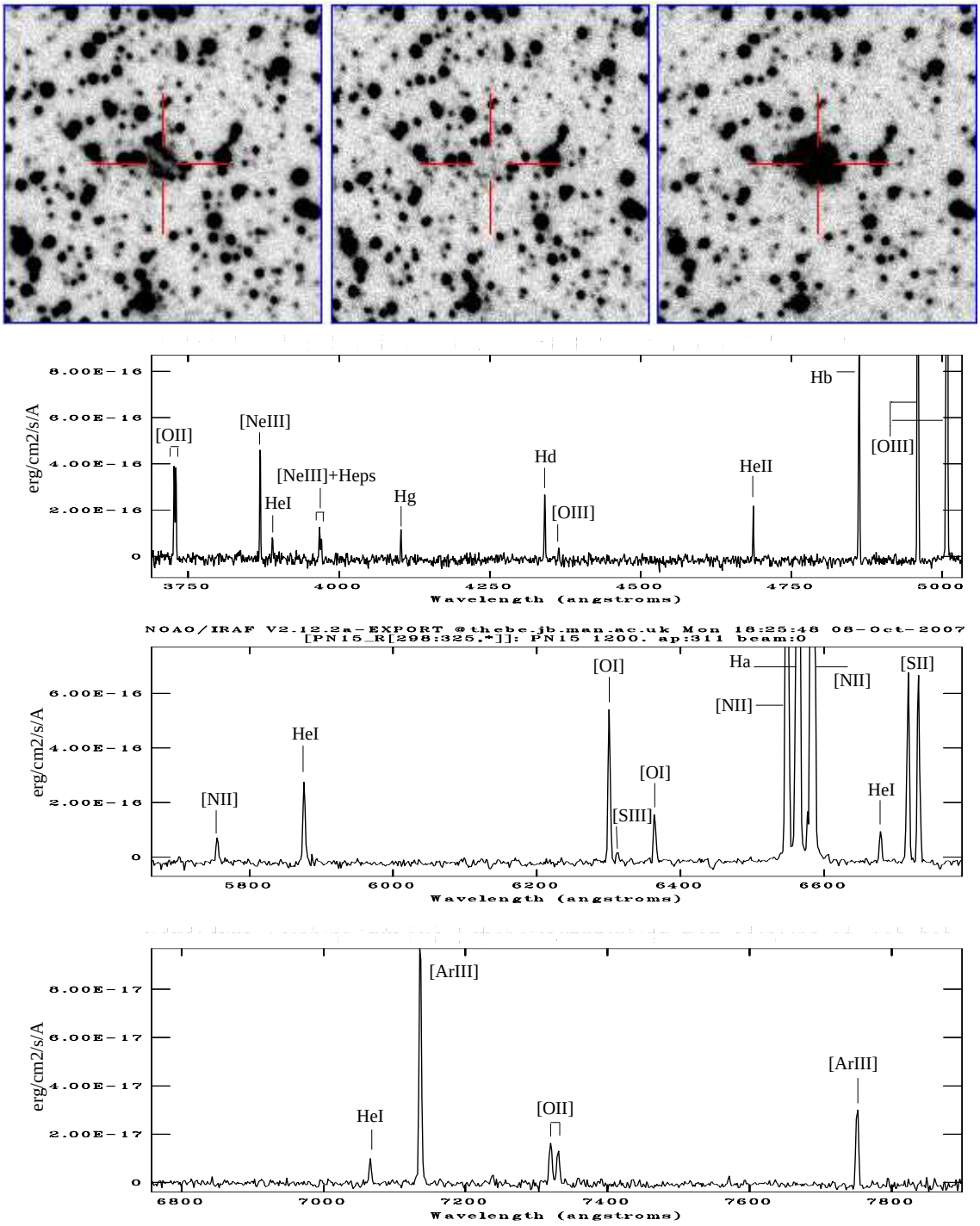

Figure 3.4: **IPHASX J185525.7-004823**. Top: r, i and Hα images with North on top and East on the Left. The total image size is 1 arcmin. Top Panel: Blue spectrum, Middle and Bottom panels: red spectra of the object taken with the WHT.

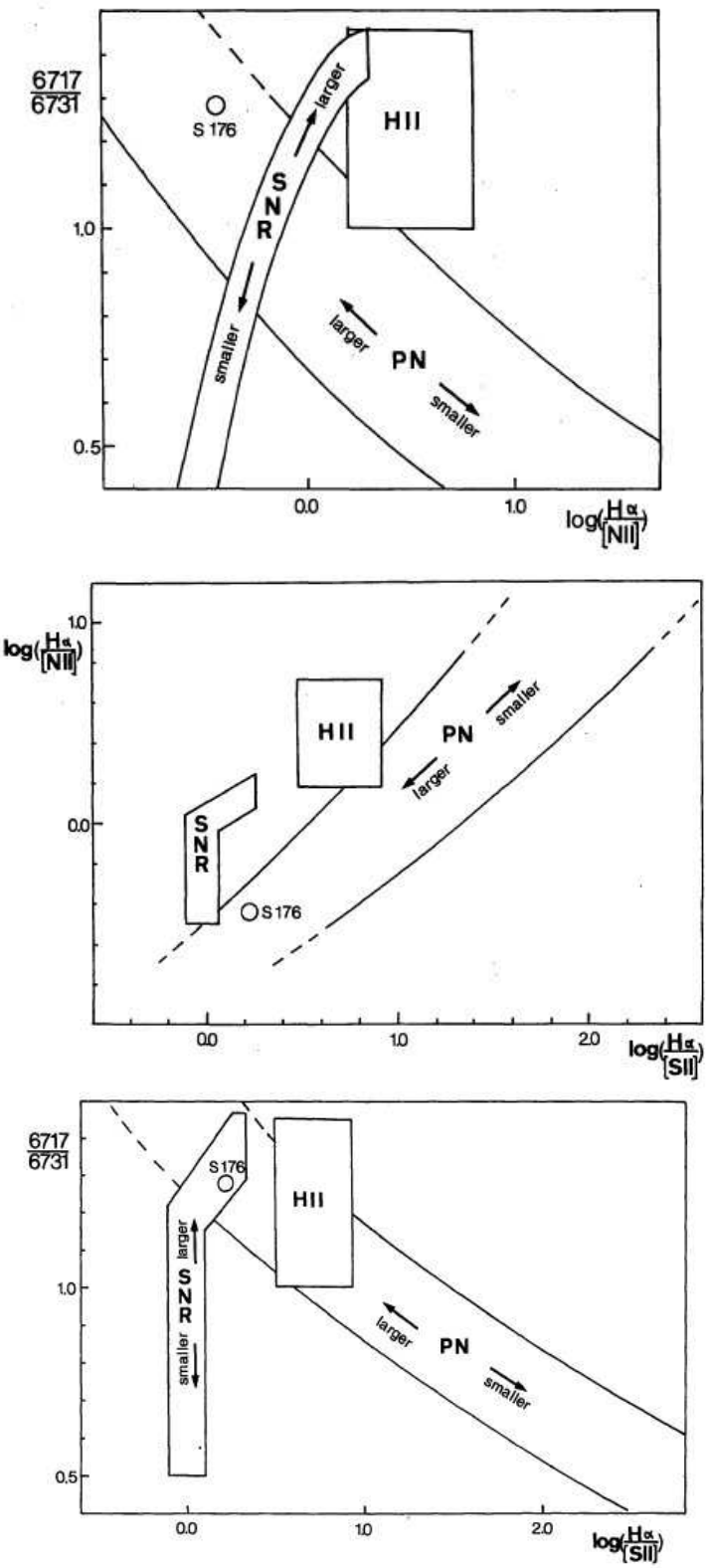

Figure 3.5: Line-ratio diagrams presented by Sabbadin et al. (1977) for the classification of the nebulae S176. Figure reproduced with the authorisation of the editors.

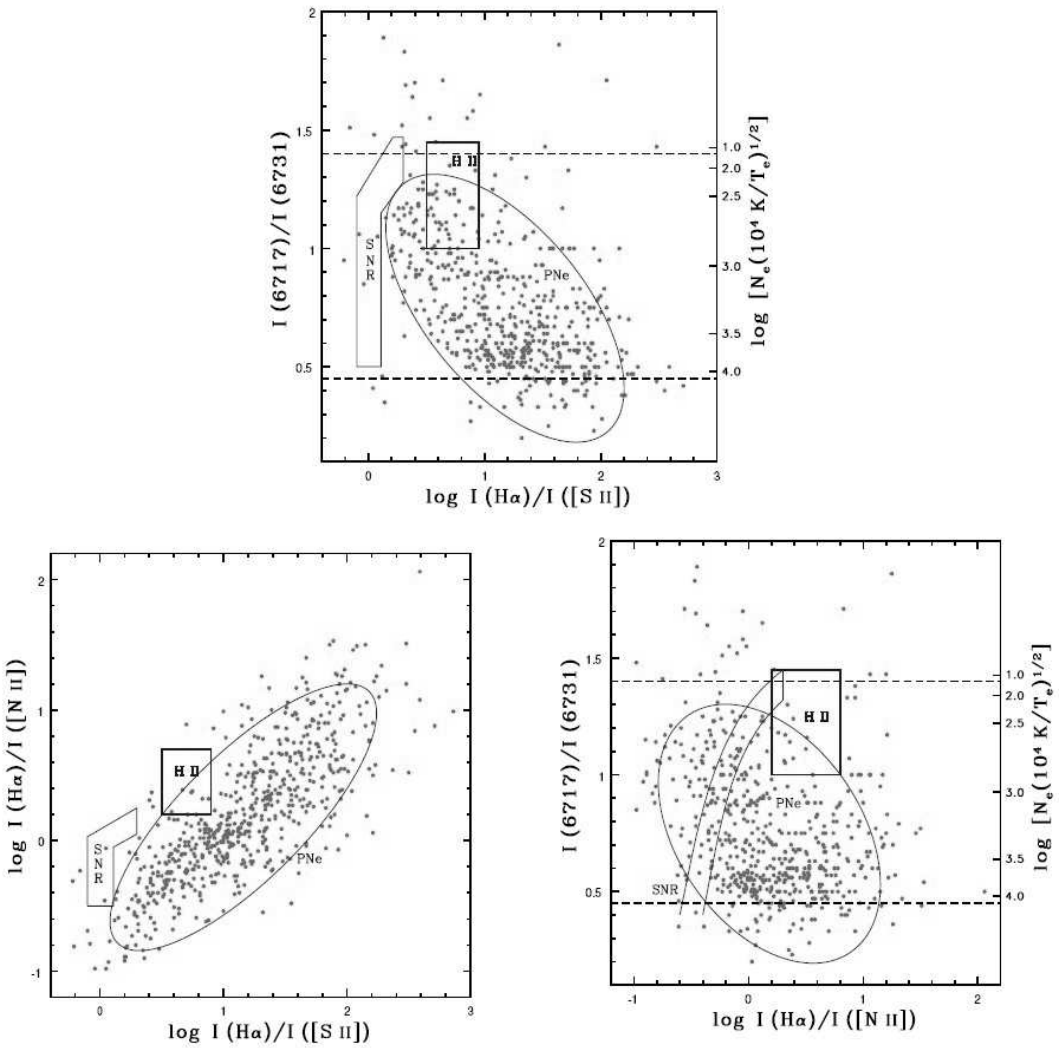

Figure 3.6: New diagnostic diagrams presented by Riesgo and López (2006). Figure reproduced with the authorisation of the editors.

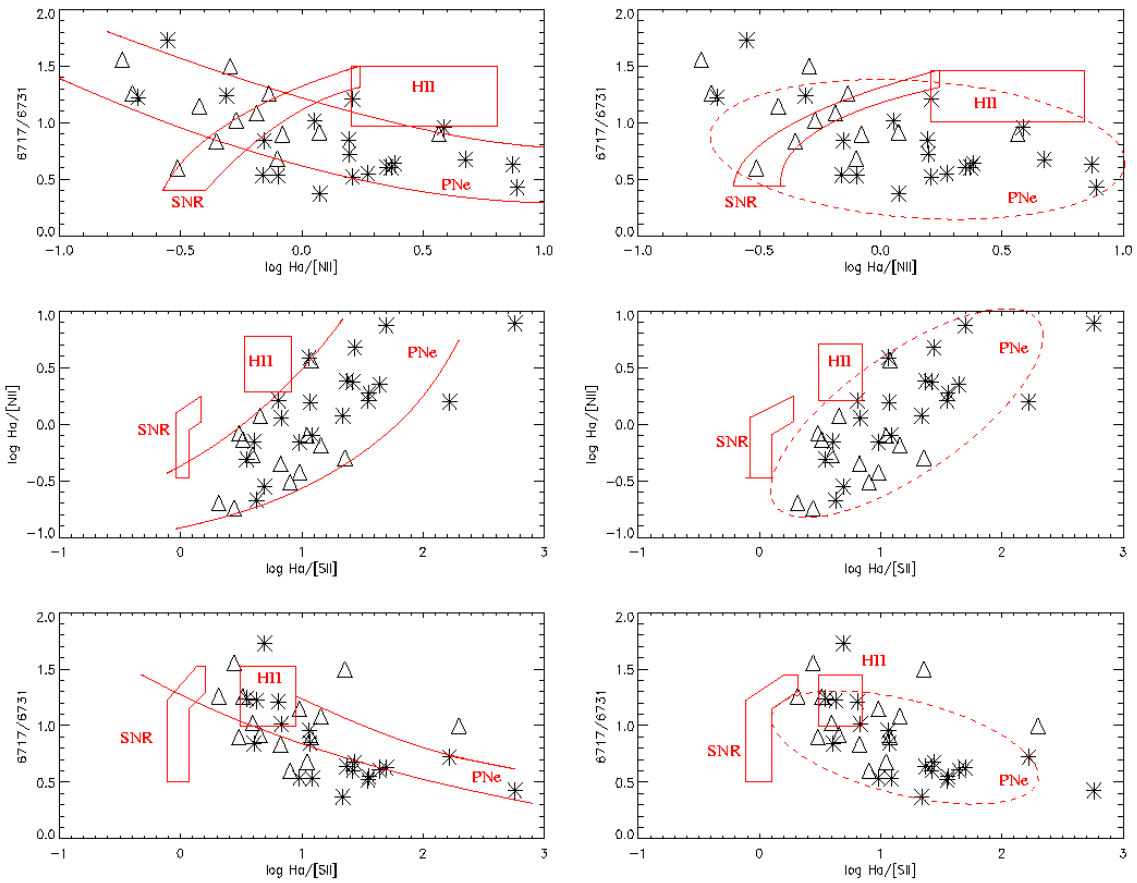

Figure 3.7: Diagnostic diagrams showing the IPHAS data with the Sabbadin et al. (1977) limitations (Left) and Riesgo and López (2006) limitations (Right). The candidate PNe are defined with triangles and the known PNe with asterisks. We only took into account the objects with all the required lines.

Table 3.4: Classification of the IPHAS candidates according Sabbadin et al. (1977) and Riesgo and López (2006).

Name	log(Hα/[NII])	log(Hα/[SII])	[SII]6717/6731	Sabbadin	Riesgo
IPHASX J184336.6+034640	-0.10	1.04	0.68	PN	PN
IPHASX J185525.7-004823	-0.35	0.82	0.83	PN	PN
IPHASX J185925.8+001734	-0.29	1.35	1.50	PN?(1)	PN
IPHASX J191124.8+002743	-0.18	1.15	1.08	PN	PN
IPHASX J191345.6+174752	1.39	2.29	1.00	PN(2)	PN?(1)
IPHASX J191445.1+133219	-0.42	0.98	1.14	PN	PN
IPHASX J192847.1+093439	-0.73	0.31	1.18	PN	PN
IPHASX J193912.0+251105	0.56	1.07	0.90	PN(2)	PN
IPHASX J194359.5+170901	-0.07	0.48	0.89	PN(2)	PN
IPHASX J194751.9+311818	0.07	0.65	0.91	PN	PN
IPHASX J194940.9+261521	-0.27	0.59	1.02	PN/HII/SNR(3)	PN
IPHASX J195248.8+255359	-0.51	0.90	0.60	PN(2)	PN
IPHASX J195657.6+265714	-0.74	0.44	1.55	PN	PN(2)

(1) Out of all boundaries, (2)Only one diagram confirms it as PN, (3) Unclear.

3.2 The IRAS and MSX based classifications

3.2.1 The infrared emission of PNe and the use of colour-colour diagrams

First introduced by Sir F. William Herschel (1738-1822) in 1800 [7], infrared astronomy has been used in the planetary nebulae field only in the last 30-40 years. Hence, after the discovery of strong infrared excess emission from dust in NGC 7027 by Gillett et al. (1967), planetary nebulae have been widely investigated for the presence of cold and warm dust, disc and torus as well as molecules like rotational CO or PAHs. The principal element in the infrared study of the PNe being their IR-colour, we can discriminate different types of objects according their IR properties. For this investigation we used data from the IRAS (Infrared Astronomical Satellite) and the MSX (Midcourse Space Experiment) surveys. Both surveys are space-based and the resulting observations have the advantage that they are not disturbed by atmospheric absorption from water vapour or other types of molecules like CO_2, CO or O_3 nor by the high background level which would otherwise prevent detection of thermal infrared sources.

The IRAS survey (Infrared Astronomical Satellite), launched in 1983 for 11 months had a 60cm telescope on board. It used four broad bands centred on 12μm, 25μm, 60μm and 100μm and all its characteristics are fully described by Beichman et al. (1988). IRAS released point sources, faint sources and small extended sources catalogues, covering more than 96% of the sky, in addition to low-resolution spectra of bright objects. But this IR survey showed some limitations:

- The spatial resolution which is about 5 arcmin is too poor to give any morphological information on distant nebulae. This is one of the *disadvantages* of space telescopes which can only have a limited mirror size. For information, the well

[7] He directed sunlight through a glass prism and measured heat radiation beyond the red of the visible part of the electromagnetic spectrum, corresponding to an invisible form of light.

confirmed IRAS point sources have angular extents less than approximately 0.5' at 12μm, 0.5' at 25μm, 1' at 60μm, and 2' at 100μm.

- The 100μm band has a poor sensitivity and there is a lot of confusion between it and interstellar cirrus. So the reliability of this band is not great, and only the remaining three will be used in our study.

- The uncertainties on the position is typically 2-16 arcseconds, hence in a crowded field the identification of the true IR emitter can be uncertain.

- The flux measurements are not always optimum and a quality factor is assigned to each flux in the associated band as: 3=high quality, 2=moderate quality, 1=upper limit. [8]

Pottasch et al. (1988) demonstrated the differences in the IR colours between HII regions, PNe, OH/IR objects, galaxies and stars (emission lines) (Fig.3.8). HII regions are well separated from the PNe and have a lower $\frac{F25\mu m}{F60\mu m}$ colour ratio, OH/IR stars share a small part of the PNe location but are otherwise well separated with a higher F12μm/ F25μm flux ratio. This is also the case for the galaxies (except the Seyfert ones showing an overlap) and the stars having an high far-IR colour. The useful boundaries taken from Pottasch et al. (1988) diagram are the following: an object is more likely to be PN if its colours are: $\frac{F12\mu m}{F25\mu m} \leq 0.35$ and $\frac{F25\mu m}{F60\mu m} \geq 0.3$, and more likely an HII region if $\frac{F12\mu m}{F25\mu m} \leq 0.3$ and $\frac{F25\mu m}{F60\mu m} \leq 0.3$ (with F the flux in Jansky). Later on Zijlstra et al. (2001) used the ratio R21=log F_{25}/F_{12} vs R32=log F_{60}/F_{25} to separate OH/IR objects, OH-Miras, HII regions, PNe and outflow sources (Fig. 3.9). In the IPHAS survey, we were also likely to find young objects associated with nebulae (like HH and T-Tauri), so we used the IRAS colour diagram by Emerson (1988) which describes the colour ranges for, among other things, "normal" stars ([F25-F12][9]: -0.7 to -0.2, [F60-F25]: -0.9 to -0.4) and T Tauri stars ([F25-F12]: 0.0 to +0.5, [F60-F25]: -0.2 to +0.4).

[8] For more information see: http://lambda.gsfc.nasa.gov/product/iras/colorcorr.cfm

[9] Define the logarithm of the ratio of the fluxes

The distinction between the T Tauri in Emerson's diagram and the OH/IR objects and Outflow Sources in Zijlstra's one, is quite narrow and further investigation would be needed to reveal its true nature.

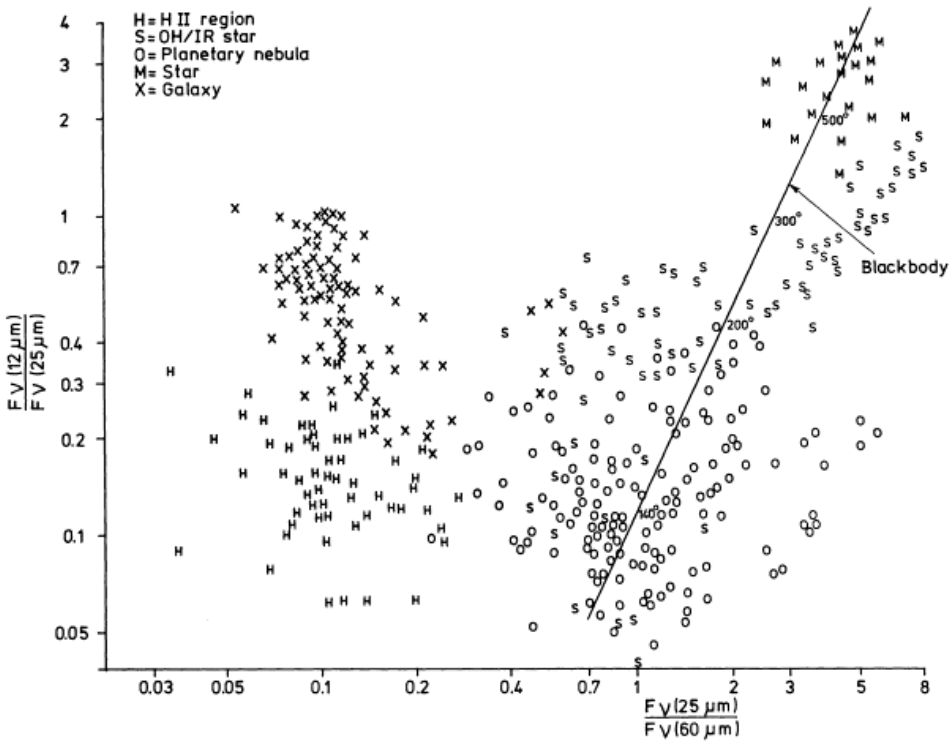

Figure 3.8: IRAS two-colours diagram for various objects from Pottasch et al. (1988). The data are issued from the point source catalogue. Figure reproduced with the authorisation of the editors.

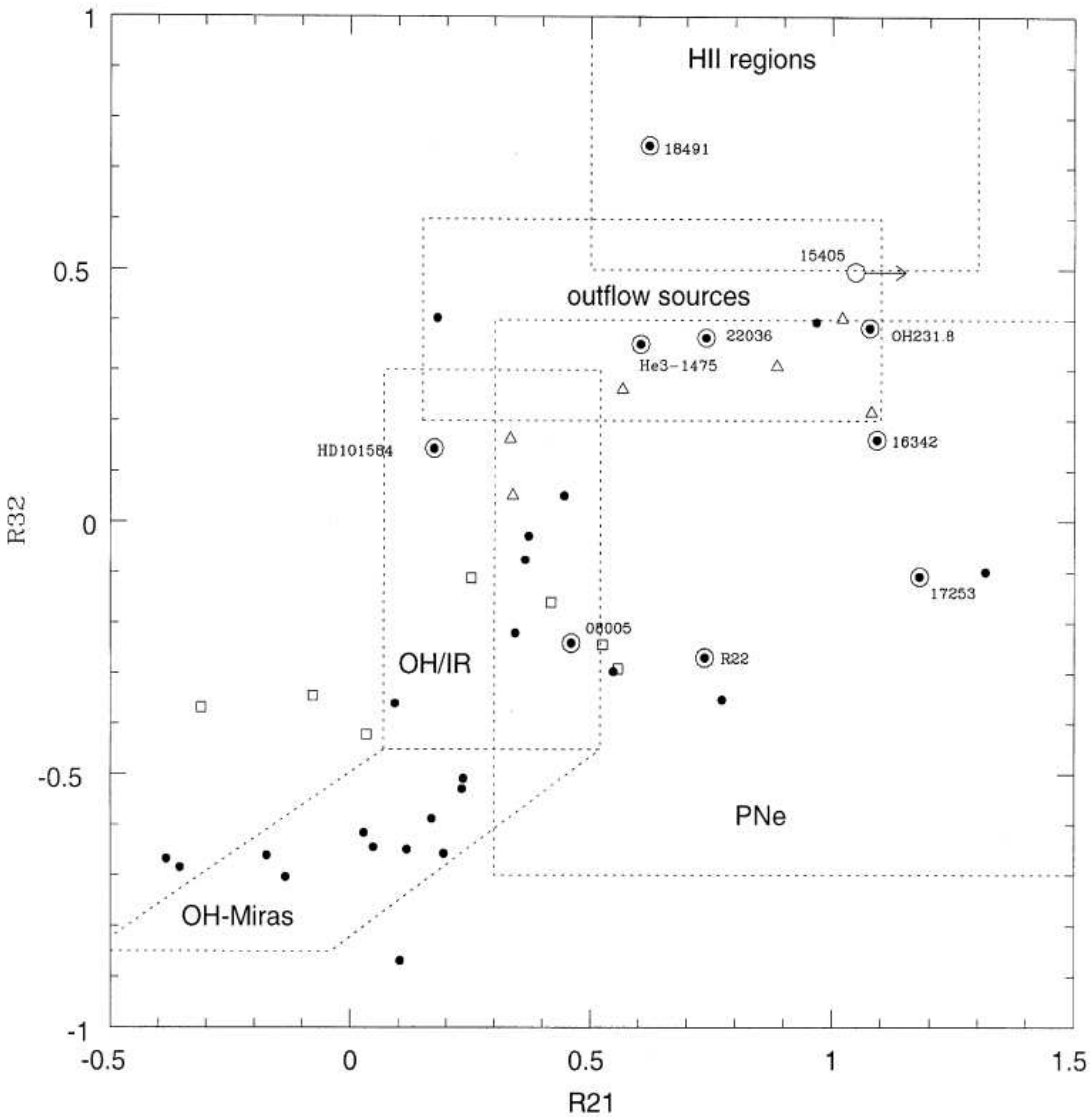

Figure 3.9: IRAS two-colours diagram from Zijlstra et al. (2001) with R21=log F_{25}/F_{12} and R32=log F_{60}/F_{25}. Figure reproduced with the authorisation of the editors.

The MSX survey (Price et al. 2001) of the galactic plane is more recent (the spacecraft was launched in April 1994) and has been designed to cover the Galaxy within b=±5° (Mill 1994). Six bands are used: A, B_1, B_2, C, D and E at 8.28, 4.29, 4.35, 12.13, 14.65 and 21.34μm respectively. The four main bands (A,C,D and E) have a spatial resolution of ~18.3 arcsec and the accuracy on the position is about 2 arcsec.

By comparison with IRAS, MSX has a better spatial resolution, sensitivity (except for the B_1 and B_2 bands) and a wider wavelength coverage. Hence, it provided not only precise data in crowded fields but also allows researchers to derive some morphological information. We did not find in the literature any extensive previous work on planetary nebulae detected or identified with MSX. In 2005, Ortiz et al. (2005), used the MSX data to trace the evolution of AGB stars (O-rich and C-rich), proto-planetary nebulae and planetary nebulae (Fig.3.10). They compared their colour and magnitude in a [14.7]-[21.3] vs [8.3]-[14.7] colour-colour diagram, and found that they can discriminate carbon stars with a blackbody temperature of 800-2000K, a first group of OH/IR objects at lower temperature: 500-800K, and a second group of OH/IR stars at the same location as the transition objects and PNe (400K-300K). The temperatures are relative to the dust.

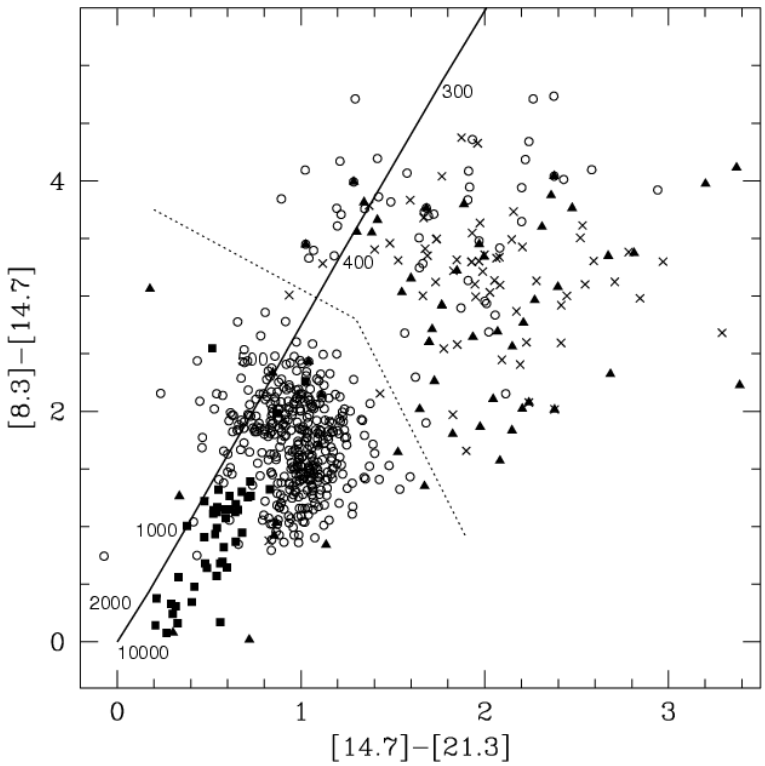

Figure 3.10: MSX colour-colour diagram from (Ortiz et al. 2005). The symbols are the following: carbon-rich stars (squares), OH/IR objects (open circles), transition objects (triangles), and planetary nebulae (crosses). Figure reproduced with the authorisation of the editors.

3.2.2 The IRAS results

Among the 233 PN candidates we could find an IRAS counterpart with enough confidence in 39 of them. By enough confidence we mean: a location of the infrared source within less than 10” from the designated object if the latter is isolated. In the case of a crowded area the IR source must coincide with the centre of the nebula or its brighter part. Although this works well for “compact” sources i.e. with a diameter lower than ∼1 arcmin, it becomes more difficult with really extended targets, and most of them were discarded. We used the point sources catalogue for our purposes. We discarded the 28 candidates with a quality flux equal to 1 in the band used to establish the diag-

nostic diagrams. We ended up with 11 candidates whose colours were compared with known PNe localised in the same area and ruled by the same flux quality law. The results are summarised in Table 3.5.

We found that according to Pottasch et al. (1988) (Fig.3.12), 4 candidates are "fully" defined as PNe (Fig. 3.13), 3 are "fully" defined as HII regions and 3 have the IRAS colours of galaxies. The presence of a known PN in the "Galaxy area" shows the possibility for the latter objects to be true PNe. The remaining candidate in our list does not find any classification in Pottasch et al. (1988)'s diagram, it fills the gap at $0.2 < F25/F60 < 0.4$ and $F12/F25 > 0.3$, between the well separated galaxies and OH/IR-PNe.

Zijlstra et al. (2001)'s diagram (Fig.3.11) allowed us to identify 4 PNe, 2 of which have a "dual" classification (mostly Outflow sources and PNe, one object also has the colour of a T-Tauri star). These four candidates correspond to the four ones defined as PNe in the Pottasch et al. (1988) diagram. This correspondence is also found for the 3 candidates classified as HII regions in Zijlstra et al. (2001)'s diagram. The 3 objects with the IRAS colours of galaxies in the Pottasch et al. (1988) diagram (IPHASX J192458.2+193434, IPHASX J192624.7+195045 and IPHASX J193912.0+251105) are outside of all known boundaries in Zijlstra et al. (2001) as well as the remaining candidate (IPHASX J195919.6+283827) with no classification in any of the diagrams. The diagrams show that these four "unknown" candidates have a particular location in both diagrams. The study of their IR-excess due to thermal radiation of circumstellar dust may help to determine their type. Hence, we introduced to Zijlstra et al. (2001)'s diagram, the IRAS data obtained for a group of Proto Planetary Nebulae (PPNe) or Post-AGBs localised in our area (Fig.3.11). The data have been obtained in the "Torùn catalogue of Galactic post-AGB and related objects" (Szczerba et al. 2007) [10]. We did not find any correlation with the location of our candidates, which showed a generally higher contribution of their 60μm flux for a similar 12μm flux as the group PNe/PPNe. A discussion about this characteristic is given in chapter 5 of this thesis.

[10] http://www.ncac.torun.pl/postagb

In conclusion the matching of our data with the IRAS catalogue only allowed us to classify 4 objects as PNe. The other few objects with available and valid data are either HII regions or objects whose characteristics do not fit with the well known diagnostic diagrams generally used. The IRAS catalogue does not provide optimum results for our identification.

Table 3.5: Results of the IPHAS/IRAS diagnostic diagrams.

Name	Size (arcsec)	F25/F60	F12/F25	log F25/F12	log F60/F25	Pottasch (1988)	Zijlstra (2001)
IPHASX J183911.8+010624	6	0.410	0.364	0.438	0.386	PN	T-Tauri/PN/Outflow
IPHASX J184336.6+034640	18	0.612	0.284	0.545	0.213	PN	PN/Outflow
IPHASX J184800.6+025420	67	0.686	0.170	0.767	0.163	PN	PN
IPHASX J185627.9+005550	48	0.431	0.313	0.503	0.365	PN	PN
IPHASX J192140.4+155354	13	0.257	0.065	1.186	0.588	HII	HII
IPHASX J192458.2+193434	29	0.070	0.307	0.512	1.154	Galaxy	Unknown
IPHASX J192624.7+195045	20	0.087	0.396	0.402	1.059	Galaxy	Unknown
IPHASX J193912.0+251105	38	0.097	0.335	0.474	1.011	Galaxy	Unknown
IPHASX J194815.0+280730	4	0.195	0.115	0.937	0.708	HII	HII
IPHASX J195015.9+272859	202	0.177	0.286	0.542	0.751	HII	HII
IPHASX J195919.6+283827	520	0.221	1.393	-0.144	0.655	Unknown	Unknown

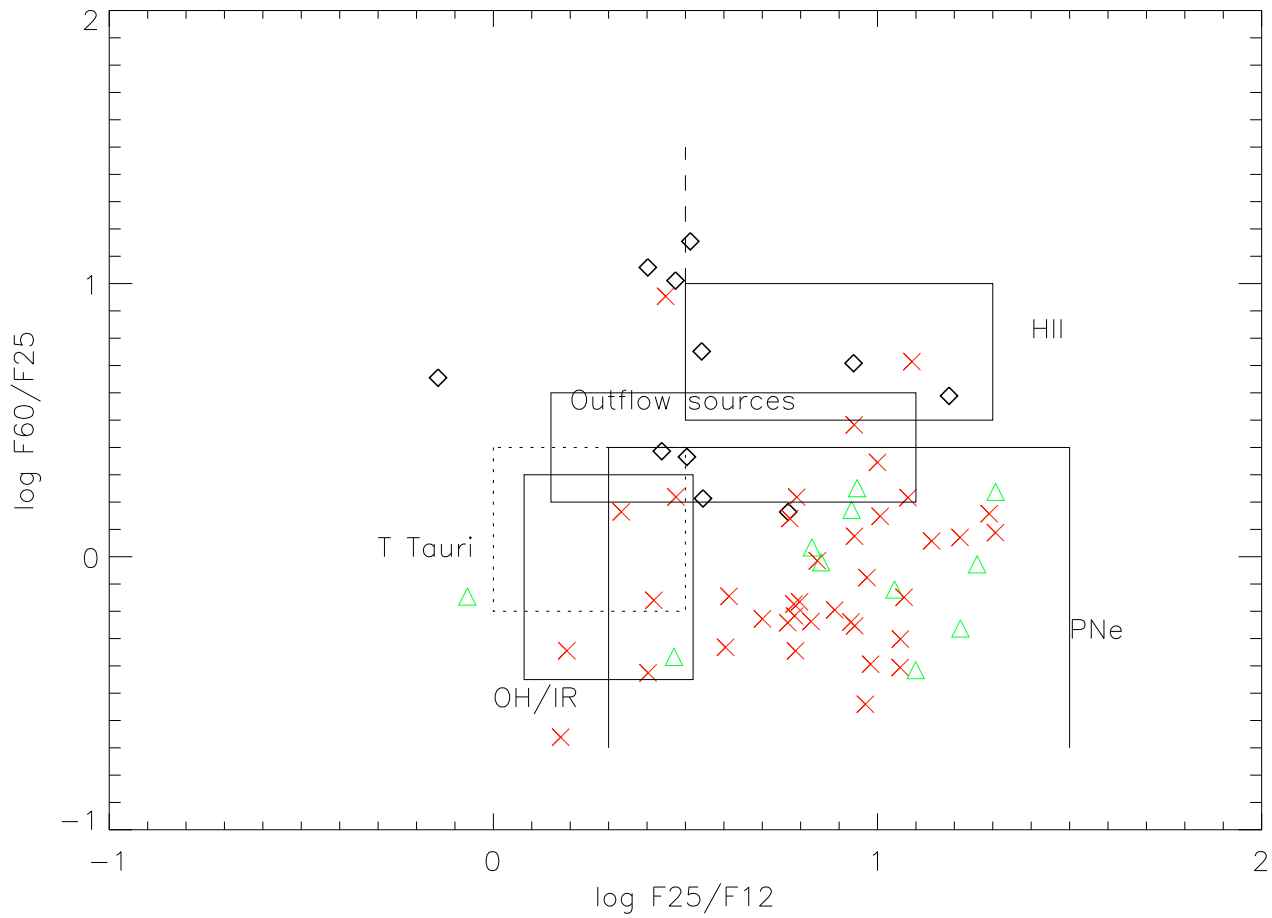

Figure 3.11: IRAS two-colour diagram from Zijlstra 2001, for evolved stars and Emerson 1987, for young stars. The diamonds represent the IPHAS candidate PNe, the red crosses show the known PNe location and the green triangles represent the PPNe.

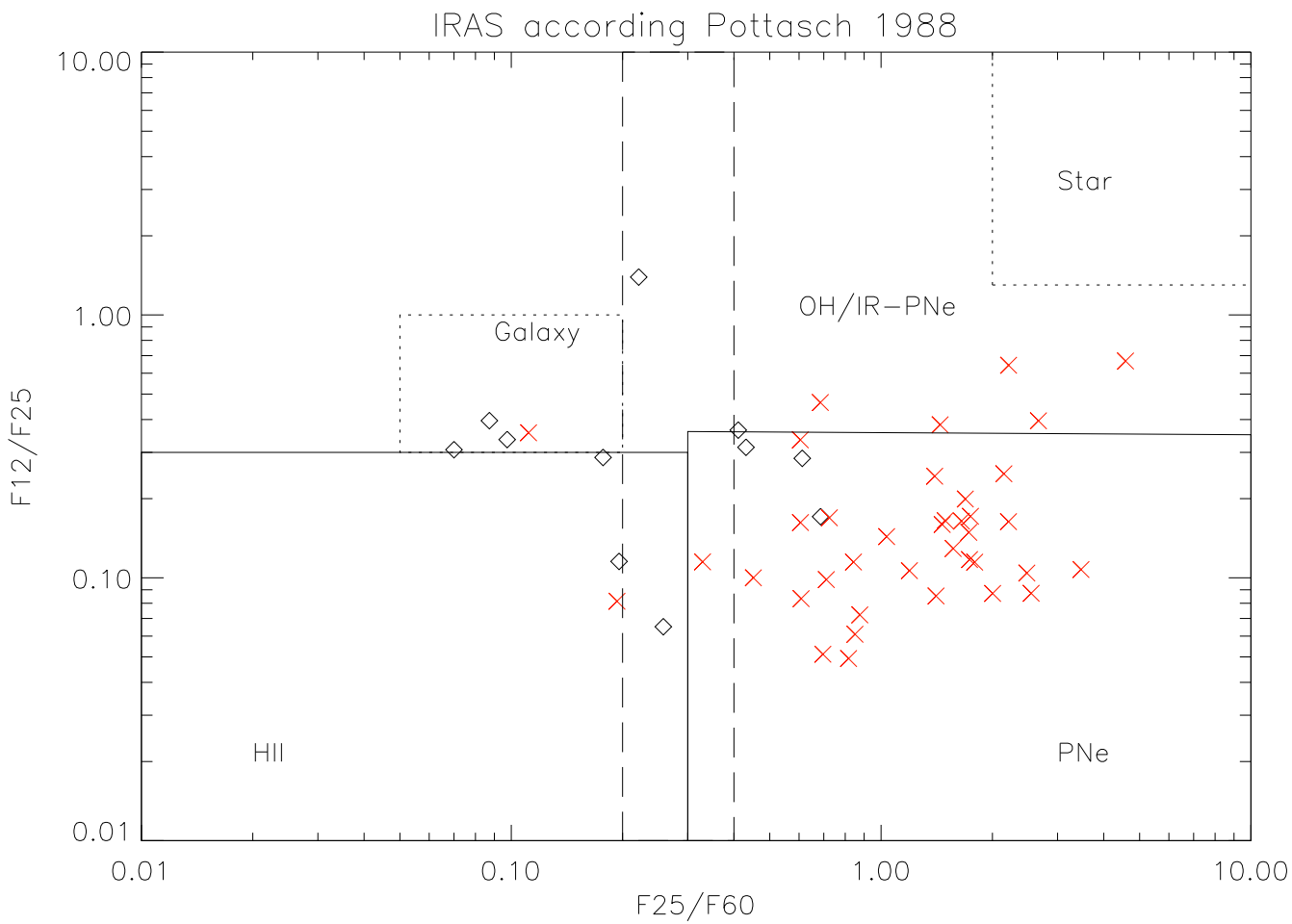

Figure 3.12: IRAS two-colour diagram from Pottasch 1988. The diamonds show the IPHAS candidate PNe and the red crosses show the known PNe location.

3.2.3 The MSX results

Among the 233 candidate PNe we found a genuine MSX positional counterpart for 27 of them i.e within the limit of the MSX accuracy and extending the research area up to 10”. The MSX targets were chosen first according their positional accuracy with the central part of the candidate nebula or its brighter part (this method discards very extended and faint nebulae), then according the quality of the measurement in each band. We chose the highest quality for the band used, hence we avoided the dataset giving only an upper limit i.e.1. The MSX flags are classified as follow: 4=excellent, 3=good, 2=fair, 1=limit, 0=not detected. The known PNe found in the area were also plotted. Their selection follows the same quality criteria as the candidate PNe. Of the 27 targets, only 10 showed an effective observed flux allowing their use in a diagnostic diagram and complying with our quality flux criterion. We used the bands A, D and E at the respective wavelengths 8.28μm, 14.65μm and 21.34 μm to fit with the criteria described by Ortiz et al. (2005) in their classification of evolved objects. The zero-magnitude flux densities used to derive the magnitude are 58.49 Jy in band A, 18.29 Jy in band D and 8.80 Jy in band E. As a result (see Table 3.6 and Fig. 3.14), 8 candidates can be classified as PNe (or PPNe) (Fig. 3.15)and the remaining two are classified as OH/IR objects. If we compare these results with the IRAS ones we can see a convergence for IPHASX J184336.6+034640 and IPHASX J184800.6+025420 which can be considered as PNe due to their infrared colours. But IPHASX J192140.4+155354, IPHASX J193912.0+25110 and IPHASX J194815.0+280730 which are defined as PNe or PPNe in the MSX survey are respectively classified as HII region, nebula of unknown nature and HII region using the IRAS diagram.

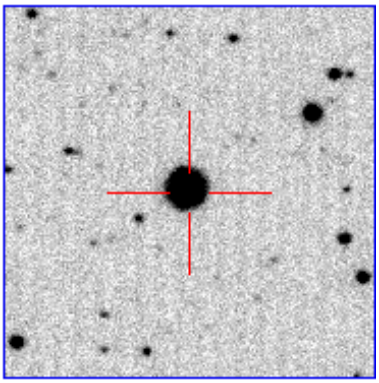

IPHASX J183911.8+010624

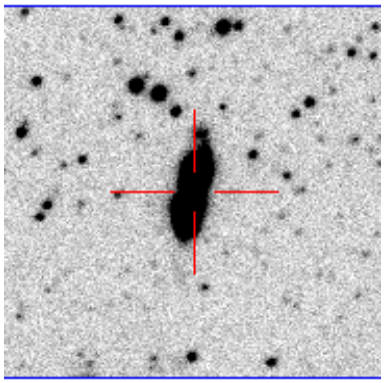

IPHASX J184336.6+034640

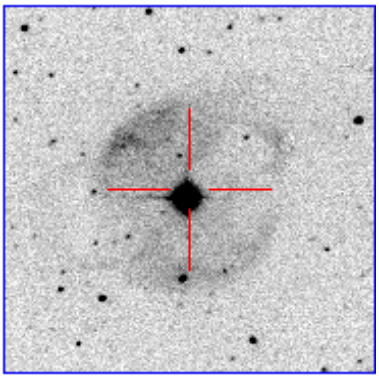

IPHASX J184800.6+025420

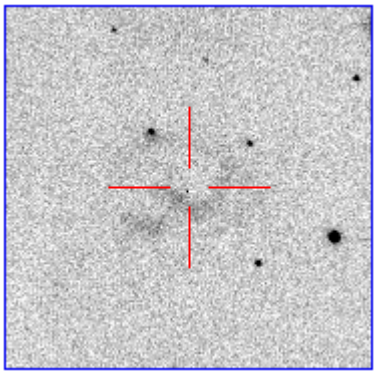

IPHASX J185627.9+005550

Figure 3.13: IPHAS planetary nebulae identified within the IRAS classification scheme. Hα+[NII], Top images: 1×1 arcmin, Bottom images: 2×2 arcmin. North on the top and East on the left.

Table 3.6: MSX identification of IPHAS sources.

Name	Size (arcsec)	Offset with MSX position (arcmin)	Identification
IPHASX J184336.6+034640	18	0.109	PNe-PPNe-OH/IR
IPHASX J184800.6+025420	67	0.033	PNe-PPNe-OH/IR
IPHASX J184932.6-004437	96	0.413	PNe-PPNe-OH/IR
IPHASX J185225.5-003326	8	0.004	PNe-PPNe-OH/IR
IPHASX J191017.4+065258	6	0.019	OH/IR
IPHASX J192038.9+160224	63	0.309	OH/IR
IPHASX J192140.4+155354	13	0.018	PNe-PPNe-OH/IR
IPHASX J192256.9+140700	68	0.178	PNe-PPNe-OH/IR
IPHASX J193912.0+251105	38	0.139	PNe-PPNe-OH/IR
IPHASX J194815.0+280730	4	0.010	PNe-PPNe-OH/IR

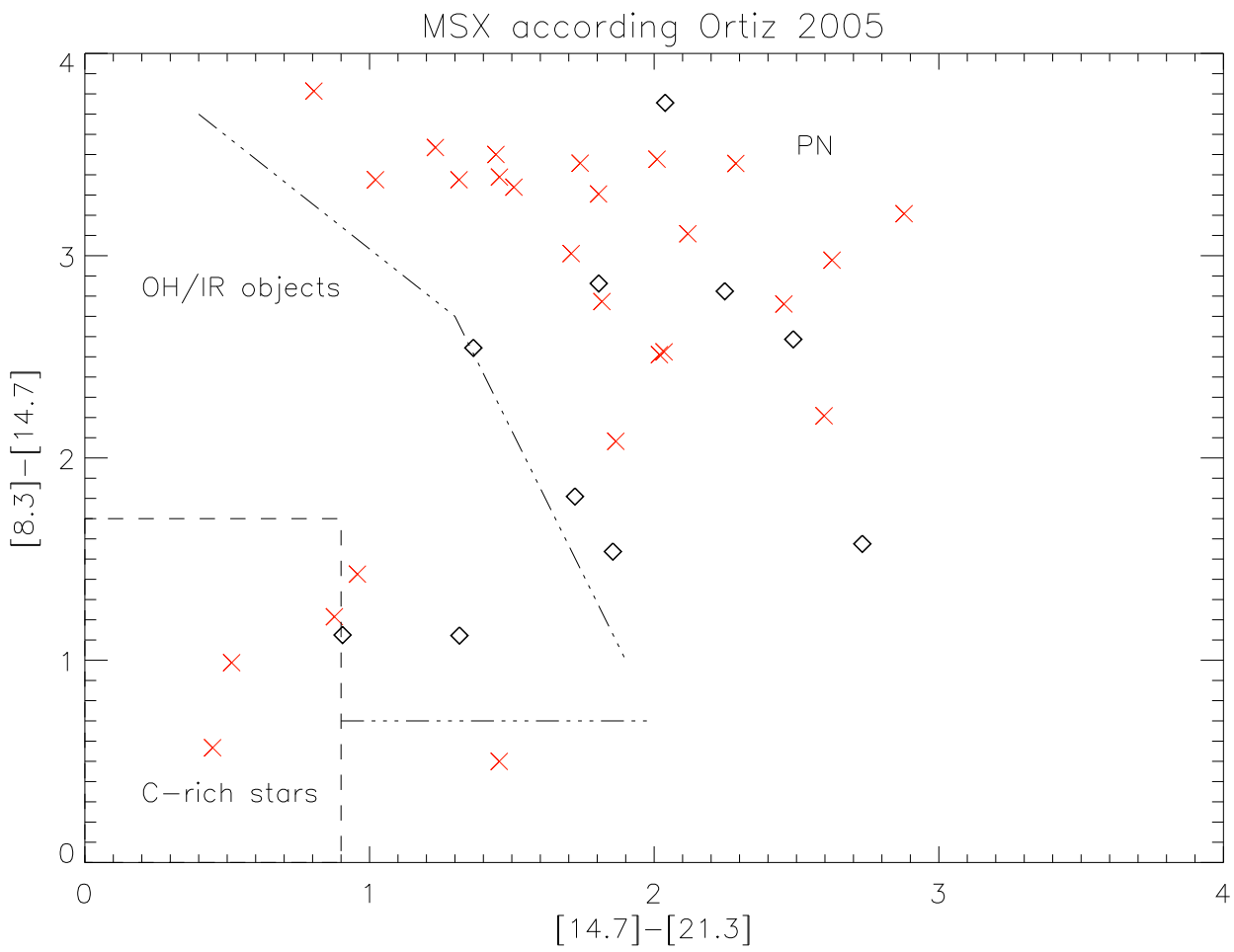

Figure 3.14: MSX colour diagram following Ortiz 2005. The diamonds refer to our candidate PNe and the crosses to the known PNe in the same sky area.

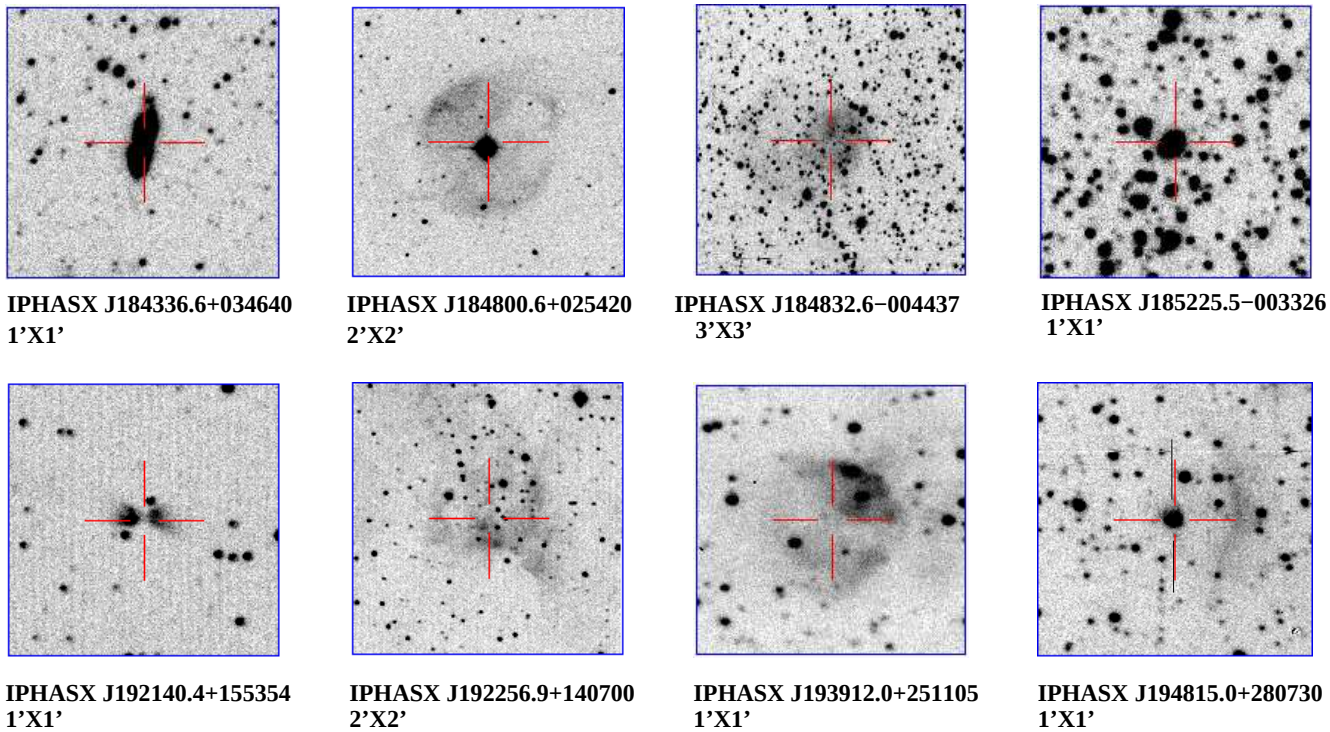

Figure 3.15: IPHAS planetary nebulae identified within the MSX classification scheme. Hα+[NII] with North on the top and East on the left.

3.3 The radio based classification

Another method used to discriminate between our objects is the use of their radio fluxes. Radio continuum radiation in planetary nebulae is due to free-free radiation. This corresponds to the emission (or radiation) resulting from the acceleration of a free electron when deflected by an ion. The electron remains free after the process. Due to their large wavelengths, much larger than the particle size of the dust, radio data are not altered by interstellar extinction.

Planetary nebulae do not generally show a strong emission in the radio band, in contrast to HII regions. The latter are usually more luminous, have higher mass and therefore have much more material which can be ionised. Moreover, as PNe evolve they become transparent (decrease of the flux) while HII regions maintain their flux much longer. Hence we will typically find PNe with a radio flux lower than ~60 mJy at 6 cm (5 GHz) (Ratag et al. (1990) (Fig. 3.16) and Zijlstra et al. (1990)) (data obtained for PNe in the Bulge at ~8 kpc: most of the PNe are located in this range). Radio data cannot be used as a single tool to determine the nature of a nebula and should be complemented by IR or optical observations. We can identify 2 different groups from their radio flux intensity. In the first group we can include HII regions and SNR, in the second we find the PNe, YSOs and Herbig Haros (Chan et al. (1996) and Curiel (1995)). This is a general approximation and some objects do not follow this rule. In that sense, the boundary between PNe and HII is not strict and some very bright PNe would show a strong radio flux like NGC 7027 with 6370 mJy at 6 cm (Pottasch 1984). In the same way we can have faint HII regions like Sh 1-118 with 21 mJy at 6cm (Zijlstra et al. 1990). We also note that a large fraction of the radio data about PNe concerns those located in the Galactic Bulge and therefore any global study based on these values can be biased.

Most of the data we were working with in the PN field were taken with the VLA. The latter, located in New Mexico (US), is an interferometer combining 27 radio an-

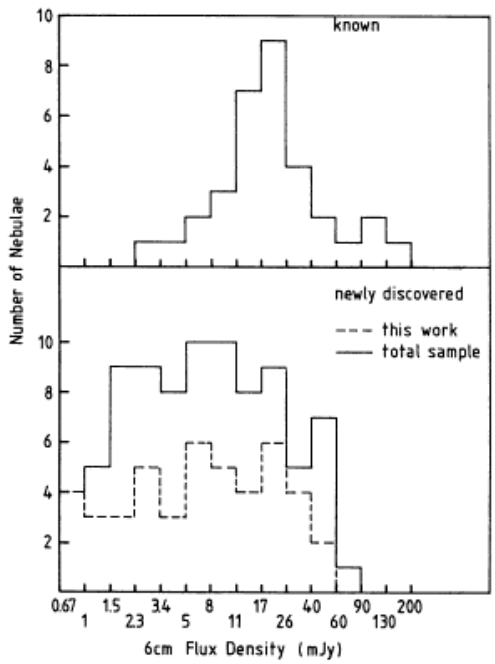

Figure 3.16: Histogram from Ratag et al. (1990) showing the 6cm flux density distribution of known PNe in the galactic bulge (top panel) and their new PNe (bottom panel). The data are from the VLA. Figure reproduced with the authorisation of the editors.

tennas in a Y-shape, each antenna having a 25m diameter. Several configurations are possible and each of them define an array. Hence we have the A array, with a maximum antenna separation of 36 km; B array with 10 km; C array with 3.6 km and D array with 1 km. The VLA covers a radio range from 4 to 50,000 MHz (i.e from 400 to 0.7 cm) separated in bands. The bands most used are those named L and C with the characteristics listed in Table 3.7[11].

A well known radio survey in the northern hemisphere is the NVSS survey meaning NRAO VLA Sky Survey (Condon et al. 1998). Operating from 1993 to 1996, the survey scanned the sky at 1.4 GHz and had a sensitivity limit of ~2.5 mJy beam^{-1}, a 45 arcsec FWHM resolution and used the D configuration of the VLA. We therefore

[11]Data obtained at http://www.vla.nrao.edu/genpub/overview/

Table 3.7: VLA characteristics for data taken at 6 cm and 21 cm.

Band	L	C
Frequency range (GHz)	1.34-1.73	4.5-5.0
Wavelength (cm)	20	6
Primary beam (arcmin)	30	9
Highest resolution (arcsec)	1.4	0.4
System Temperature (K)	37-75	44

compared our list of candidates, more precisely their optical position, with the NVSS database, which includes the radio sources values and the associated maps. We found a good correlation for 60 objects. The accuracy on the position, implying the true correspondence between the PN candidate and the radio source, can be difficult depending on the size of the nebulae. The “compact” ones have less than 5” offset with respect to the optical position, providing of course that the object is not in a crowded area, where it is more difficult to distinguish the emitter. The offset can become wider for more extended sources and we relied on the radio maps to confirm the coincidence (althought the VLA can become insensitive for very extended and faint sources). The results are shown in Table 3.9 at the end of this section. In order to compare the behaviour of the IPHAS objects with known PNe we also added the NVSS data for 95 confirmed PNe found in the same sky area.

In Fig.3.17, the distribution of the candidate PNe is plotted against the distribution of the known PNe. We found that there are proportionally slightly more candidates (77%) with a low radio flux i.e up to 20 mJy than known PNe (64%) in the same region. Between 20 mJy and 60 mJy, the tendency is inverted and we found more known PNe (25%) than candidates (15%). Finally, slightly more confirmed PNe (11%) have a high radio flux, i.e. greater than 60 mJy, compared to the candidates (8%). The general trend observed for the PNe is confirmed for the IPHAS nebulae with a decrease in the number of objects and with an increase of the radio flux. The mean radio flux

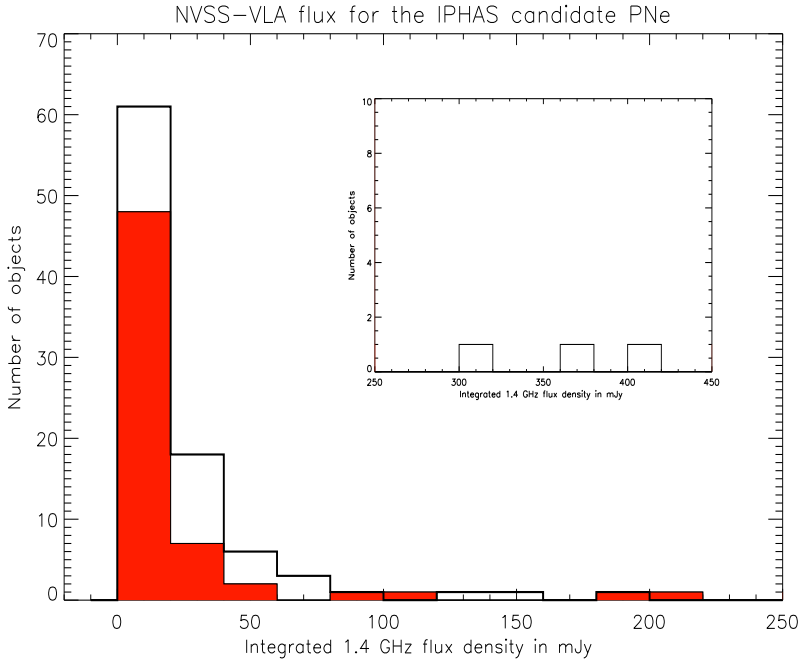

Figure 3.17: Results of the NVSS/VLA survey applied to 60 IPHAS targets (red) and 95 confirmed PNe (thick black line delimitation). For display purposes we do not show the only candidate with a flux of 5419.1 mJy.

for our candidate PNe is 107 mJy if we include the relatively high flux of IPHASX J192349.9+143330 with 5419.1 mJy, and decreases to 20.6 mJy without this object, compared to the mean 33.9 mJy for the known PNe. In conclusion, **IPHAS nebulae have a generally lower radio flux than the previously known PNe**. This low flux can be accounted for a large expansion of the nebulae and therefore a more advanced evolutionary stage.

In the framework of this radio analysis, we also derived the brightness temperature (T_b) at 1.4 GHz of the candidate PNe, which corresponds to the temperature of the radio surface (and is independent of the distance to the nebula). T_b is defined as:

$$T_b = \frac{c^2}{2\pi k \nu^2} \frac{S_\nu}{\theta_r^2} \tag{3.5}$$

with c the speed of light, k the Boltzmann constant, S_ν the flux in mJy and θ_r the angular radius in arcsecond. We also added to our data, the measurements done for the previously mentioned known PNe and those of 37 HII regions located in the sky area we are studying, taken from the "Catalogue of H II Regions" from Sharpless (1959a). The corresponding optical thickness τ_ν is linked to T_b by the relation :

$$T_b = T_e(1 - e^{-\tau_\nu}) \tag{3.6}$$

with T_e the electronic temperature (K) set at 10 000 K. If we go through the literature we hardly find PNe for which 1.4 GHz fluxes have been used to derive T_b. Instead the 5 GHz fluxes are generally used (e.g. van de Steene and Zijlstra (1995), Zijlstra et al. (1989) and Siódmiak and Tylenda (2001)), as it provides a better resolution. Therefore we convert our depth to that at 5GHz, and recalculate the brightness temperature at 5GHz, knowing that:

$$\tau_\nu = \tau_0(\nu/\nu_0)^{-2.1} \tag{3.7}$$

with τ_0 the optical thickness at the reference frequency ν_0 i.e. at 1.4 GHz.

Figure 3.18 shows the distribution in brightness temperature for IPHAS nebulae, known PNe and HII regions. Planetary nebulae follow a clear $1/\theta^2$ trend with a decrease of T_b while the angular size increases. This trend reflects a biased effect as we worked with known objects in the sky area (of study) with available radio data, hence nebulae surely exist below the curve, like more compact PNe, but we have no indication of their radio fluxes. While most of the PNe are located on the left part of the graphic (with their angular diameter lower than ~50 arcsec), the HII regions are mostly located away from the curve described by the PNe and have larger dimensions. We noticed first that we do find PNe in the "HII area" and then, our sample of HII regions does not contains ultra-compact objects which may be located in the "PN area". The IPHAS nebulae are for the majority in agreement with the PNe location, although some are

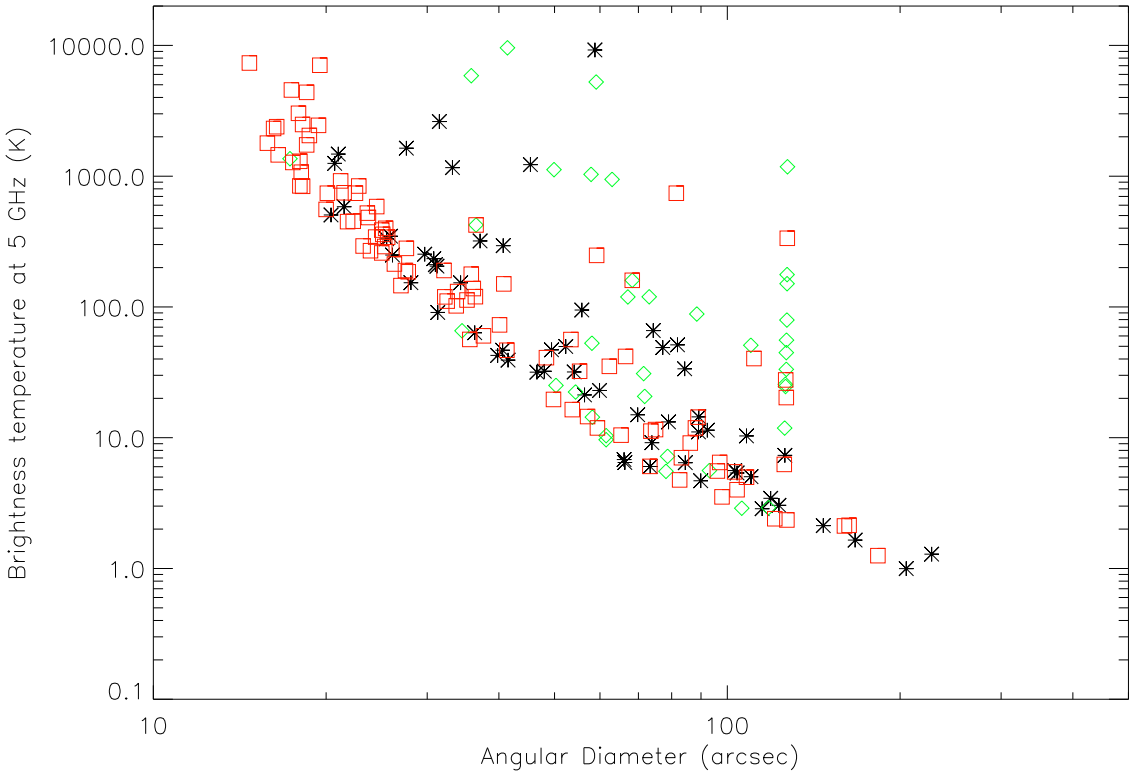

Figure 3.18: Brightness temperature evolution of the IPHAS targets (asterisk), the confirmed PNe (red square) and the HII regions (green diamond) according their size.

found in an "intermediate zone" between the PNe and the HII regions. It is therefore more difficult to define their nature. But one IPHAS nebula shows a clear location in the "HII area". Indeed, IPHASX J192349.9+143330 (Fig. 3.19) has a very high brightness temperature of 9230 K and a large radio size and is very likely a HII region. This classification is corroborated by a high radio flux of 5.4 Jy. We note a caveat in the use of "known objects", given the misclassification which can occur i.e. some of the known PNe may be in fact HII regions.

In term of radio surface brightness (RSB) (see Fig.3.20), we observed that there are proportionally more IPHAS nebulae with a lower RSB than confirmed PNe. Hence while 95% of the candidates have a RSB between 0 and 0.02 mJy/arcsec^2, only 70%

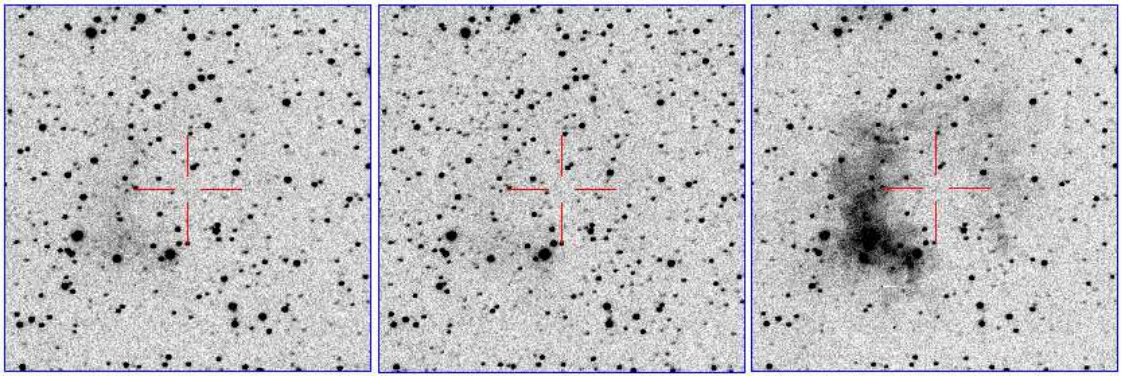

Figure 3.19: r, i and Hα images of the newly discovered HII region IPHASX J192349.9+143330. Image size: 3×3 arcminute, with the North on the top and the East on the left.

of the known PNe are in this interval. The 30% left of the known PNe spanned up to a RSB of 0.24 mJy/arcsec^2, while the remaining 5% candidate PNe have a RSB of 0.04 mJy/arcsec^2. The faintness of the IPHAS sources, which has nothing to do with interstellar extinction, can be accounted for by larger size and then a greater evolutionary stage: extended sources are likely to have a low surface brightness. By comparison, the known PNe are generally brighter and younger.

Although, in most of the cases, we cannot derive the precise nature of a nebula, we can estimate the likelihood of it being a planetary nebula. This is based on 3 criteria:

- The position on the T_b vs size diagram.
- The limiting flux for a larger sample of known planetary nebulae.
- The flux delimitation between a larger sample of PNe and HII regions.

For our purpose we used all the PNe found in the VLA survey by Condon and Kaplan (1998) and all the HII regions from the “Catalogue of H II Regions” from Sharpless (1959a) with available fluxes. This added up to 833 PNe and 160 HII regions.

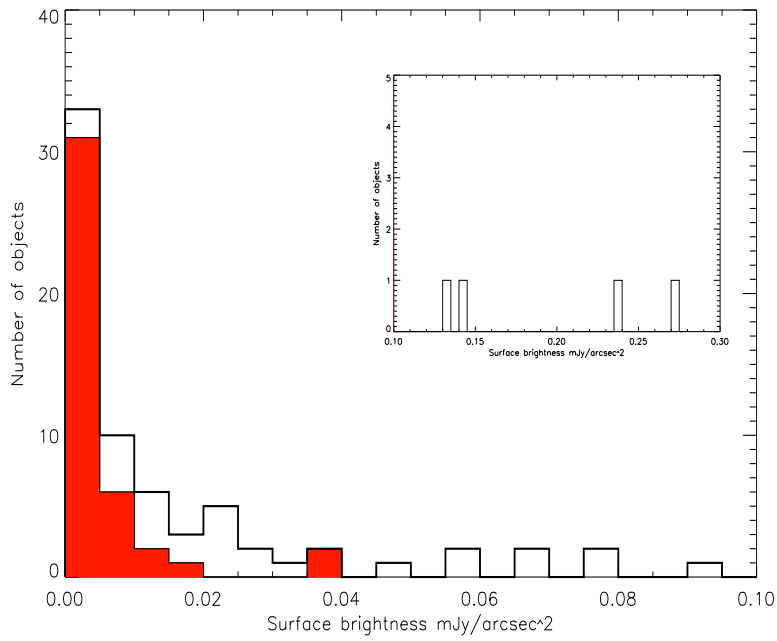

Figure 3.20: Comparison of the radio surface brightness of the IPHAS targets (red) and the known PNe (black delimitation).

Figure 3.21 shows the boundaries (quoted L1, L2, L3 and L4) we established to differentiate both populations. First, the concentration of PNe decreases as we move away from the boundary L1 i.e from L1 to L3. In the range [L1,L2], the probability for an object to be a PN is higher than above L3, where the probability for an object to be a HII region is higher. The range [L2,L3] is an intermediate zone where it is more complicated to determine the nature of the nebulae. The boundary L4 separates the nebulae according their angular diameter. Hence, on the left of L4 (size $< \sim 35$”), we only find PNe and on the right (size $> \sim 35$”) both populations are found. The association of the 4 borders forms a grid which will help to better determine the location of PNe and HII regions, or at least to estimate the probability for a nebula to be either a PN or HII region according to its location on the net. Therefore we defined 5 zones, whose characteristics are listed in Table 3.8.

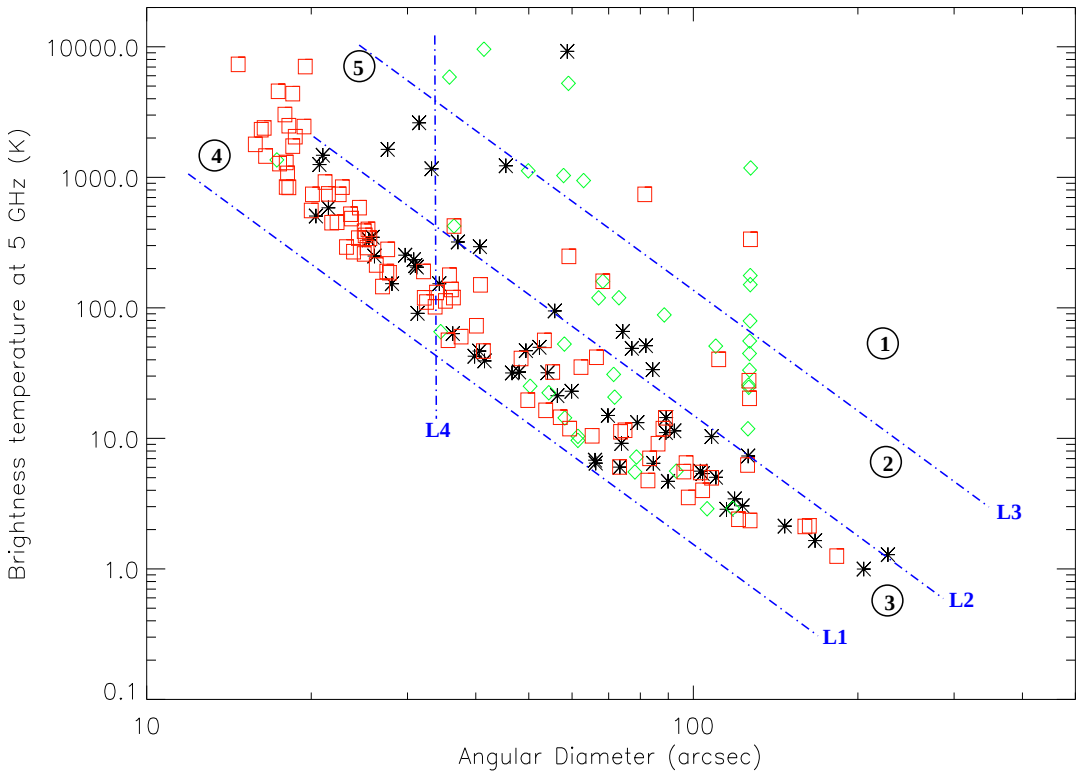

Figure 3.21: Limits on the location of PNe and HII regions on the T_b vs size diagram.

Table 3.8: Probability on the nature of the nebulae occupying the different zones described in the T_b vs size diagram.

N° Zone	Type of Nebulae
1	Very likely HII regions
2	Probable HII regions: Not conclusive
3	Mixed populations
4	Very likely PNe
5	Probable PNe: Not conclusive

This analysis can be cross-checked with our knowledge of the limiting radio flux of planetary nebulae i.e. the upper flux reached by most of the planetary nebulae. Figure

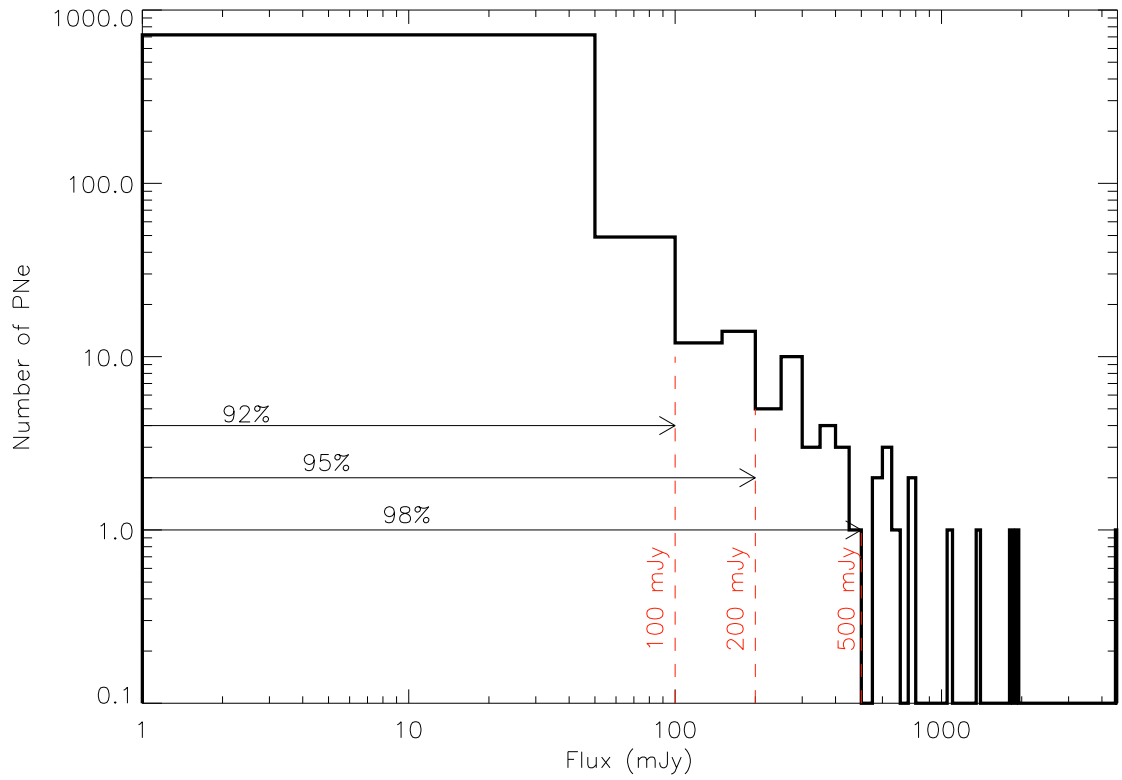

Figure 3.22: Percentage of PNe for limiting fluxes of 100, 200 and 500 mJy.

3.22, shows that 98% of the PNe are contained in a flux range between 1 and 500 mJy. So below 500 mJy, there is a reasonable probability for the nebula to be a PN.

In order to include the HII regions, the last test consisted of determining the turning point (or radio flux) when the fraction of PNe over HII regions changes. The Figure 3.23 indicates that up to ~200 mJy (225 to be precise), the number of PNe is greater than the number of HII regions. This area is dominated by planetary nebulae. Between ~200 mJy and 500 mJy, we have a transition zone, where both populations coexist. This fits in well with the results shown in Fig. 3.22. Therefore nothing can be stated in terms of classification. After 500 mJy, the fraction of PNe/HII regions is below unity, and we are in a zone mostly dominated by HII regions.

The radio data obtained from the 1.4 GHz VLA survey showed, firstly, some

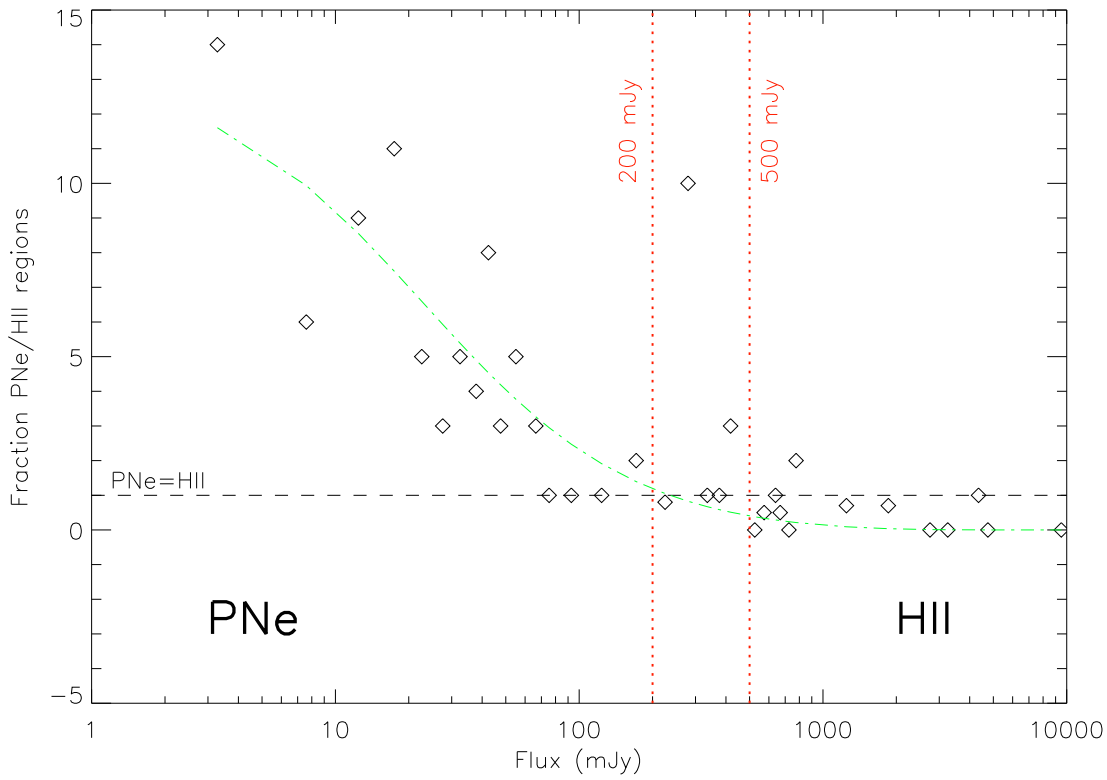

Figure 3.23: Fraction of PNe/HII regions according to the radio flux.

characteristics of the IPHAS sources, like the generally low radio flux and low surface brightness, both consistent with evolved and extended nebulae, in comparison to known PNe. We also defined a scheme exploring the likelihood of being a planetary nebula using the brightness temperature, the general PN flux and studying the evolution of the fraction of PNe/HII regions along with the radio flux. Although, as we said at the beginning of this section, this scheme doesn't give an absolute and definitive classification, it does help to determine our data in one direction (PN) or the other (HII regions) or more generally objects with weak or strong radio emissions. The classification for our 60 targets are listed in Table 3.9. We introduced the following nomenclature for probability on the objects' nature: 2-Very Likely (PN or HII), 3-Probable (PN? or HII?), 4-Not conclusive (-). In the absence of spectra we did not use the "1-True" no-

tation. We found that 22% of the nebulae can be classified as “very likely” and include 1 HII region and 12 PNe, 63% of the sample (38 objects) are classed as “probable” PNe and 15% (9 objects) show a “non conclusive” classification. In conclusion our radio cross-identification technique was revealed to be a good tool to find PNe. The new planetary nebulae are shown in Figure 3.24.

A more accurate determination of the radio fluxes is needed for these new sources, and we expect it to be done with the CORNISH survey (Co-Ordinated Radio ’N’ Infrared Survey for High-mass star formation)[12]. Unfortunately, this survey does not cover all the IPHAS fields and is limited to l=10 to 65 deg and $|b|\leq 1$ deg but in this range the data obtained at radio wavelengths, from the Very Large Array in B configuration at 5 GHz, will have 1 arcsecond resolution comparable to the IPHAS survey and an uniform sensitivity over a large area.

[12]http://www.ast.leeds.ac.uk/Cornish/index.html

Table 3.9: Radio classification of the candidate PNe identified in the NVSS survey. The classification is set as: 2-very likely, 3-probable and 4-non conclusive.

IPHAS Name	Flux at 1.4 GHz (mJy)	T_b vs Size	PN flux Limit	PNe/HII vs Flux	Classification
IPHASX J183438.7+000803	12.7	PN	PN?	PN?	2
IPHASX J183602.4-000226	4.3	-	PN?	PN?	3
IPHASX J183652.8-011536	6.9	-	PN?	PN?	3
IPHASX J183911.8+010624	6.1	-	PN?	PN?	3
IPHASX J184104.6-014050	4.4	-	PN?	PN?	3
IPHASX J184211.4+005031	15.1	PN	PN?	PN?	2
IPHASX J184253.2-022642	4.9	-	PN?	PN?	3
IPHASX J184336.6+034640	5.1	-	PN?	PN?	3
IPHASX J184745.4+013248	13.4	-	PN?	PN?	3
IPHASX J184800.7+025416	21.6	HII?	PN?	PN?	4
IPHASX J184836.2+022050	5.7	-	PN?	PN?	3
IPHASX J184932.6-004437	100.0	PN?	PN?	PN?	3
IPHASX J185225.5-003326	20.5	PN	PN?	PN?	2

Table 3.9 – continued .

Name	Flux at 1.4 GHz (mJy)	T_b vs Size	PN flux Limit	PNe/HII vs Flux	Classification
IPHASX J185309.4+075241	9.0	PN	PN?	PN?	2
IPHASX J185321.7+055641	5.0	-	PN?	PN?	3
IPHASX J185640.1-003804	2.4	-	PN?	PN?	3
IPHASX J185722.5+010929	6.5	-	PN?	PN?	3
IPHASX J185759.6+020706	99.7	PN?	PN?	PN?	3
IPHASX J185815.8+073753	16.6	PN	PN?	PN?	2
IPHASX J185925.8+001734	3.7	-	PN?	PN?	3
IPHASX J190155.1+011211	197.8	HII?	PN?	PN?	4
IPHASX J190340.7+094640	6.1	-	PN?	PN?	3
IPHASX J190346.8+050935	6.2	-	PN?	PN?	3
IPHASX J190418.6+050635	17.7	HII?	PN?	PN?	4
IPHASX J190432.9+091656	17.5	PN	PN?	PN?	2
IPHASX J190633.6+090720	14.9	PN	PN?	PN?	2
IPHASX J190654.9+052216	3.1	-	PN?	PN?	3
IPHASX J190700.7+043041	10.1	-	PN?	PN?	3
IPHASX J190759.4+050519	8.5	-	PN?	PN?	3
IPHASX J191022.1+110538	5.0	-	PN?	PN?	3

Table 3.9 – continued .

Name	Flux at 1.4 GHz (mJy)	T_b vs Size	PN flux Limit	PNe/HII vs Flux	Classification
IPHASX J191104.7+060845	8.5	-	PN?	PN?	3
IPHASX J191124.8+002743	3.4	-	PN?	PN?	3
IPHASX J191345.6+174752	2.1	-	PN?	PN?	3
IPHASX J191716.6+181518	3.6	-	PN?	PN?	3
IPHASX J192038.9+160224	33.0	HII?	PN?	PN?	4
IPHASX J192146.7+172053	16.7	PN	PN?	PN?	2
IPHASX J192349.9+143330	5419.1	HII	HII	HII	2
IPHASX J192410.6+133443	8.9	-	PN?	PN?	3
IPHASX J192458.2+193434	42.1	PN	PN?	PN?	2
IPHASX J192510.8+113353	2.2	-	PN?	PN?	3
IPHASX J192615.4+191358	25.5	HII?	PN?	PN?	4
IPHASX J192624.7+195045	51.6	PN	PN?	PN?	2
IPHASX J192717.1+193408	3.5	-	PN?	PN?	3
IPHASX J192902.5+244646	2.8	-	PN?	PN?	3
IPHASX J193008.9+192137	5.4	-	PN?	PN?	3
IPHASX J193718.7+202102	6.6	PN	PN?	PN?	2
IPHASX J193721.9+233607	2.8	-	PN?	PN?	3

Table 3.9 – continued .

Name	Flux at 1.4 GHz (mJy)	T_b vs Size	PN flux Limit	PNe/HII vs Flux	Classification
IPHASX J193740.6+203548	16.2	PN	PN?	PN?	2
IPHASX J193912.0+251105	218.9	PN?	PN?	PN?/HII?	4
IPHASX J194226.1+214521	5.5	-	PN?	PN?	3
IPHASX J194359.5+170901	5.0	-	PN?	PN?	3
IPHASX J194408.9+284845	8.6	-	PN?	PN?	3
IPHASX J194533.8+210751	3.4	-	PN?	PN?	3
IPHASX J194641.5+264820	21.9	HII?	PN?	PN?	4
IPHASX J194810.6+280724	7.2	-	PN?	PN?	3
IPHASX J194815.0+280730	36.5	HII?	PN?	PN?	4
IPHASX J194852.7+222516	3.4	-	PN?	PN?	3
IPHASX J195015.9+272859	3.4	-	PN?	PN?	3
IPHASX J195248.8+255359	15.9	HII?	PN?	PN?	4
IPHASX J195919.6+283827	27.0	-	PN?	PN?	3

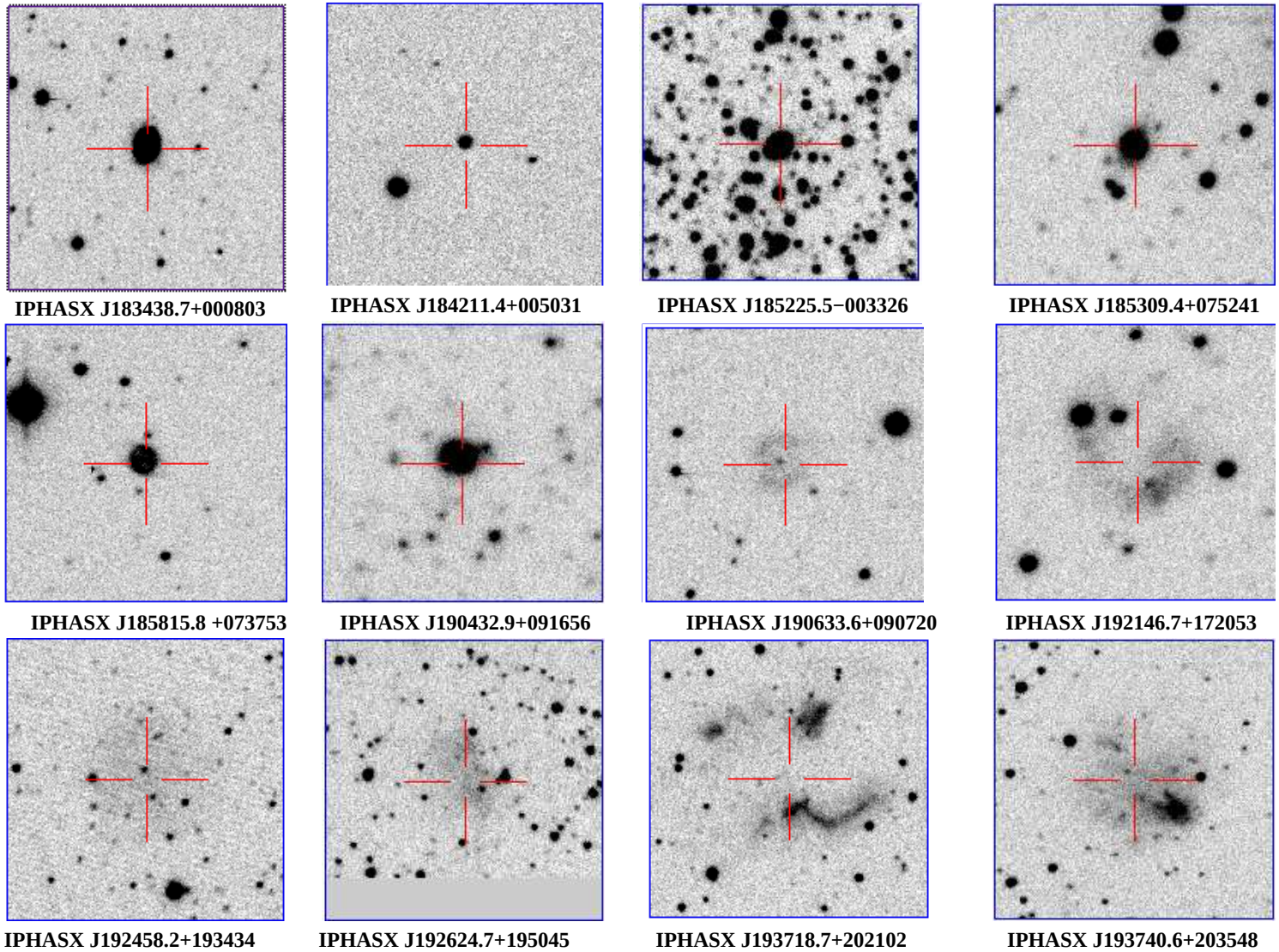

Figure 3.24: IPHAS planetary nebulae identified thanks to their radio flux. 1×1 arcminute Hα images with the North on the top and the East on the left.

3.4 Morphology based classification

In order to complete our object classification, the last criterion used will be the morphology. It is not a tool that can be used alone as different types of nebulae can show the same form. But combined with other analytical methods it can help to mark the difference. Planetary nebulae mostly have a well defined symmetrical shape (round or Strömgren sphere, elliptical, bipolar, multipolar...etc), and this is also the case for symbiotic stars and some HII regions. In contrast, the majority of HII regions are bright and shapeless. As they are generally at the same location as the SNR, they suffer from close interaction. Herbig Haros and YSO objects often show bow shocks and symmetrical jets can be seen in HH objects. Finally SNR are generally filamentary and less diffused than HII regions. What follows here is a gallery of Hα+[NII] images of all our candidate PNe (Figure 3.25) as well as a qualitative description of each of them in Appendix B. The images have been taken using the INT Hα filter.

We found that 146 sources (nearly 2/3 of the whole sample) can be classified from "very likely" to "probable" PNe due to their shape, although this a quite subjective classification. We cannot state the nature of the 87 remaining sources, which are generally shapeless, faint and/or large.

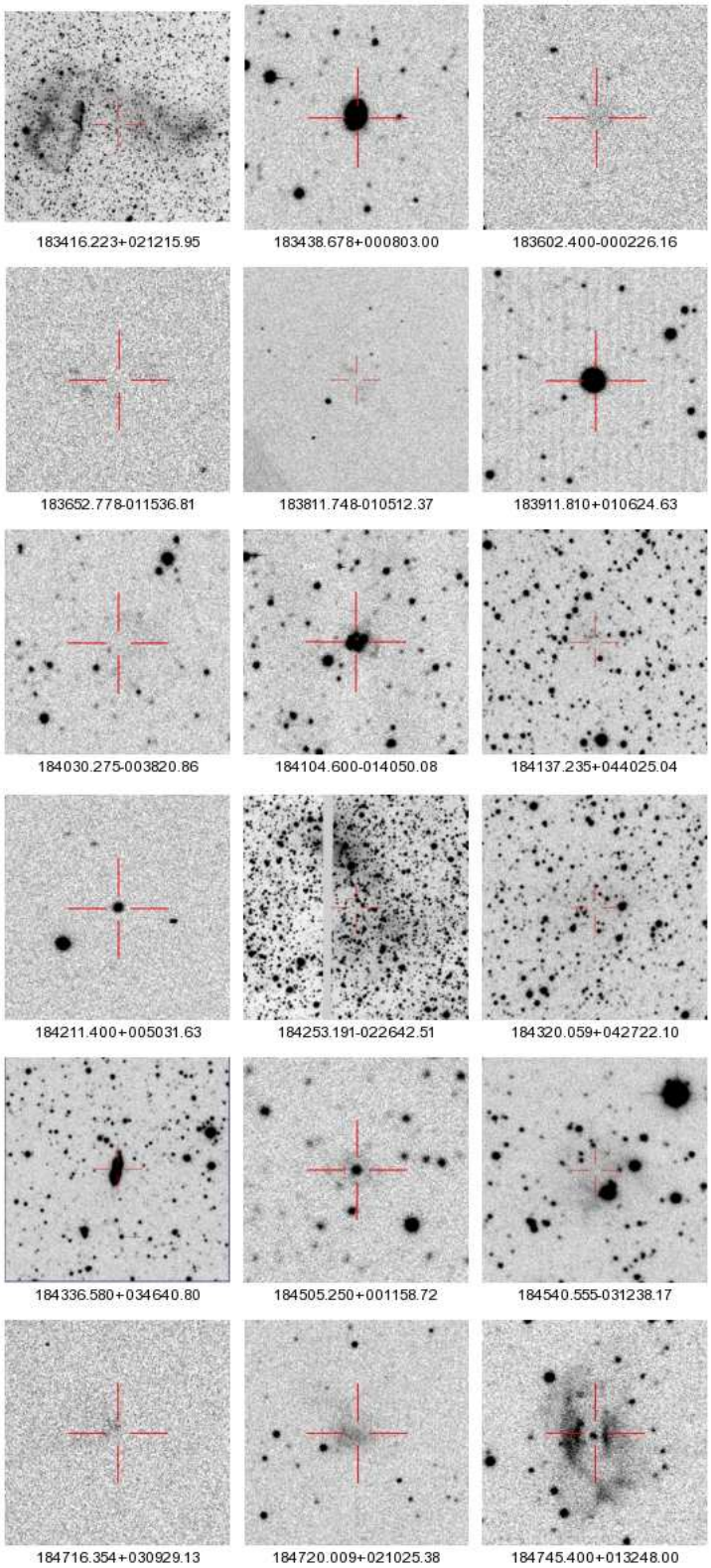

Figure 3.25: Hα+[NII] images of the IPHAS candidate PNe. North on the Top and East on the left.

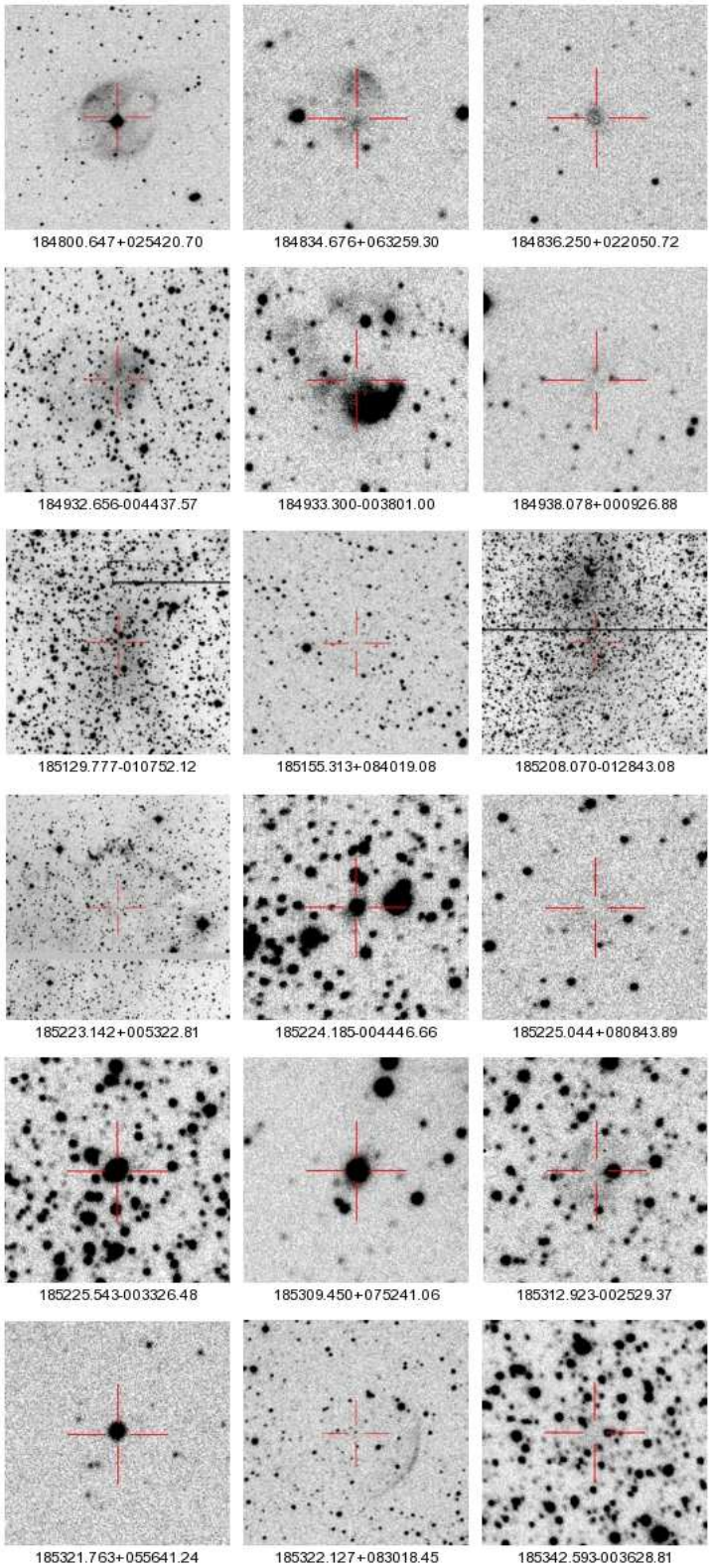

Figure 3.25 (continued)

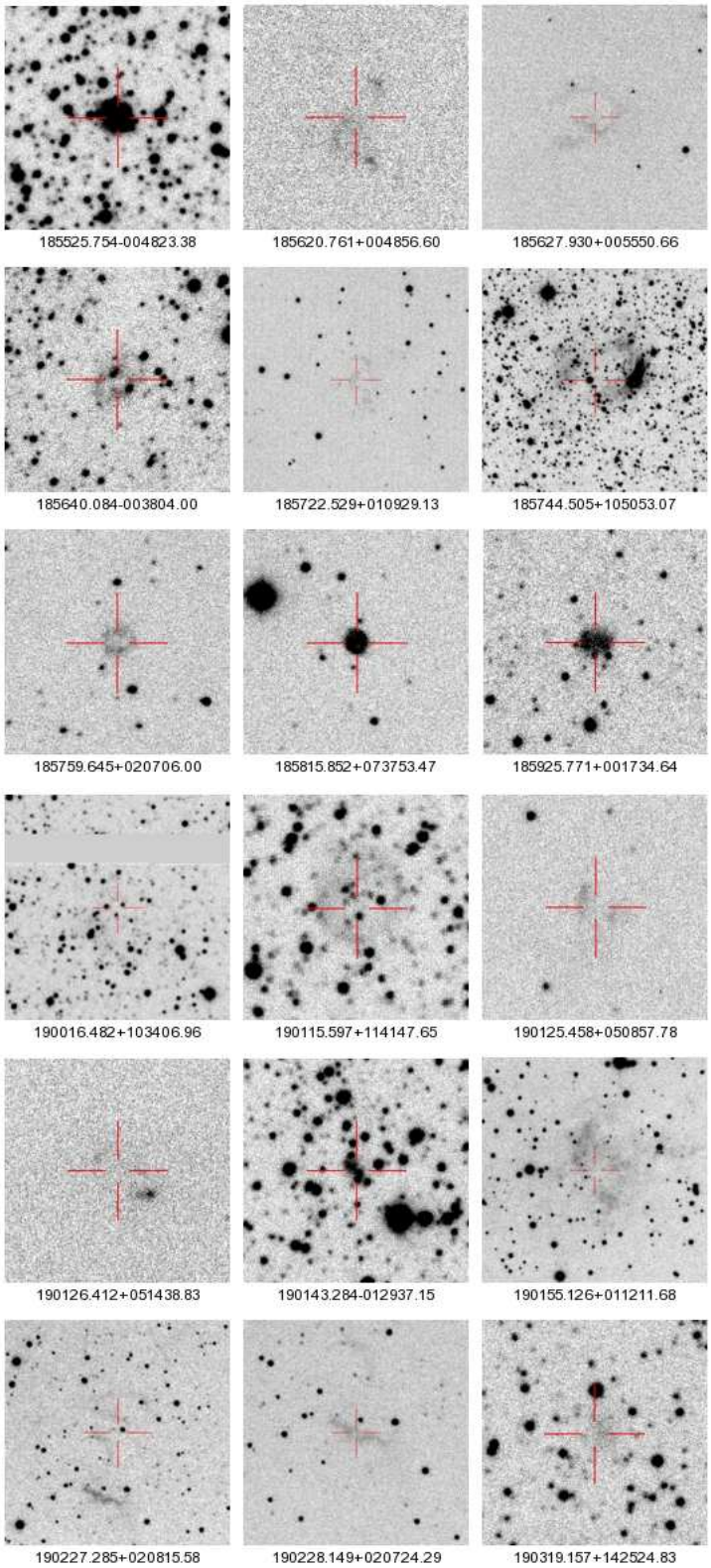

Figure 3.25 (continued)

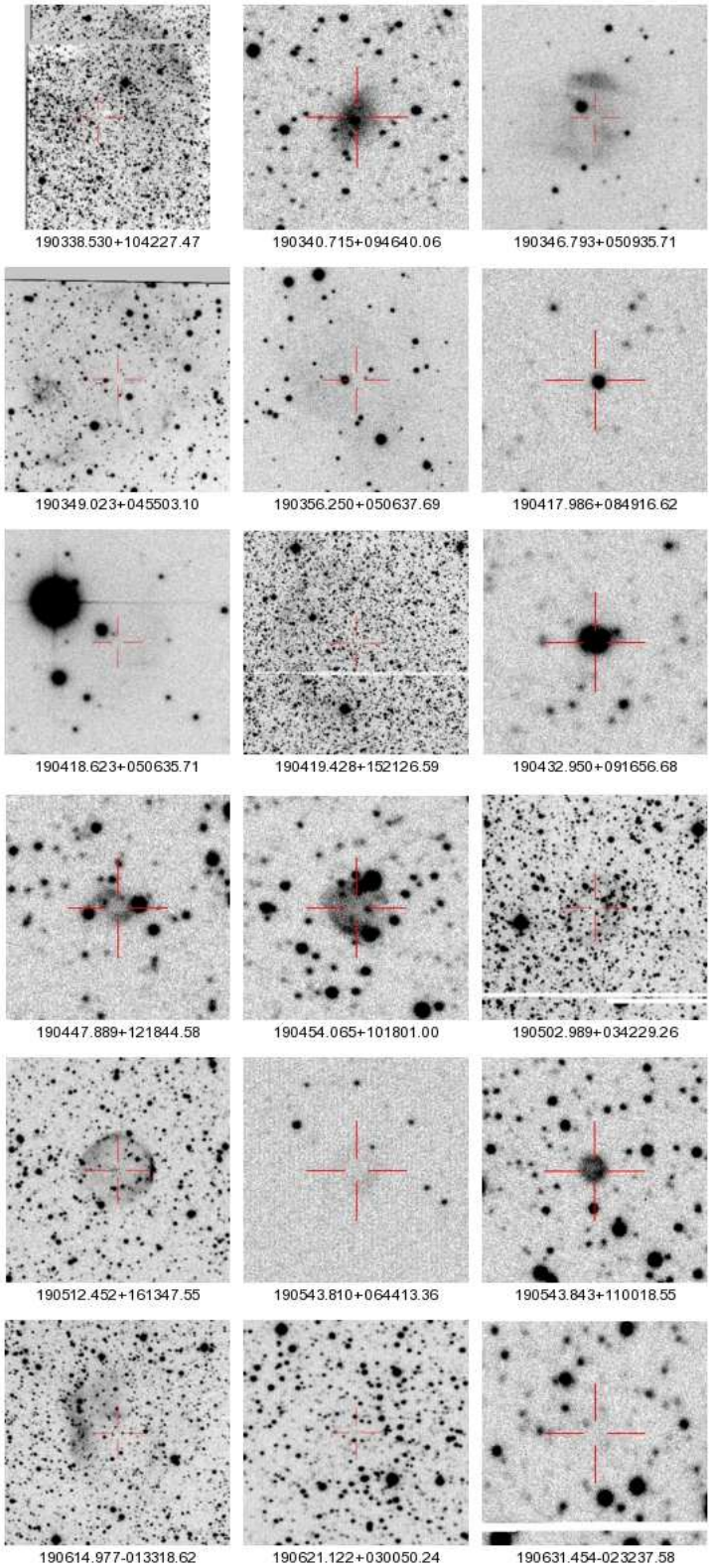

Figure 3.25 (continued)

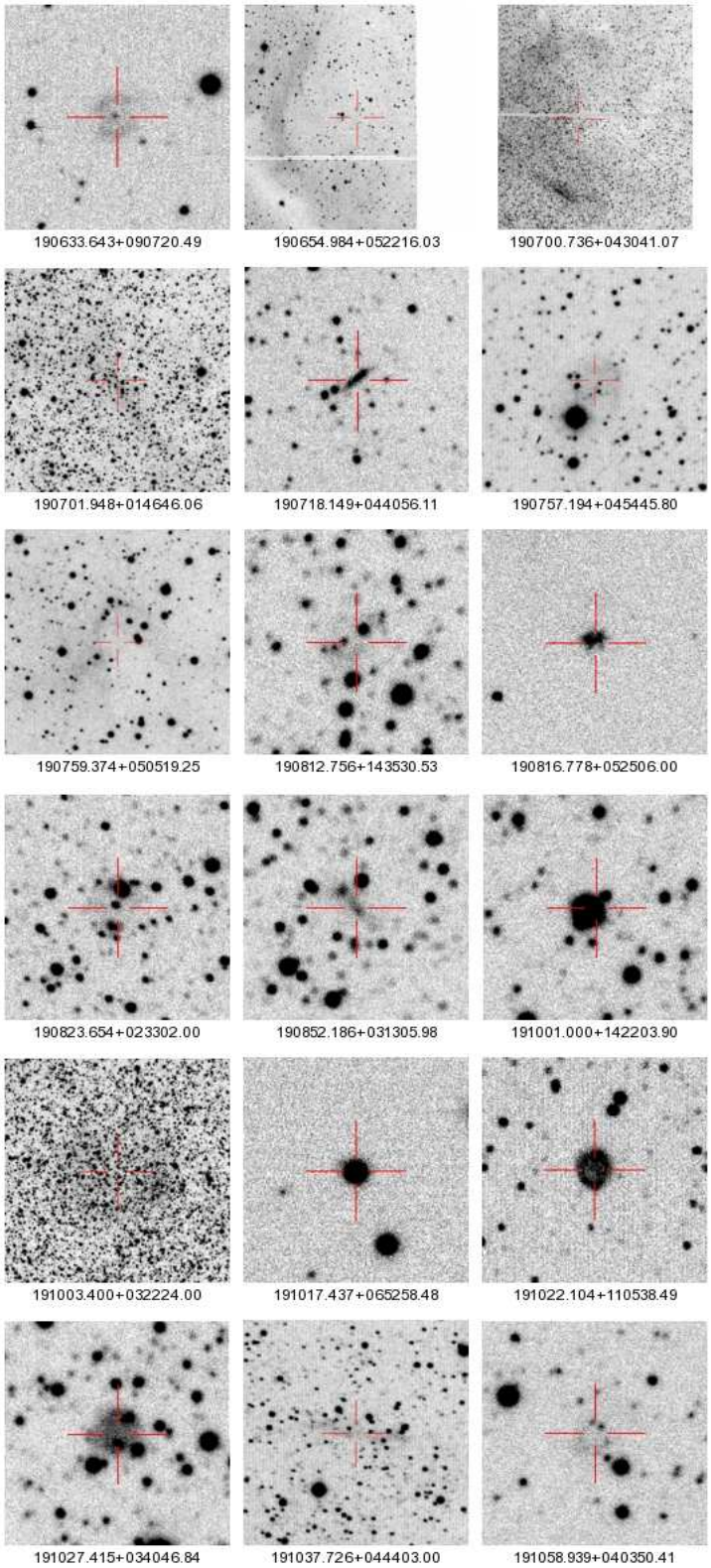

Figure 3.25 (continued)

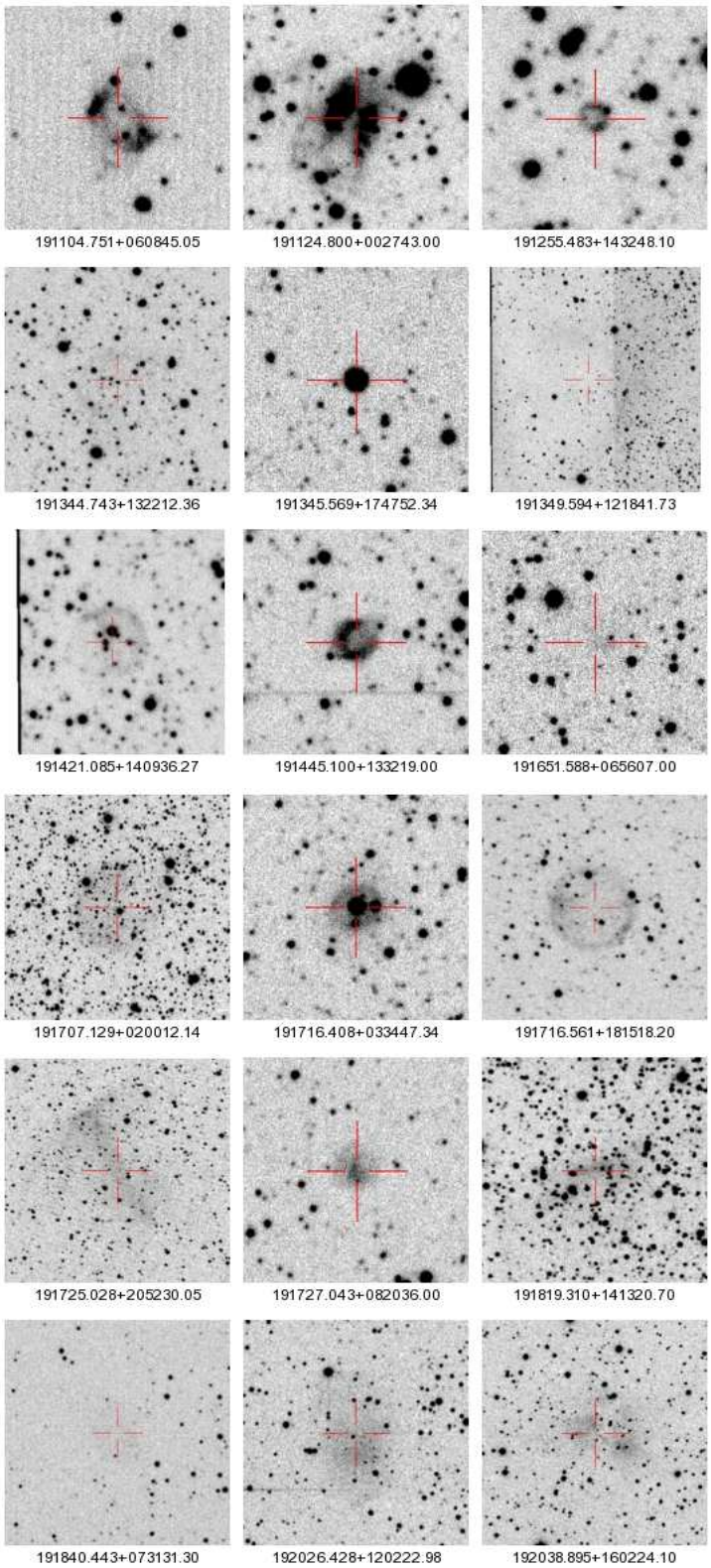

Figure 3.25 (continued)

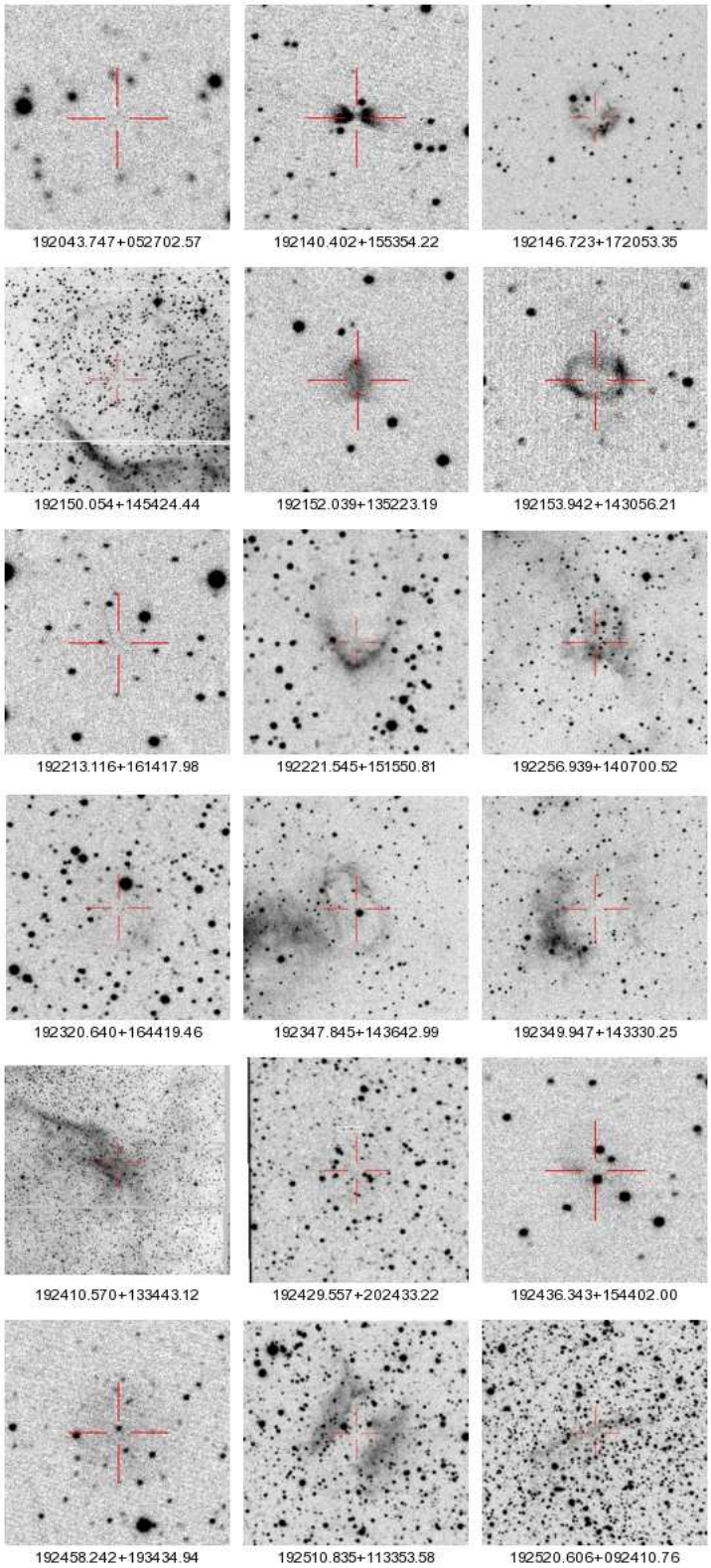

Figure 3.25 (continued)

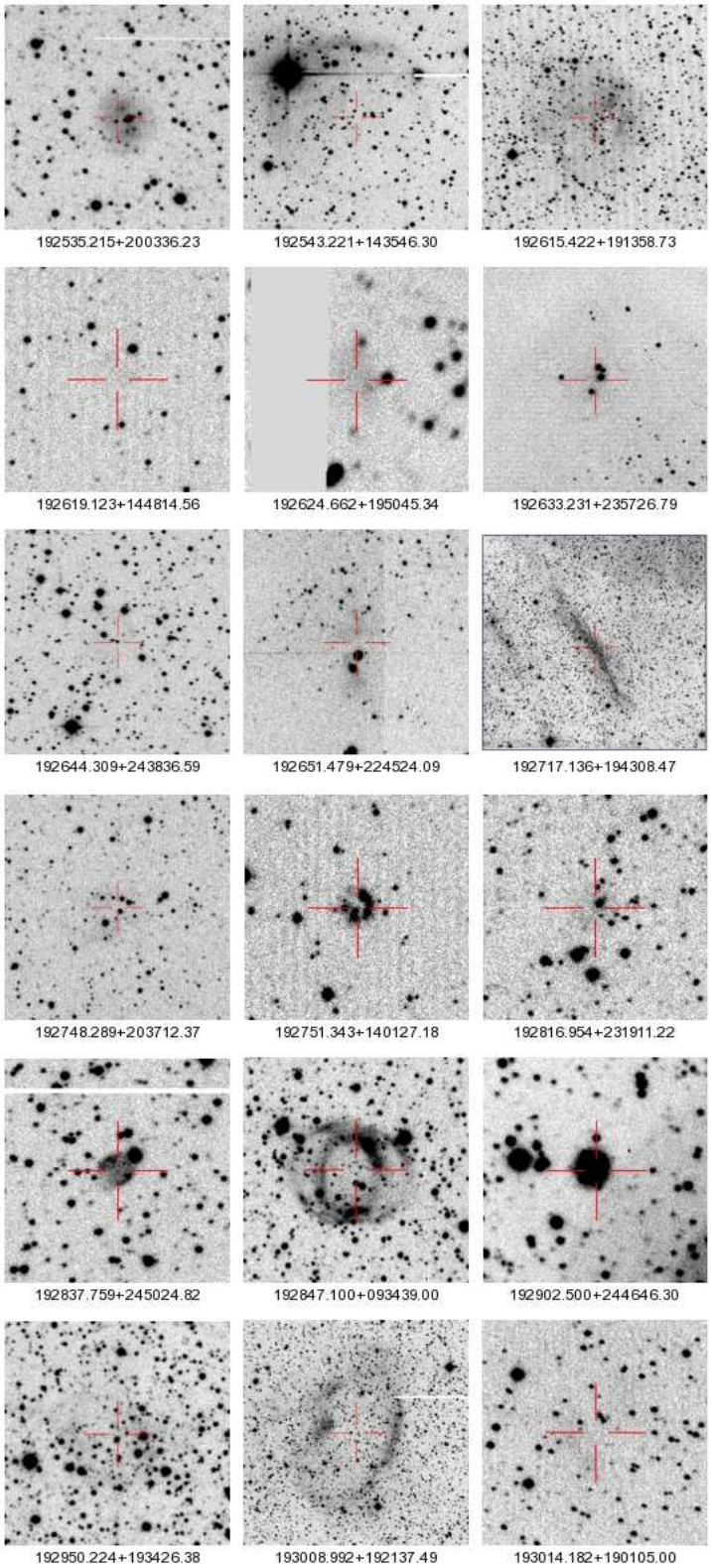

Figure 3.25 (continued)

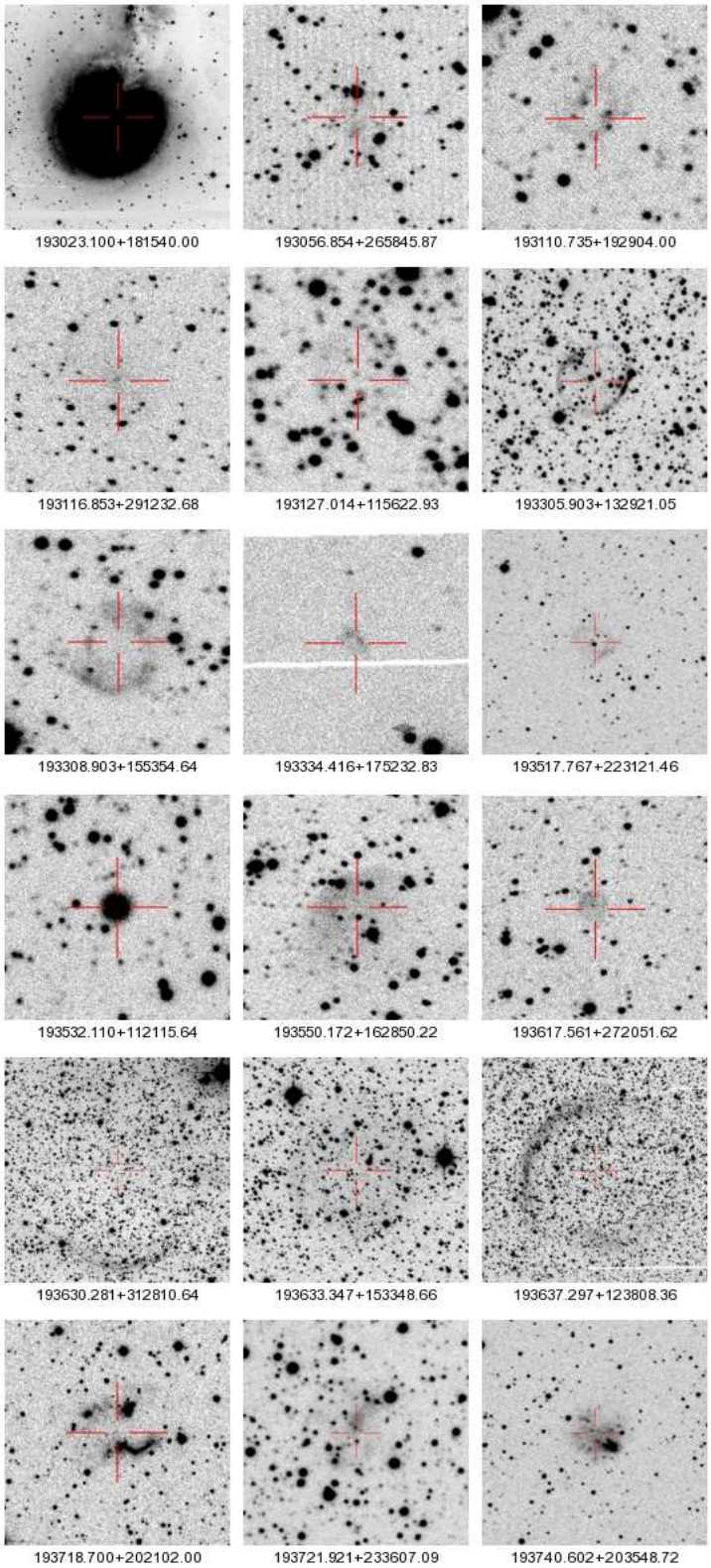

Figure 3.25 (continued)

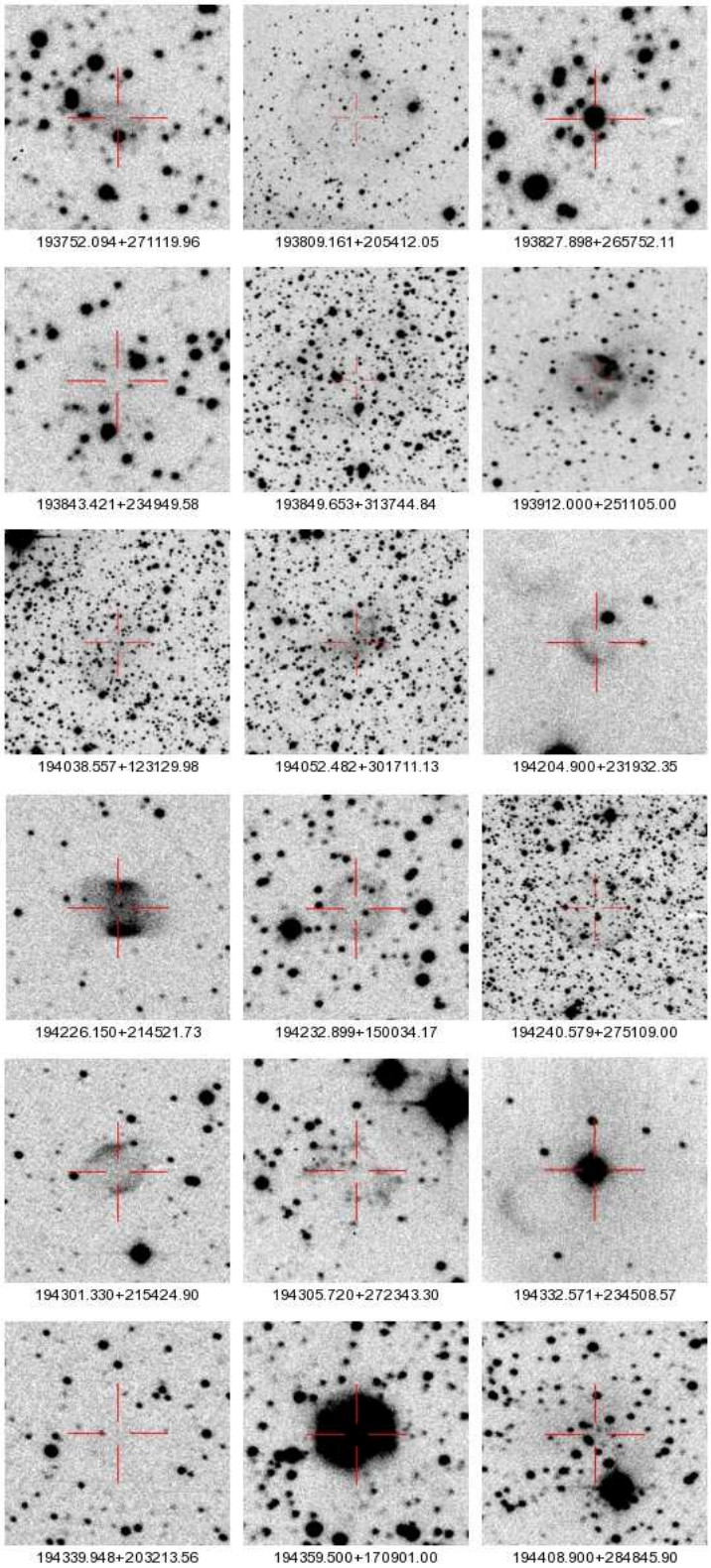

Figure 3.25 (continued)

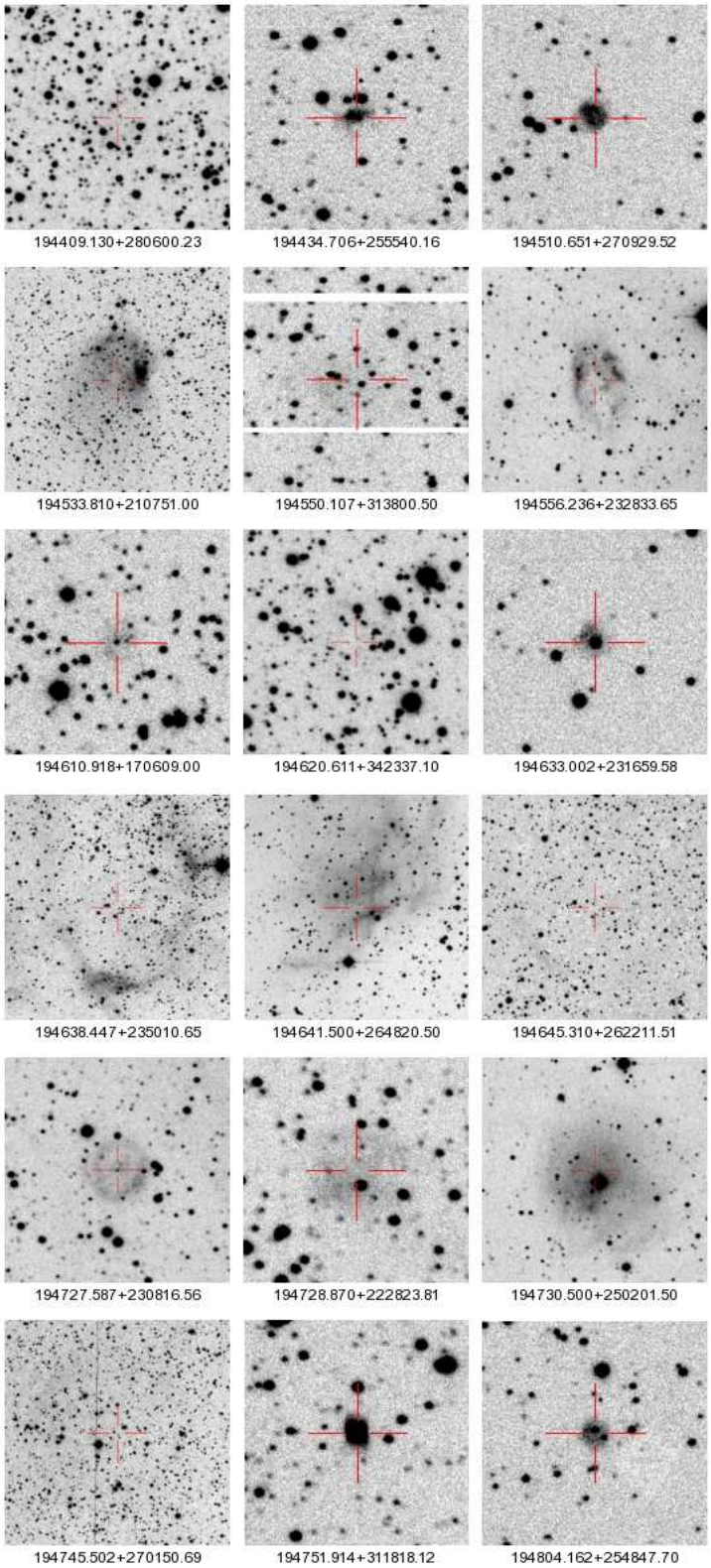

Figure 3.25 (continued)

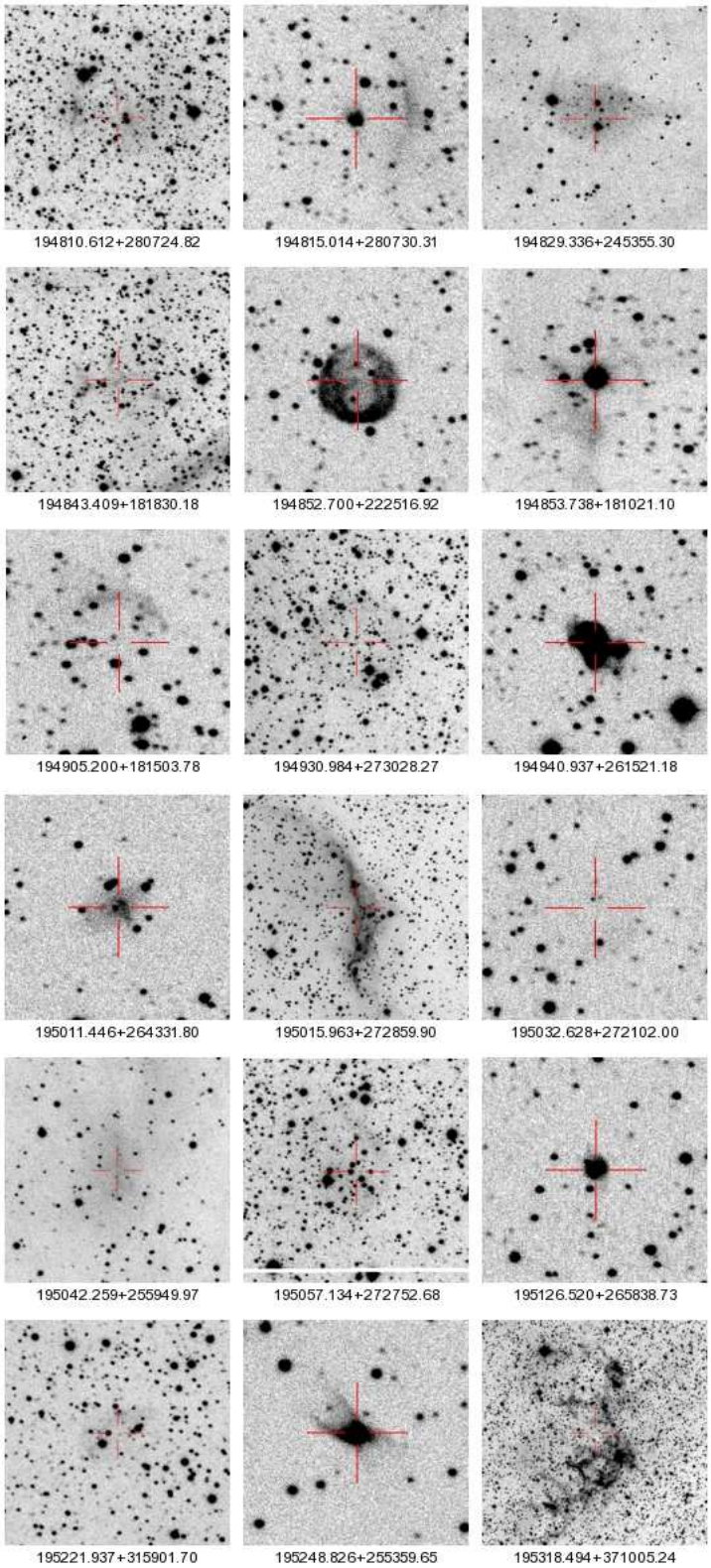

Figure 3.25 (continued)

3.5 Summary

Visual inspection, in the right ascension range between 18h and 20h, of 2 degrees mosaics created from the IPHAS data has revealed a large number of new Hα emitters among which we found 233 candidate planetary nebulae. We were not able to spectroscopically prove the nature of all of them. So using other tools like infrared (IRAS and MSX) and radio data (NVSS/VLA), supported by the morphology, we either derived the candidate's nature or at least give some hypothesis concerning their nature. Our classification is divided into 4 categories listed below. We emphasize that this classification overrides individual ones. Hence, as an example, a nebula **only** identified as "radio PN" will have its general classification set to "probable: 3".

- 1: True planetary nebula i.e. confirmed at least spectroscopically.
- 2: Very Likely planetary nebula; with at least three corroborations including (or not) spectroscopic data.
- 3: Probable planetary nebula; with no spectroscopic data and at least one or two identifications, or only a convincing morphology.
- 4: Unlikely or non-conclusive planetary nebula; with no spectroscopic data and no other conclusive identification or an unconvincing morphology.

We summarise in Table 3.10 the results obtained for the IPHAS candidate PNe presented in the classification process. Of the 233 objects we were able to gather data for 72 of them (31%). In this group, 12 have the highest probability to be a PN (17%) and are therefore classified as "true" PNe and 2 objects are classified as "very likely" PN (2%). 22 candidates are "probable" PNe (30%) among which 1 could be coincident with a HII region. Finally, concerning the remaining 36 candidates (50%), we have either not enough information or conflicting designations, to give a definitive classification. For most of those, rather than "unlikely" we should read "non conclusive". Of course, one can rely on the partial analysis (IRAS, MSX and radio) to have an idea of

the nature of the nebulae. Among the 161 candidates left, we have morphologically classified all the ones which are diffuse and with no symmetry as “unlikely/non conclusive planetary nebula” (this will stand until further analysis), they represent 53% of the remaining candidates (85 objects). The 76 nebulae (with symmetry) left, are classified as “probable” PNe (47%).

We also notice that in our list of candidate PNe, 6 detected objects may be possible new SNRs (Fig 3.26). This is a very interesting result as we can expect to detect many more of these objects and increase the statistics on the number of supernovae remnants in the galactic plane as well as making a study of “small size” SNR i.e. young outbursts. These nebulae are characterised by the presence of ROSAT x-ray data inside or outside the nebula, their filamentary aspect or even the presence of a nearby young pulsar (less than 10^6 years). These objects are discussed in Appendix E.

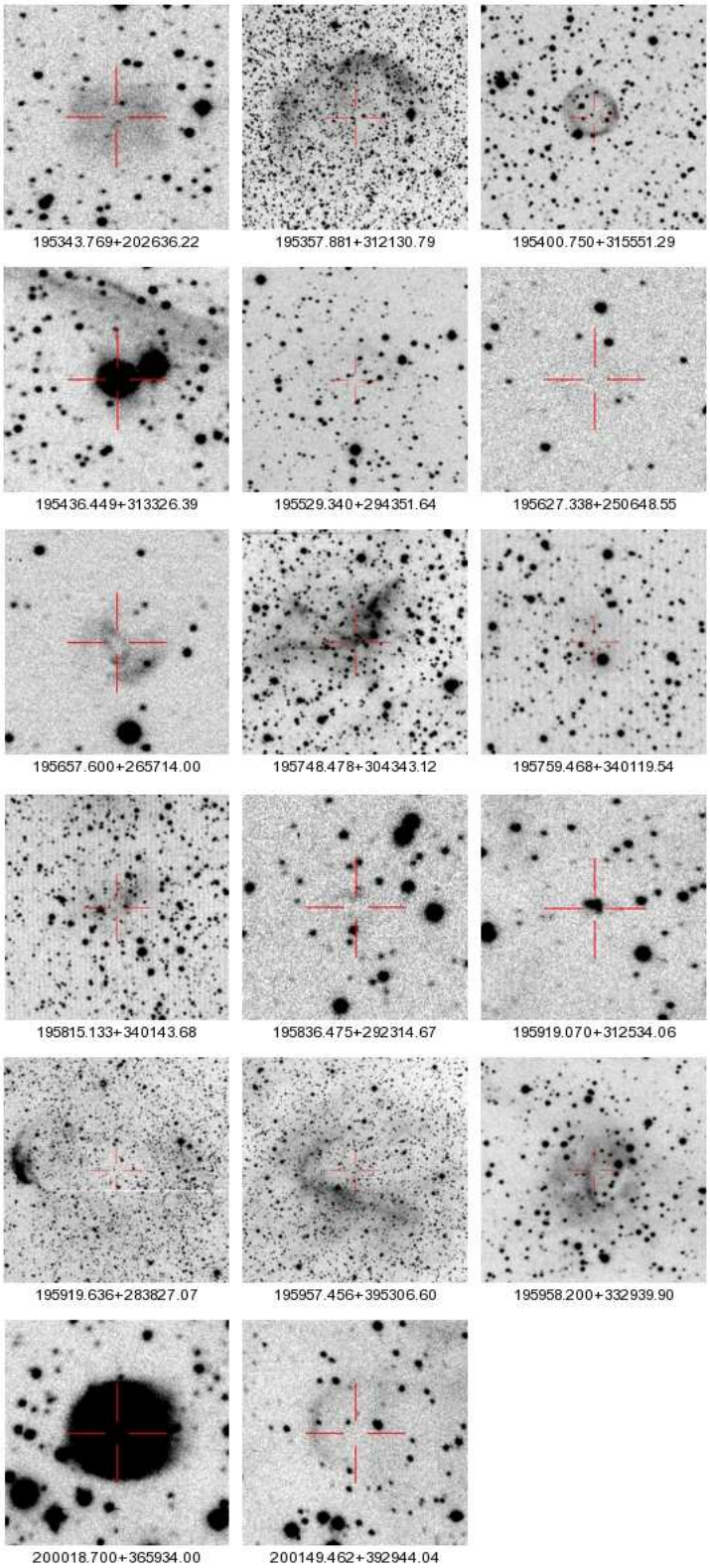

Figure 3.25 (continued)

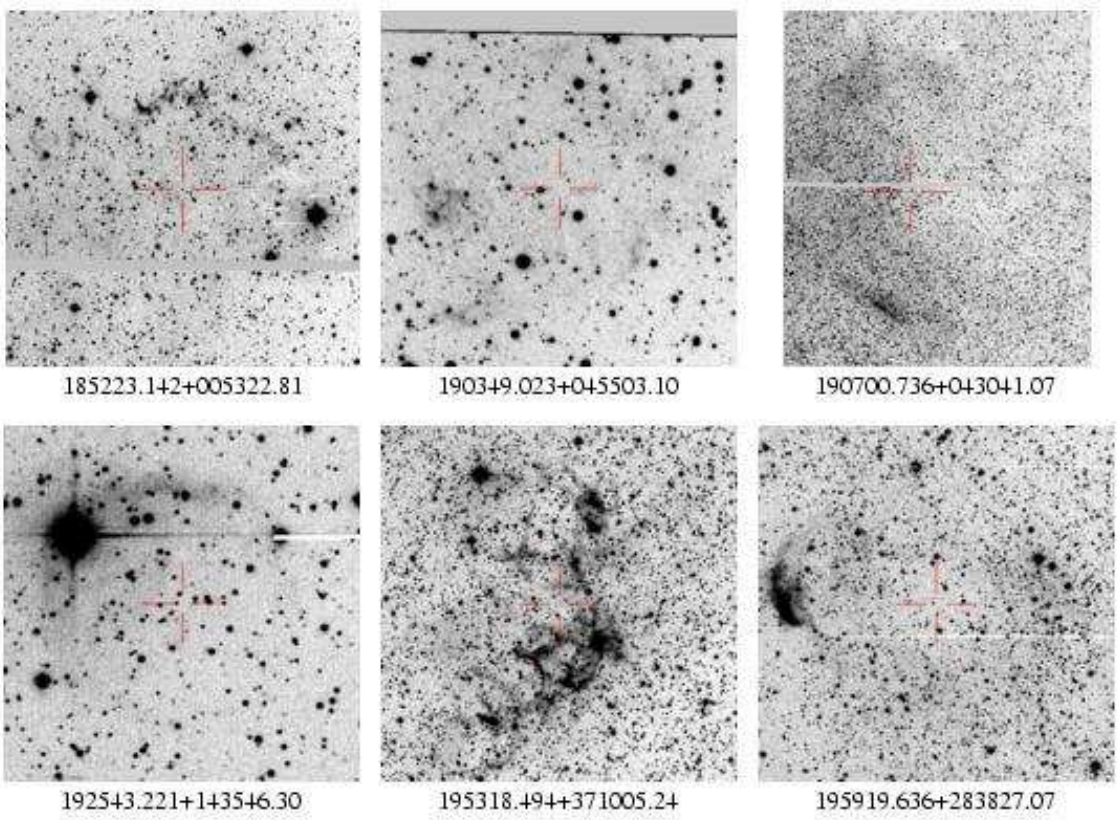

Figure 3.26: Young IPHAS Supernovae Remnant candidates also notified as PN candidates.

Table 3.10: Summary of the classification of IPHAS candidate PNe. Lines stands for the Emission lines study. The last column indicates the likelihood on the true nature of the nebulae

Name(IPHASX J)	**Spectroscopy**			**IRAS**			**MSX**	**NVSS**	**Morpho**	**N°**
	Sabbadin	**Riesgo**	**Lines**	**Zijlstra**	**Pottasch**	**Emerson**				
183438.7+000803								PN	E	3
183602.4-000226								PN?	I	4
183652.8-011536								PN?	I	4
183911.8+010624	-	-	PN?	PN/Outflow	PN	T-Tauri		PN?	R	2
184104.6-014050								PN?	I	4
184211.4+005031								PN	R	3
184253.2-022642								PN?	I	4
184336.6+034640	PN	PN		PN/Outflow	PN		PN/PPN	PN?	B	1
184745.4+013248	-	-	HII/PN					PN?	B	3
184800.6+025420				PN	PN		PN/PPN	HII?/PN?	R	2
184836.2+022050								PN?	R	4
184932.6-004437							PN/PPN	PN?	I	3

Table 3.10 – continued .

Name (IPHASX J)	Spectroscopy			IRAS			MSX	NVSS	Morpho	N°
	Sabbadin	Riesgo	Lines	Zijlstra	Pottasch	Emerson				
185224.2-004446	-	-	PN?						R	3
185225.5-003326							PN/PPN	PN	R	3
185309.4+075241								PN	E	3
185321.7+055641								PN?	R	4
185525.7-004823	PN	PN							B	1
185627.9+005550				PN	PN				I	3
185640.1-003804								PN?	E	3
185722.5+010929								PN?	I	4
185759.6+020706								PN?	R	4
185815.8+073753								PN	E	3
185925.8+001734	PN?	PN						PN?	E	1
190155.1+011211								HII?/PN?	I	4
190340.7+094640								PN?	I	4
190346.8+050935								PN?	I	4
190418.6+050635								HII?/PN?	I	4
190432.9+091656								PN	R	3

Table 3.10 – continued .

Name (IPHASX J)	Spectroscopy			IRAS			MSX	NVSS	Morpho	N°
	Sabbadin	Riesgo	Lines	Zijlstra	Pottasch	Emerson				
190633.6+090720								PN	R	3
190654.9+052216								PN?	R	4
190700.7+043041								PN?	R	4
190759.4+050519								PN?	I	4
191017.4+065258							OH-IR		R	3
191022.1+110538								PN?	R	4
191104.7+060845								PN?	B	4
191124.8+002743	PN	PN						PN?	B	3
191345.6+174752	PN	PN?						PN?	R	1
191445.1+133219	PN	PN							B	1
191716.6+181518								PN?	R	3
192038.9+160224							OH-IR	HII?/PN?	I	4
192140.4+155354				HII	HII		PN/PPN		B	3
192146.7+172053								PN	R	3
192256.9+140700							PN/PPN		I	3
192349.9+143330								HII	I	3

Table 3.10 – continued .

Name (IPHASX J)	Spectroscopy			IRAS			MSX	NVSS	Morpho	N°
	Sabbadin	Riesgo	Lines	Zijlstra	Pottasch	Emerson				
192410.6+133443								PN?	I	4
192458.2+193434				Unknown	Galaxy			PN	R	4
192510.8+113353								PN?	B	4
192615.4+191358								HII?/PN?	R	4
192624.7+195045				Unknown	Galaxy			PN	I	4
192717.1+193408								PN?	I	4
192847.1+093439	PN	PN							B	1
192902.5+244646	-	-	HII?					PN?	R	4
193008.9+192137								PN?	E	4
193718.7+202102								PN	B	3
193721.9+233607								PN?	I	4
193740.6+203548								PN	I	3
193827.9+265752	-	-	-						R	3
193912.0+251105	PN	PN		Unknown	Galaxy		PN/PPN	PN?	I	1
194226.1+214521								PN?	B	4
194359.5+170901	PN	PN						PN?	B	1

Table 3.10 – continued .

Name (IPHASX J)	Spectroscopy			IRAS			MSX	NVSS	Morpho	N°
	Sabbadin	Riesgo	Lines	Zijlstra	Pottasch	Emerson				
194408.9+284845								PN?	I	4
194533.8+210751								PN?	I	4
194641.5+264820								HII?/PN?	I	4
194751.9+311818	PN	PN							B	1
194810.6+280724								PN?	I	4
194815.0+280730				HII	HII		PN/PPN	HII?/PN?	R	4
194852.7+222516								PN?	R	4
194940.9+261521	Unclear	PN							B	1
195015.9+272859				HII	HII			PN?	I	4
195248.8+255359	PN	PN						HII?/PN?	B	1
195657.6+265714	PN	PN							B	1
195919.6+283827				Unknown	Unknown			PN?	I	4

The spectroscopy, infrared and radio analysis carried out on some IPHAS nebulae, allowed us to classify some IPHAS nebulae, but it also underlined that they exhibit some particular characteristics when compared to known planetary nebulae. Thus the radio data have shown that the IPHAS candidate PNe are probably more evolved than their known counterparts. In the next part, we will use the results obtained previously to show to which extent IPHAS contributes to enhancing our knowledge about planetary nebulae, the key question being: *what does IPHAS contribute further to our knowledge ?*

We will therefore focus on the general distribution and number of the IPHAS sources, but also on the analysis of their infrared properties, their distance determination, their evolutionary phase and finally their interaction with the interstellar medium.